AD-A146 289 NONLINEAR SYSTEM IDENTIFICATION METHODOLOGY DEVELOPMENT 1/2
BASED ON F-4S FLI..(U) SYSTEMS CONTROL TECHNOLOGY INC
PALO ALTO CA J H VINCENT ET AL. DEC 83
UNCLASSIFIED N00421-81-C-0289 F/G 14/2 NL

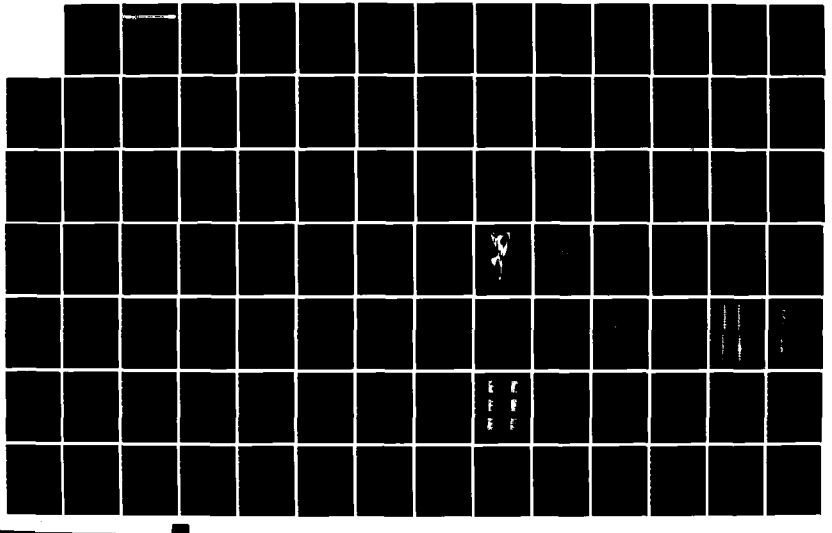

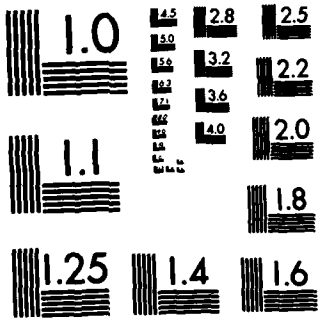

MICROCOPY RESOLUTION TEST CHART

SCT SYSTEMS CONTROL TECHNOLOGY, INC.
1801 PAGE MILL RD. □ P.O. BOX 10180 □ PALO ALTO, CALIFORNIA 94303 □ (415) 494-2233

DECEMBER 1983

FINAL REPORT

NONLINEAR SYSTEM IDENTIFICATION METHODOLOGY DEVELOPMENT BASED ON F-4S FLIGHT TEST DATA ANALYSIS

Project No. 5273

Prepared by
J.H. Vincent
S.N. Franklin
U.H. Rabin
T.L. Trankle

Prepared for the
NAVAL AIR TEST CENTER
NAS Patuxent River, Maryland 20670
Under Contract No. N00421-81-C-0289

and the

OFFICE OF NAVAL RESEARCH
800 N. Quincy Street
Arlington, Virginia 22217
Under Contract No. N00014-78-C-0641

FOREWORD

This report describes the work performed by Systems Control Technology, Inc. (SCT) under Contract No. N00421-81-C-0289 for the Strike Aircraft Test Directorate of the NAVAIRTESTCEN and under Contract No. N00014-78-C-0641 for the Office of Naval Research. The objective of the initial work was to develop a system identification methodology suitable for extracting a nonlinear aerodynamic data base from flight test measurements. The second objective of this work was to apply this methodology to the development of an aerodynamic data base for an F-4S simulator at the NAVAIRTESTCEN.

Mr. Roger Burton served as the technical monitor for this work. The program manager was Mr. James Vincent. Mr. Norm Franklin was principally responsible for producing the system identification results. Report preparation efforts were directed by Ms. Clare Walker, with assistance from Mrs. Toshi Furukawa.

LIST OF SYMBOLS

a_x, a_y, a_z	Axial, lateral, and vertical accelerations	ft/sec^2
b_w	Wing span (38.67 ft)	ft
$b_{(\cdot)}$	Bias for the $(\cdot)$ sensor	-
$\bar{c}_w$	Wing mean aerodynamic chord (16.04 ft)	ft
C_D	Drag coefficient	-
$C_{D_{(\cdot)}}$	$\partial C_D/\partial(\cdot)$	-
C_L	Lift coefficient	-
C_ℓ	Rolling moment coefficient	-
$C_{\ell_{(\cdot)}}$	$\partial C_\ell/\partial(\cdot)$	-
C_n	Yawing moment coefficient	-
$C_{n_{(\cdot)}}$	$\partial C_n/\partial(\cdot)$	-
C_x	Axial force coefficient	
$C_{x_{(\cdot)}}$	$\partial C_x/\partial(\cdot)$	-
C_y	Side force coefficient	-
$C_{y_{(\cdot)}}$	$\partial C_y/\partial(\cdot)$	-
C_z	Normal force coefficient	-
$C_{z_{(\cdot)}}$	$\partial C_z/\partial(\cdot)$	-
F_x, F_y, F_z	Total applied axial, lateral, and vertical forces in body axis	lb
F_{ax}, F_{ay}, F_{az}	Aerodynamic forces in body axis	lb
F_{sx}, F_{sy}, F_{sz}	Aerodynamic forces in stability axis	lb
F_{Tx}, F_{Ty}, F_{Tz}	Propulsion forces in body axis	lb
F_G	Gross thrust	lb
F_I	Inlet ram force	lb

LIST OF SYMBOLS (Continued)

F_N	Net thrust	lb
g	Acceleration due to gravity	ft/sec^2
h	Altitude	ft
h_p	Pressure altitude	ft
I_x, I_y, I_z	Moments of inertia	slug-ft^2
I_{xz}	Cross moment of inertia	slug-ft^2
J	Matrix of partial derivatives of measurements with respect to parameters	-
K_α	Angle of attack numerator gain	-
ℓ_x, ℓ_y, ℓ_z	Noseboom location relative to c.g.	ft
$\ell_{x_A}, \ell_{y_A}, \ell_{z_A}$	Accelerometer location relative to c.g.	ft
ℓ_{N_y}, ℓ_{N_z}	Net thrust moment arms relative to MRC	ft
$\ell_{G_x}, \ell_{G_y}, \ell_{G_z}$	Gross thrust moment arms relative to MRC	ft
$\ell_{I_x}, \ell_{I_y}, \ell_{I_z}$	Inlet ram force moment arms relative to MRC	ft
M	Mach number	-
M	Fisher information matrix	-
M_x, M_y, M_z	Total applied rolling, pitching, and yawing	lb-ft
M_{Ax}, M_{Ay}, M_{Az}	Aerodynamic moments in body axis	lb-ft
M_{sx}, M_{sy}, M_{sz}	Aerodynamic moments in stability axis	lb-ft
M_{Tx}, M_{Ty}, M_{Tz}	Propulsion moments in body axis	lb-ft
m	Aircraft mass	slug
$\dot{m}_a$	Engine air mass flow	slub/sec
N_x	Axial load factor	g's

LIST OF SYMBOLS (Continued)

N_y	Lateral load factor	g's
N_z	Vertical load factor	g's
P	Roll rate	rad/sec
Q	Pitch rate	rad/sec
$\hat{q}$	Dynamic pressure	lb/ft^2
R	Roll rate	rad/sec
S_w	Wing surface (530 ft^2)	ft^2
s	LaPlace operator ($\sigma \pm j\omega$)	-
t	time	sec
u	System input	-
V	Inertial velocity along y body axis	ft/sec
V_T	True airspeed	ft/sec
Var( )	Covariance of ( )	-
W	Inertial velocity along z body axis	ft/sec
w	Process noise vector	-
w_f	Fuel flow	lbs/hr
x	System state	-
y	System output	-
GREEK		
α	Angle of attack	rad
β	Angle of sideslip	rad
γ	Flight path angle	rad
δ	Control surface deflection	rad
δ_A	Effective aileron deflection (spoiler effectiveness included)	rad

LIST OF SYMBOLS (Continued)

δ_{LES}	Leading-edge slat deflection	rad
δ_R	Rudder deflection	rad
δ_S	Stabilator deflection	rad
δ_{TEF}	Trailing-edge flap deflection	rad
θ	Euler pitch angle	rad
θ_T	Thrust line inclination relative to x-axis	rad
ν_k	Measurement error of measurement K	-
ρ	Measurement autocorrelation	-
ρ	Air density	$lb\ sec^2/ft^4$
σ_k	Root mean square error of measurement K	-
τ	Time delay	msec
ϕ	Euler roll angle	rad
ψ	Euler yaw angle	rad

SUBSCRIPTS

A	Airspeed component in body axes
AA	Accelerometer location
cg	center of gravity location
L	Left
m	Measurements
MRC	Moment reference location

SUBSCRIPTS (Continued)

NB	Nose boom
R	Right
REF	Body reference location
x, y, z	Axial, lateral, and vertical body axes
W	Wind component in body axes

ABBREVIATIONS

AMB	Ambient conditions
CR	Cruise
HSI	High stability index
FCS	Flight control system
LSI	Low stability index
LSI*	Low stability index (for comparison with HSI)
PA	Power approach
TO	Take-off

TABLE OF CONTENTS

TABLE OF CONTENTS (Continued)

I. INTRODUCTION AND SUMMARY

1.1 INTRODUCTION

1.1.1 Motivation for Nonlinear System Identification

The Naval Air Test Center (NATC) and Systems Control Technology, Inc. (SCT) have worked jointly to develop an advanced flight test data processing technique that supports an integrated flight testing procedure (i.e., extraction of test data for multiple test requirements from common flight conditions). This data processing technique is commonly referred to as system (or parameter) identification. The development of the system identification methodology has been pursued by a number of organizations during the last decade [1-7].

Realization of this goal for an integrated flight testing procedure is dependent on the ability to identify nonlinear aerodynamic characteristics and propulsion system performance from flight test data. The identified models can be used to define performance, stability and control, and unaugmented airframe dynamic characteristics of the aircraft being evaluated. By identifying the nonlinear aerodynamic models in a multivariable, table-look-up format, direct correlations can be made with preflight aerodynamic predictions (e.g., wind tunnel data) and simulation models.

By using a data processing technique that can identify aerodynamic and installed propulsion models from many large-amplitude dynamic test conditions, it is possible to enhance the test productivity through a reduction in required test time. For the dynamic maneuvers, the test time is defined in terms of seconds, compared to minutes for static tests. Other motivating factors that support the development of this technology include improvements in safety of flight, and a general expansion of requirements for higher fidelity aerodynamic models of the aircraft.

Safety of flight can be enhanced during a flight envelope expansion test program by using system identification techniques to validate the aircraft simulation model for flight regimes already tested. The updated mathematical

model can then be used to make preflight predictions for flight envelope expansion test conditions. In addition, when nonlinear identification models and identification techniques are used, the pilot's task is greatly simplified since he is not required to maintain small perturbation flight about a trimmed operating point.

The need for improved modeling of aircraft aerodynamic characteristic has been, and continues to be apparent in numerous areas of technical and operational importance. Four such areas are: 1) flying quality military specification compliance testing, 2) training simulations, 3) design methods for specification of aircraft characteristics, and 4) the development of mission profiles that make optimum use of the airplane's capabilities. In general, there is a need for an improved understanding of an airplane's aerodynamic characteristics to support design improvements for increased cost effectiveness, expanded mission flexibility and enhanced operational safety.

1.1.2 F-4S System Identification Research Program Overview

NAVAIRTESTCEN initiated its program to develop advanced system identification techniques in 1971 in a joint program with the Office of Naval Research, Naval Air Systems Command (NAVAIRSYSCOM), and Systems Control, Inc. The original purpose of this development effort was not directed towards enhancing simulation fidelity, but rather to improve flight test stability and control analysis techniques. However, system identification was quickly recognized as an ideal analysis tool for improving the accuracy of the aerodynamic data bases used in aircraft simulations. Thus, during the 1970's, NAVAIRTESTCEN applications of system identification were equally divided between stability and control analysis, and enhancing the fidelity of aircraft simulatons. These simulation improvement programs were motivated by either:

(1) the requirement to improve the aerodynamic data bases of Navy fleet aircraft so that accurate simulations were available to study and solve operational problems; or

(2) the requirement to provide an accurate aerodynamic data base so that Navy operational trainer simulated flight characteristics would be representative of actual fleet aircraft.

Development of a nonlinear system identification capability has been pursued through a multiphase research program spanning 1979 through 1982. The NAVAIRTESTCEN F-4S (BUNO 286) has been used throughout the research program. The test aircraft and its instrumentation have remained fairly constant throughout the research program. The F-4S parameter identification program included three separate phases, which are summarized as follows.

Each phase had a separate objective and its own set of flight test data.

Phase I

Flight test data for the Phase I research program were generated during the proof of concept flight test program for the F-4S design. The objective in processing the Phase I data was to assess the general quality of the F-4S flight test data. The purpose of this analysis was to generate a basis for formulating a flight test plan and instrumentation specification for the Phase II program.

Flight data processing from this phase provided valuable insight for subsequent phases. Useful parameter identification results were not obtained from the Phase I flight test program because of the developmental status of the nonlinear system identification technology.

Phase II

The purpose of the Phase II flight test program was to generate a comprehensive flight test data base which could be used to develop and validate nonlinear system identification analysis techniques. The Phase II flight test plan was based on experience gained from the first program phase.

The flight test program was conducted in a clean configuration with the throttles fixed for each maneuver and with flight near and beyond stall. Test conditions were generally initiated from wing-level, constant altitude flight with $\alpha \approx 10^{\circ}$ and $M \approx .6$. For some test conditions, the pilot applied variable aft stick to maneuver the aircraft through the desired angle-of-attack test range. For some of the stall entry conditions lateral stick and/or pedal doublets were combined with the longitudinal stick

command. Other flight conditions included single axis and multi-axis sequented doublet inputs. These inputs were made by the pilot and were not intended to be repeatable nor precise with regard to their spectral characteristics, but were generally effective in creating large-amplitude motions. The overall test goal was to force the aircraft through a broad range of test conditions. The level of excitation of primary test variables achieved during the F-4S flight test program is summarized as follows:

- Angle of attack: $-1^\circ < \alpha < 40^\circ$
- Sideslip: $|\beta| < 18^\circ$
- Mach No: $M < .6$
- Rotational Rates: $|P| < 90^\circ/S$, $|Q| < 20^\circ/S$, $|R| < 25^\circ/S$
- Full amplitude control inputs

The nonlinear system identification data processing techniques were validated through the processing of the Phase II flight test data. Useful aerodynamic data were obtained from the Phase II program. The lateral directional aerodynamic characteristics presented in this report are primarily from this analysis. The low-speed, longitudinal model for the clean configuration was also extracted from the Phase II flight test data set.

Phase III

The objective of the third program phase was to generate an aerodynamic data base for an F-4S simulation at the NAVAIRTESTCEN. This updated simulation model has been used to evaluate aft c.g. flying qualities of the F-4S with a high stability index store configuration. These simulation tests were used to evaluate the consequences associated with moving the aft c.g. limit further aft.

The Phase III F-4S flight test program included three flap configurations (power approach, take-off, and cruise) and two loading configuraitons (clean and a high stability index store configuration). The flaps-up flights were flown for $.7 < M < .9$. All flight conditions were flown at low to moderate

angles of attack ($0^\circ < \alpha < 24^\circ$). Sinusoidal stick and pedal pumping inputs covering a range of frequencies were used to excite the airplane.

A majority of the aerodynamic models presented in this report are from the analysis of the Phase III flight test. An important aspect of the Phase III system identification data processing task was a demonstration of the ability to produce flight-validated aerodynamic models in a reasonable period of time.

1.2 REPORT SUMMARY

Section II provides a technical background for the presentation described by this report. An overview of an integrated system identification procedure is presented. This is followed by a discussion of several algorithms which can be used for system identification. Finally, a methodology for representing nonlinear models is presented.

Section III describes the test aircraft, the flight test instrumentation system, and the test conditions evaluated for the F-4S identification program described by this report. The descriptions presented in Section III are provided as background information for the discussions on model structure determination and parameter identification.

Section IV describes the steps involved in the analysis and preprocessing of flight test data. This is a major element of the integrated system identification procedure. The overall objectives of this task are to evaluate the suitability of the flight test data for identifying aerodynamic characteristics and to develop a complete set of kinematically consistent measurements.

Section V presents the aerodynamic and propulsion model data which were identified from both the Phase II and Phase III flight test programs. This data base, along with the mathematical model presented in Appendix A, comprise a simulation of the F-4S.

Conclusions for this study are presented in Section VI.

II. SYSTEM IDENTIFICATION METHODOLOGY

This section provides a technical background for the presentation described by this report. An overview of an integrated system identification procedure is presented. This is followed by a discussion of several algorithms which can be used for system identification. Finally, a methodology for representing nonlinear models is presented.

2.1 OVERVIEW OF AN INTEGRATED SYSTEM IDENTIFICATION PROCEDURE

The capability of processing large quantities of data from flight tests has led to the parallel development of data processing algorithms, which greatly increase the amount of useful knowledge that can be extracted from the data. These algorithms, based on dynamical and statistical principles, yield very precise information about the characteristics of the data and the system that produced it. This methodology (often called system identification) has been extensively documented in previous technical reports and technical journals [1-7]. Key contributions in this field include:

- The development of an integrated system identification procedure that includes a model structure determination phase.
- The use of system identification for supporting flight test planning: instrumentation selection (type and accuracy), telemetry requirements (sample rate, bandwidth, and digitization) and input design.
- Algorithm improvements for the implementation of maximum likelihood techniques.

The steps in the integrated system identification procedures are illustrated in Figure 2.1 with the salient objectives of each step noted. Five basic steps are shown: Flight Data Processing and Analysis, Model Structure Determination, Parameter Identification, Model and Parameter Validation, and Flight Test Planning. The following discussion reviews the first three steps shown in Figure 2.1. Model and parameter validation techniques are addressed later in this report and examples of the application of system identification to flight test planning are presented in Refs. 2, 4, and 5.

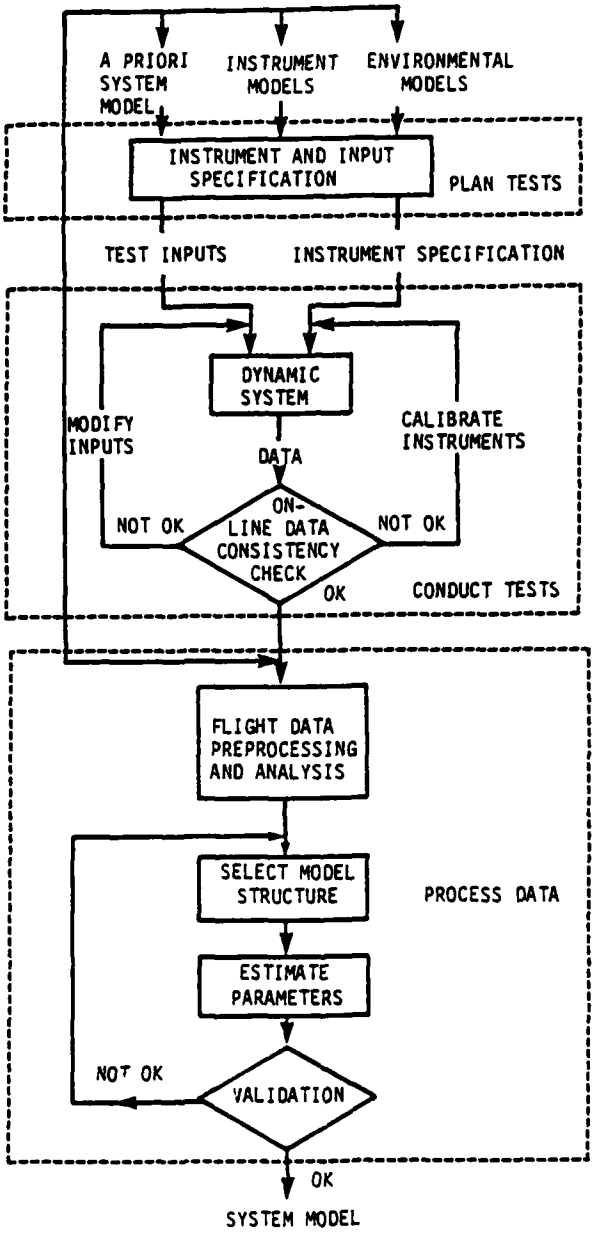

Figure 2.1 Integrated System Identification Procedure

2.1.1 Flight Data Processing and Analysis

The processing and analysis of flight test data is a major element of the integrated system identification procedure. The overall objectives of this task are to review measurement excitation, remove wildpoints, reconstruct unmeasured quantities (i.e., acceleration of the aircraft at the center of gravity), and develop a set of kinematically consistent measurements. Where measurement consistency cannot be established, requirements for instrumentation system error source modeling are defined. Measurement consistency has a significant impact on parameter identification accuracy since unaccounted-for errors will bias parameter estimates.

2.1.2 Model Structure Determination

Model structure determination is the next step of the integrated system identification procedure. The purpose of this step is to identify significant terms of a math model and to generate an initial estimate of the parameters for the parameter identification program. By identifying a significant model structure first, the potential for having a divergent solution with the parameter identification optimization algorithm due to "overparameterization" is reduced. Furthermore, the cost of running the parameter identification program is reduced when good initial parameter estimates are used since fewer program iterations are required for convergence.

2.1.3 Parameter Identification

Parameter identification is the final data processing step in the integrated system identification procedure. For this step, refined parameter estimates are obtained by using a maximum likelihood algorithm with the model structure identified from the previous step. There are several reasons for using a maximum likelihood algorithm to refine the parameter estimates. Equation error techniques, which are used to identify the model structure, are formulated to minimize the squared error difference between reconstructed and estimated equation variables (i.e., C_L and C_m, etc.) along the flight trajectory. If any of the measurements are in error (e.g., bias or scale factor), the resulting parameter values will also be in error. The maximum likelihood program, on the other hand, minimizes the squared error of the

estimated measurements by estimating both aerodynamic and instrumentation error parameters.

2.1.4 Model and Parameter Verification

The validity of the parameter estimates can be established from three different considerations.

(1) Engineering judgement: Are the estimates reasonable from the point of view of general agreement with preflight predictions?

(2) Estimation uncertainty: What is the magnitude of the $\pm 2\sigma$ bands about the estimate?

(3) Prediction accuracy: How well does the identified model predict flight test measurements for many test maneuvers? Does the identified model predict these measurements better than a model based on preflight parameters?

2.2 DATA PROCESSING ALGORITHMS

A large number of methods exist for performing system identification data processing. The best algorithm for any given application depends strongly on the type of model and on the nature of the available data. No one type of processing algorithm can handle all possible applications.

This section outlines three processing methods (Table 2.1) which have been found to be effective in a variety of applications. These methods are:

- equation error minimization methods,
- output error minimization methods, and
- simultaneous state and parameter estimation methods.

2.2.1 Equation Error

The equation error minimization methods estimate unknown parameters by choosing them to minimize a performance index. A continuous dynamic system must be represented as:

$$dx/dt = f(x, u, t, \theta) + w$$

where θ is a set of p unknown parameters and w is a time-varying unobservable disturbance. An analogous formulation exists for a discrete dynamic system. The performance index $\mathscr{L}_e(\theta)$ to be minimized is:

$$\mathscr{L}_e(\theta) = \left\{ \sum_{i=1}^{M} \frac{dx(t_i)}{dt} - f[x(t_i),\, u(t_i), t_i,\, \theta] \right\}^2 \qquad (1)$$

The equation error minimization method is often called the least squares method because of the form of the performance index $\mathscr{L}_e(\theta)$.

The effective use of the equation error minimization requires the a priori determination of system states x, controls u, and state derivatives dx/dt over the time interval of the test. A priori here means that these quantities must be determined before the unknown system parameters are estimated. This determination may be done using direct measurements or using system characteristics which are independent of the parameters. For example, an unmeasured state derivative may be determined by (very carefully) numerically differentiating a measured state time history.

The term w is a stochastic quantity which represents unmeasurable process disturbances in the system. w includes wind gusts and unmodeled, high-order aerodynamic effects.

The special advantage of the equation error minimization method lies in the fact that many nonlinear dynamic system functions $f(x, u, t, \theta)$ are linear in the parameters θ. In other words,

$$f(x, u, t, \theta) = \sum_{j=1}^{P} \theta_j f_j(x, u, t) + f_{p+1}(x, u, t) \qquad (2)$$

The functions f_j, $j=1,2,\ldots p+1$ are independent of the p unknown parameters θ_j. The parameter values which minimize $\mathscr{L}_e(\theta)$ can be found explicitly using linear algebraic operations [14]. The disadvantages of the equation error minimization method arise primarily from the requirement for very accurate measurements of states and controls. States will inevitably be measured with some error. No measurement at all may be available for other states.

Table 2.1

System Identification Data Processing Methods

METHOD	ADVANTAGES	DISADVANTAGES	PERFORMANCE INDEX	MINIMIZATION ALGORITHM TYPICALLY USED	EXAMPLES OF APPLICATIONS
EQUATION ERROR	• EFFECTIVE IN PRESENCE OF PROCESS NOISE • COMPUTATIONAL SIMPLICITY	SENSITIVE TO MEASUREMENT ERRORS	$\Sigma[\frac{dx}{dt} - f(x,u,\theta,t)]^2$	LINEAR LEAST SQUARES [14]	AERONAUTICS [20]
OUTPUT ERROR	• EFFECTIVE IN PRESENCE OF MEASUREMENT ERRORS	SENSITIVE TO PROCESS NOISE	$\Sigma[y - \hat{y}(t,\theta)]^2$	GAUSS-NEWTON [16]	RAIL VEHICLES [21] GAS TURBINES [4]
COMBINED STATE AND PARAMETER ESTIMATION	• EFFECTIVE IN PRESENCE OF BOTH MEASUREMENT AND PROCESS NOISE	COMPUTATIONAL COMPLEXITY	$\Sigma[y - \hat{y}(t,\theta,y)]^2$	GAUSS-NEWTON [16] KALMAN FILTER [17]	AERONAUTICS [22]

2.2.2 Output Error

Output error minimization methods, like equation error minimization methods, estimate unknown parameters by choosing them to minimize a performance index. The dynamic system must be represented as

$$dx/dt = f(x, u, t, \theta), \quad x(t_0) = g(\theta) \tag{3}$$

$$y = h(x, u, t, \theta) + \nu \tag{4}$$

where θ is a set of p unknown parameters and ν is a time-varying, unobservable, additive measurement error. The performance index $\mathscr{L}_0(\theta)$ to be minimized is

$$\mathscr{L}_0(\theta) = \sum_{i=1}^{m} [y_i - \hat{y}(t_i, \theta)]^2 \tag{5}$$

Here y_i is the observed system output at time t_i. $\hat{y}(t_i, \theta)$ is the system output y predicted for time t_i by solving the system state equations and measurement equations using the measured system inputs $u(t_i)$ and the a priori parameter values θ.

The effective use of the output error minimization requires the very accurate measurement of system inputs u and the measurement of system outputs y. The method will tolerate errors in the measurement of y.

The term ν is a stochastic quantity which represents instrument measurement errors, e.g., analog-to-digital quantization noise.

The special advantage of the output error minimization method, with respect to the equation error method, is that the measurement requirements are greatly relaxed. The method does not require the accurate measurement of all state and state derivatives. Rather, it is effective using noisy measurements of the limited number of outputs that are available.

The actual determination of the parameter values θ which minimize the performance index $\mathscr{L}_0(\theta)$ is computationally more complex than the minimization $\mathscr{L}_e(\theta)$. This is because $\mathscr{L}_0(\theta)$ is a nonlinear function of the parameter set θ. Finding the minimizing parameter set requires an iterative numerical scheme [15, 16]. The application of such numerical methods is often not straightforward.

The principal disadvantage of the output error minimization scheme is that it does not explicitly allow for the presence of unmodeled disturbances in the state dynamics. Such disturbances are represented in the equation error method by the term w. "Process noise" is the term often used to describe these unmodeled effects.

It should be noted that the output error method can account for system dynamics disturbances of unknown magnitude if the form of these disturbances is accurately represented. The disturbance w must be explicitly represented as

$$w = w(t, \theta) \tag{6}$$

The unknown elements of the disturbance are represented using part of the unknown parameter vector θ. One might estimate the horizontal plane components of a steady wind present during a flight test, for example.

2.2.3 Combined State and Parameter Estimation

Methods which combine state and parameter estimation are required if significant levels of both unknown, unmodeled disturbances and measurement errors are present in the system under study. The performance index used here is very similar to the output error index $\mathscr{L}_0(\theta)$. However, the estimated outputs y are now direct functions of the observed outputs y. The performance index is

$$\mathscr{L}_s(\theta) = \sum_{i=1}^{M} [y_i - \hat{y}(t_i, \theta, y)]^2 \tag{7}$$

The estimated outputs are determined using both the system dynamic equations and the observed values of the outputs themselves.

Methods for the determination of $\hat{y}$ given measurements y and an assumed form of the system dynamics have been widely studied under the topics of state estimation [17] and linear system observation [18]. The use of the

Kalman filter to estimate y in the modified output error performance index $\mathscr{L}_s$ leads to "maximum likelihood" parameter estimates [19]. The procedure requires that $\mathscr{L}_s$ be evaluated as a function of θ using the Kalman filter to estimate y. The parameter values are estimated by choosing them to minimize $\mathscr{L}_s(\theta)$ using a Gauss-Newton method [20]. The use of this maximum likelihood estimation procedure often allows the estimation of system noise levels as well as of parameters describing the physical plant.

2.3 SOME PRACTICAL CONSIDERATIONS

This section briefly discusses a number of practical considerations which should be taken into account in an effective system identification data processing scheme.

2.3.1 Assumptions Regarding Measurement Noise Statistics

A common problem is to assume that the measurement error should be modeled as a Gaussian white process when in fact systematic errors such as bias and scale factor exist. Systematic measurement errors will usually cause larger parameter estimation errors than random noise errors of the same root-mean-square level. A very common scale factor found when dealing with any instrument using electronic pickoffs is -1.0. This is due to simple polarity errors made when installing the instrument. Reference 11 covers methods of assessing the relative significance of systematic measurement errors and random measurement errors.

2.3.2 Number of Independent Parameters In The Model

Problems can arise from an attempt to fit too complex a model to the available data. The chief symptom of this is that a large scatter of estimated parameter values will be seen if several data sets are used independently to estimate values for the same parameter set.

2.3.3 Extrapolation of Results

An identified model should not be used to predict system behavior for operating regimes far beyond those encountered during data collection. Operating regime predictions should be limited in both input bandwidth and amplitude to those tested.

2.3.4 Excitation of All System Modes

This problem can be avoided by careful choice of inputs during the test planning stage. A second solution is to process multiple maneuvers simultaneously which contain different control inputs. By doing this, the required modal information is extracted from a set of simpler maneuvers, rather than one complicated maneuver.

2.3.5 Effective Use of Sequential Data Processing Schemes

System identification data processing requires the computational steps of model structure determination, parameter estimation, and model validation. An additional preliminary step of prefiltering measurements may also be required for effective use of an equation error parameter estimation method. An effective overall computational scheme may require that the operations of prefiltering, model structure determination, and parameter estimation be carried out in a sequential rather than in a more nearly simultaneous manner. Care must be taken to ensure that the algorithms employed at any given stage do not remove critical information from the data. As a simple example, the bandpass of a noise prefilter should be higher than that of the modes of the system to be identified.

2.3.6 Process Noise

The term "process noise" refers to unmodeled factors in the state dynamics of the system being identified. Sources of process noise include:

Any other linear, unbiased estimator has a covariance matrix which exceeds

(1) unmeasured environmental disturbances - wind gusts acting on an aircraft, for example,

(2) unmodeled nonlinearities or degrees of freedom in the state dynamics, and

(3) errors in measuring input signals.

The effect of process noise is usually, but not always, to degrade estimation accuracies. If measurements of system states are highly accurate, then the process noise becomes the major source of estimation error. Under some circumstances, process noise in the form of unmeasured environmental disturbances can improve estimation accuracy. The environmental disturbances might excite modes of the system which are not excited by the known input test signal.

The relative significance of process noise in an identification effort depends roughly upon the ratio

$$r = \text{RMS(process noise)}/\text{RMS(known inputs)} \tag{8}$$

where RMS( ) refers to the root-mean-square state excursion due to the indicated source of excitation. If r is large, then the process noise is significant. If r is small, then the process noise is not significant. It is difficult, however, to specify a value of r indicating the boundary between significant or insignificant process noise levels which will be valid for all systems.

Effective system identification methods exist for use when available data contain process noise. The equation error formulation is preferred if all system states can be measured or estimated accurately, otherwise the formulation combining state and parameter estimation will be required.

2.3.7 Initialization

Many parameter estimation formulations require the iterative, numerical solution of nonlinear equations. The output error and the combined state and parameter estimation formulations fall into this category. Iterative numerical algorithms require initial estimates of parameter values in order to

begin execution of the first iteration. Inaccurate initial estimates may cause:

(1) convergence of the estimation method (which usually employs some form of performance criterion minimization algorithm) to a local minimum, or

(2) divergence of the estimated parameter values as iterations proceed. Divergence may occur, for example, if the values of the initial parameter estimates cause an instability in the dynamic system model.

An effective way to obtain initial parameter estimates for starting iterative algorithms is often to employ the equation error estimation formulation. As noted in Section 2.3.1, the equation error formulation usually requires only the solution of a linear set of algebraic equations in order to obtain parameter estimates. Such equations may be solved without a priori parameter estimates. An effective two-step parameter estimation procedure is:

(1) estimate initial parameter values using the equation error formulation, then

(2) refine these estimates using either the output error or the combined state and parameter estimation formulations.

The values of parameters estimated using the equation error formulation are sensitive to errors in measuring states (measurement noise). However, the parameter estimates calculated using an equation error criterion even with data corrupted by measurement noise are often sufficiently accurate for use as start-up values for iterative algorithms.

2.3.8 Numerical Methods

System identification algorithms engender a variety of numerical mathematical requirements. Table 2.2 lists four of these:

- solution of differential equations,
- solution of linear algebraic systems of equations,
- solution of least squares problems, and
- minimization of general nonlinear multivariable functions.

Table 2.2

Numerical Methods Used in System Identification

NUMERICAL MATHEMATICAL REQUIREMENT		EFFECTIVE METHOD OF APPROACH
SOLUTION OF DIFFERENTIAL EQUATIONS	LINEAR	TRANSITION MATRIX [23]
	NONLINEAR	MULTISTEP METHODS (ADAMS-BASHFORTH) [24]
SOLUTION OF LINEAR ALGEGRAIC SYSTEMS OF EQUATIONS	POSITIVE DEFINITE, SYMMETRIC	CHOLESKY [25]
	GENERAL	GAUSSIAN ELIMINATION [25]
SOLUTION OF LEAST SQUARES PROBLEMS	LINEAR	FACTORIZATION OR SQUARE ROOT METHODS [26]
	NONLINEAR	GAUSS-NEWTON [27]
MINIMIZATION OF GENERAL NONLINEAR MULTIVARIABLE FUNCTIONS		QUASI-NEWTON [28]

Effective methods to handle these problems range from the classical systematic elimination method of Gauss [25] for the solution of systems of linear algebraic equations to more recent developments in the solution of linear least squares problems [26].

An important consideration in using any of the methods of Table 2 is that of numerical conditioning. Numerical conditioning refers to the sensitivity of the output of a numerical algorithm to small changes in the input to the algorithm. For example, assume that in solving a system of n linear equations

$$Ax = b,$$

the matrix A is known exactly, but the vector b is subject to uncertainty δb. The norm of the resulting uncertainty in x, δx, is bounded by [25]

$$\frac{\|\delta x\|}{\|x\|} \leq \frac{\sqrt{\mu_1}}{\sqrt{\mu_n}} \quad \frac{\|\delta b\|}{\|b\|} \tag{9}$$

where μ_1 is the largest eigenvalue of AA^T and μ_n is the smallest eigenvalue of AA^T. The quantity

$$\text{cond}(A) = \sqrt{\mu_1/\mu_n} \tag{10}$$

is called the condition number of A and is always greater than 1.0. Similar bounds for solution sensitivities exist for least squares parameter estimation problems [26].

The condition number of a numerical problem can give insight into the precision required to obtain acceptable accuracy of solution. The uncertainty δb, for example, might be due to rounding due to finite precision in computer word length. If the condition number of a problem is 10^6, then eight significant figures of accuracy would be required to maintain 1 percent accuracy in the solution.

2.4 CONSIDERATIONS FOR NONLINEAR PARAMETER IDENTIFICATION

Methods for the maximum likelihood identification of linear state dynamic models are well established [29]. Such methods have been applied to problems of linear modeling of aircraft aerodynamics using flight test [22] data. These methods are sometimes applied in a piecewise manner to fundamentally nonlinear systems.

The intrinsic nonlinear nature of aircraft aerodynamic models may inhibit the effective use of linear identification methods. For example, if a limited amount of data is available, it may not be possible to identify many linear perturbation models. A single nonlinear model may have fewer total free parameters. Also, excursions through the nonlinear portion of the model's dynamic range may be so rapid that no single linearized model can represent a significant portion of the trajectory.

The use of a nonlinear model may be required if the goal of the analysis is to determine which one of several competitive phenomenological mathematical models best fits available data. A "phenomenological" model is one that is constructed from fundamental physical principles. Such a model may have a very complex form mathematically but may have a minimum number of unknown coefficients.

There are certain computational difficulties associated with the use of a nonlinear dynamic model in a maximum likelihood parameter estimation algorithm.

Calculation of Sensitivities

The estimation of parameters through the use of the maximum likelihood criterion requires the maximization of the likelihood of the data with respect to the unknown parameters. The determination of the maximizing parameter values requires numerical optimization techniques. The most efficient of these [27] are descendents of the Levenberg-Marquardt nonlinear least squares method [16,30]. These algorithms require the evaluation of the partial derivative of modeling residuals with respect to parameter values. This partial derivative is often called a "sensitivity". The calculation of these sensitivities is not difficult in principle. They satisfy differential equations which are closely related to the system dynamic equations, but which

contain terms based on the algebraic partial derivatives of the dynamic equations (see Section 3.1). The difficulty is one of practice. Any time that the structure of the nonlinear model is changed, then the sensitivity differential equations must be changed also. This requires tedious algebraic differentiation of the modified dynamic equations.

Evaluation of Covariance of Parameter Estimates

A parameter covariance matrix can be estimated using the Cramer-Rao bound [31]. The most common use of this bound assumes that the errors in predicting the response of the system are due to an additive, white (negligible autocorrelation) random process. If the analyst also desires confidence intervals for parameter estimates, then the additional assumption that the errors have a normal distribution must also be made. These assumptions are commonly violated when a nonlinear system is modeled. In particular, the whiteness assumption is typically violated.

Generic Model Structure

There is a need to represent nonlinear functions of several variables in the model used in the identification algorithm. Ideally, a single generic form should represent multidimensional surfaces of arbitrary shape. These functions represent total aerodynamic force or moment coefficients as functions of angle of attack, angle of sideslip, and angular rates.

2.4.1 Problem Definition

The dynamic system is modeled as nx first order nonlinear differential equations.

$$\dot{\underline{x}} = \underline{f}(\underline{x}, \underline{u}, \underline{w}, t, \underline{\theta}) \tag{11}$$

having an output measured at discrete times t_k

$$y(t_k) = h\,(\underline{x}, \underline{u}, t_k, \underline{\theta}) + v\,(t_k) \tag{12}$$

Here

$\underline{x}$ = nx component state

$\underline{u}$ = nu component inputs measured without error

$\underline{\theta}$ = nth component unknown parameter vector

$\underline{w}$ is a nw component random input (process noise source) having statistics

$$E(\underline{w}) = \underline{0} \tag{13}$$

$$E[\underline{w}(t_i)\,\underline{w}^T(t_j)] = Q(t_i)\,\delta_{ij} \tag{14}$$

The scalar $v(t_k) = v_k$ is a random measurement error having the statistics

$$E(v_k) = 0 \tag{15}$$

$$E(v_k^2) = r \tag{16}$$

Note that the assumption of scalar measurements does not cause a great loss of generality. This formulation can accomodate multiple sensors simply by assuming that the interval between measurements is sometimes very small. The only loss of generality regards the representation of correlation of measurement error between sensors.

If we assume that the stochastic quantities have normal distributions then the joint density or likelihood function of a sample of nt measurements $y(t_k) = y_k$ is

$$\mathscr{L}(y_1, y_2, \ldots, y_{nt}\,;\,\underline{\theta})$$

$$\mathscr{L} = \left\{ \prod_{k=1}^{nt} \frac{\exp\left[-\frac{1}{2}\,(y_k - y_k(\underline{\theta}))^2/\sigma_k{}^2(\underline{\theta})\right]}{(2\pi)^{1/2}\,\sigma_k(\underline{\theta})} \right\} \tag{17}$$

An extended Kalman filter [17] can generate both the measurement estimates y_K and the measurement uncertainties σ_K. The estimate of θ having the

smallest variance is the one which maximizes $\mathscr{L}(\underline{y} ; \underline{\theta})$ with respect to θ. The maximization of $\mathscr{L}$ is equivalent to the minimization of the negative log likelihood function given by

$$-\log \mathscr{L}(\underline{y} ; \underline{\theta}) = \tag{18}$$

$$\frac{1}{2} \sum_{K=1}^{nt} \left\{ [y_k - y(\underline{\theta})]^2 / \sigma_k^2(\underline{\theta}) + 2 \log \sigma_k(\underline{\theta}) \right\}$$

Note that if the σ_k are known, then the minimization of $-\log \mathscr{L}$ can be treated as a nonlinear least square problem.

Aspects of this problem addressed here are the following.

(1) The minimization of Eq. (18) with respect to $\underline{\theta}$ requires the use of an iterative numerical procedure similar to a Newton or quasi-Newton method. If the σ_k are known, then the most effective procedure is that of Levenberg and Marquardt [16,30]. A drawback to the Levenberg-Marquardt method is the requirement for the evaluation of $\partial y/\partial \underline{\theta}$. Direct analog finite difference methods [32] avoid this problen by approximating the partial derivative by a finite difference. Section 2.4.2 extends the finite difference analog of the Levenberg-Marquardt procedure to the more general form of Eq. (18).

(2) Validation of an identified model should include the determination of confidence intervals or variances for estimated parameters. These may be estimated using the Cramer-Rao bound, which states that

$$E[(\hat{\theta} - \underline{\theta}^*)(\hat{\theta} - \underline{\theta}^*)^T] \geq M^{-1} \tag{19}$$

where M is the information matrix, given by

$$[M]_{ij} = -[\partial^2(\log \mathscr{L}(\underline{y} ; \underline{\theta})/\partial\theta_i \, \partial\theta_i] \tag{20}$$

and $\underline{\theta}^*$ is the true parameter value.

Experienced analysts in the system identification field are aware that the Cramer-Rao bound is usually optimistic [33]. That is, it tends to predict parameter variances which are very small in comparison to variances observed among estimates derived from multiple data sets. The most easily implemented expressions for the information matrix assume that the measurement errors are not autocorrelated. If autocorrelation is accounted for, then the Cramer-Rao bound more realistically approximates the true parameter variance. Section 2.4.3 outlines methods based on principles of generalized least squares which automatically account for first order autocorrelation of measurements. This method produces parameter estimates which have a lower variance than those which do not account for autocorrelation.

(3) Modeling nonlinear aerodynamics requires the representation of nonlinear functions of several variables. For example, pitch moment of an aircraft is a nonlinear function of angle of attack α, angle of sideslip β, pitch rate Q, and elevator angle δ_e.

$$C_m = C_m(\alpha, \beta, Q, \delta_e) \tag{21}$$

Much work in the identification of these functions has been based on their representation as multidimensional polynomials [34]. This approach is effective for local models. A local model is one that is valid over a restricted region of the flight envelope, say for an α interval of 10°. Such models often use expansions for functions like C_m in the states of degree no higher than two. The representation of a global model using polynomial expansions may require very high order polynomials. The representation of a pitch moment curve for one particular aircraft through a 40° angle of attack region requires a ninth degree polynomial [35]. Section 2.4.4 indicates how the use of local, low degree polynomial models leads very naturally to a spline formulation for a global model.

2.4.2 Derivative-Free Minimization of the Negative Log Likelihood Function

Finding the parameter values $\hat{\underline{\theta}}$ which minimize Eq. (18) requires the use of a numerical optimization scheme. Typically, each iteration of the algorithm updates $\underline{\theta}$ as

$$\underline{\theta}_{n+1} = \underline{\theta}_n + \Delta\underline{\theta} \tag{22}$$

where $\Delta\underline{\theta}$ satisfies

$$M\Delta\underline{\theta} = -\underline{g} \tag{23}$$

$$g_i = \partial \log \mathscr{L}(\underline{y}, \underline{\theta})/\partial\theta_i \tag{24}$$

and M is defined in Eq. (20).

Differentiating Eq. (18) gives [35]

$$g_i = -\sum_{k=1}^{nt} \Big\{ [\nu_k(\partial\nu_k/\partial\theta_i) - \tfrac{1}{2}\ \nu_k^2(\partial\sigma_k^2/\partial\theta_i)/\sigma_k^2 + \tfrac{1}{2}\ \sigma_k^2/\partial\theta_i]/\sigma_k^2 \Big\} \tag{25}$$

$$\begin{aligned} M_{ij} = -\sum_{k=1}^{nt} \Big\{ & (\partial\nu_k/\partial\theta_i)(\partial\nu_k/\partial\theta_j)/\sigma_k^2 + [-(\partial\nu_k/\partial\theta_i)(\partial\sigma_k^2/\partial\theta_j) \\ & -(\partial\nu_k/\partial\theta_j)(\partial\sigma_k^2/\partial\theta_i) + \nu_k(\partial\theta_k^2/\partial\theta_i)(\partial\theta_k^2/\partial\theta_j) \\ & + \sigma_k(\partial^2\nu_k/\partial\theta_i\partial\theta_j) - \nu_k(\partial^2\sigma_k/\partial\theta_i\partial\theta_j)]\ \nu_k/\sigma_k^4 \\ & - \tfrac{1}{2}(\partial\sigma_k^2/\partial\theta_i)(\partial\sigma_k^2/\partial\theta_j)/\sigma_k^4 + \tfrac{1}{2}(\partial^2\sigma_k^2/\partial\theta_i\ \partial\theta_j)/\sigma_k^2 \Big\} \end{aligned} \tag{26}$$

where

$$\nu_k = y_k - \hat{y}_k\ (\underline{\theta}). \tag{27}$$

Following the spirit of the Levenberg-Marquardt method, we simplify the expression for the Hessian by dropping the terms proportional to ν_k. If the model fits the data well, ν_k should approach zero near convergence. With the exception of the last term of Eq. (26), it is now possible to evaluate both gradient and Hessian if only the first-order sensitivities ν_k and σ_k^2 to changes in θ are known.

It is possible to derive analytically ordinary differential equations for $\partial\nu_k/\partial\theta_i$ and $\partial\sigma_k^2/\partial\theta_i$. When the plant dynamic equations are linear, these differential sensitivity equations (also called "sensitivity equations") have a particularly simple form [36]. When the plant dynamics are nonlinear, however, a much more practical method is to approximate the partial derivatives with finite differences.

$$\partial\nu_k/\partial\theta_i \tilde{=} [\nu_k(\underline{\theta} + \underline{\varepsilon}_i) - \nu_k(\underline{\theta})]/|\underline{\varepsilon}_i| \tag{28}$$

or

$$\partial\nu_k/\partial\theta_i \tilde{=} [\nu_k(\underline{\theta} + \underline{\varepsilon}_i) - \nu_k(\theta - \varepsilon_i)]/2|\underline{\varepsilon}_i| \tag{29}$$

where $(\underline{\varepsilon}_i)_j = \varepsilon\delta_{ij}$.

Partial derivatives of $\sigma^2(\theta)$ are approximated similarly.

The "direct analog" [32] type of optimization algorithms use the finite difference approximations to the partial derivatives as direct substitutes for the partial derivatives. These algorithms have been studied carefully for the solution of the nonlinear least square problem and have been found to have convergence properties nearly identical to algorithms which use analytic expressions for the sensitivities.

Alternate methods for minimization of the negative log likelihood function without evaluating derivatives use algorithms which are not direct analogs of derivative methods. We have tested one of these methods [37] in a nonlinear system identification algorithm and found it to be not as effective as the direct analog method.

In partial implementations of the finite difference method for the solution of system identification problems, we typically simultaneously solve a set of nx nominal state equations together with nth sets of nx perturbed parameter state equations. This is required in order to implement the one-sided approximation to the sensitivity given in Eq. (28).

The last term of Eq. (26) cannot be eliminated by assuming that ν_k is small near the minimum. The term cannot be constructed from first order partial derivatives of ν and σ^2. It can be estimated, however, using methods similar to those employed in solving large residual nonlinear least square problems [38]. This topic will not be treated in further detail here.

2.4.3 Autocorrelated Measurement Errors

It is desireable to determine the expected accuracy of the parameters estimated from flight data. The usual method for doing this is to compute a parameter covariance matrix as the inverse of the Fisher information matrix M.

Methods of generalized least squares [39] indicate expressions for parameter estimation covariance using the assumption that measurement errors are autocorrelated. This autocorrelated process is the output of a first order difference equation driven by white noise. Not only parameter covariances but also parameter estimates themselves are altered by the autocorrelation assumption. An estimation algorithm which does not explicitly account for the measurement error autocorrelation will still produce unbiased parameter estimates. However the actual variance of such estimates, as opposed to the Cramer-Rao predicted variance, will be higher than those produced by an algorithm which does explicitly account for autocorrelation.

We consider here only the output error case (no process noise) of the maximum likelihood estimator for dynamic systems. The estimated measurements $\hat{y}$ are functions of the unknown parameter set $\underline{\theta}$. The information matrix M is given by

$$M \tilde{=} \frac{1}{\sigma^2} J^T J \tag{30}$$

where J is the matrix of sensitivities

$$[J]_{k\ell} = - \partial \hat{y}(\underline{\theta}, t_k) / \partial \theta_\ell \tag{31}$$

for the case of white measurement noise. Iterations of the identification algorithm solve

$$M \Delta \underline{\theta} = -\underline{g} \tag{32}$$

where

$$\underline{g} = \frac{1}{\sigma^2} J^T \underline{\nu} \tag{33}$$

$$_k = y(t_k) - \hat{y}(t_k)$$

The covariance of the measurement error is a diagonal matrix

$$E(\underline{\nu}\ \underline{\nu}^T) = \sigma^2 I \tag{34}$$

where $\nu_k = \nu(t_k)$, the measurement error at t_k. (35)

Now suppose that the measurement errors have a nondiagonal covariance matrix of

$$E[\underline{\nu}\ \underline{\nu}^T] = \sigma^2 V \tag{36}$$

For a purely linear estimation problem, (i.e. $y = J\underline{\theta} + \underline{\theta}$), the "generalized least squares" estimate of $\underline{\theta}$ satisfies [39]

$$[J^T V^{-1} J]\underline{\theta} = J^T V^{-1} \underline{y} \tag{37}$$

The covariance of the parameter estimates is

$$E[(\hat{\underline{\theta}} - \underline{\theta}^*)(\hat{\underline{\theta}} - \underline{\theta}^*)^T] = \sigma^2 (J^T V^{-1} J)^{-1} = \mathrm{Var}(\hat{\theta}) \tag{38}$$

Any other linear, unbiased estimator has a covariance matrix which exceeds that given in Eq. (38).

If the noise vector $\underline{v}$ is generated by a first order autoregressive process

$$v(t_k) = \rho v(t_{k-1}) + \epsilon_k \tag{39}$$

where ϵ_k is a zero mean, constant variance process, then V has the form

$$V = \begin{bmatrix} 1 & \rho & \rho^2 & \cdots & \rho^{n-1} \\ \rho & 1 & \rho & & \rho^{n-2} \\ \rho^2 & \rho & 1 & & \rho^{n-3} \\ \vdots & & & & \vdots \\ \rho^{n-1} & \rho^{n-2} & \rho^{n-3} & \cdots & 1 \end{bmatrix} \tag{40}$$

The inverse of V is $V^{-1} = P^T P$ where

$$P = \begin{bmatrix} \sqrt{1-\rho^2} & 0 & \cdots & 0 \\ -\rho & 1 & & 0 \\ 0 & -\rho & & 0 \\ \cdot & & 1 & 0 \\ \cdot & & & \\ \cdot & & & \\ 0 & \cdots & -\rho & 1 \end{bmatrix} \frac{1}{\sqrt{1-\rho^2}}$$

The generalized least square estimator for $\underline{\theta}$ can be easily implemented by writing Eq. (37) as

$$[(P\ J)^T(P\ J)]^{-1}\ \hat{\underline{\theta}} = (P\ J)^T\ P\ \underline{y} \tag{42}$$

The multiplications $P\ J$ and $P\ \underline{y}$ are simple because $\underline{P}$ is sparce.

For application to the output error system identification problem, a nonlinear least square problem, Eq. (42) is applied to parameter variations $\Delta\underline{\theta}$ on each iteration of a successive approximation algorithm.

$$(P\ J)^T(P\ J)\Delta\underline{\theta} = (P\ J)^T\ P\ [\underline{y} - \hat{\underline{y}}\ (\theta)] \tag{43}$$

If ρ is unknown, then it can be estimated using

$$\hat{\rho} \simeq \frac{\sum_{k=1}^{nt-1} (t_k)\ (t_{k+1})}{\sum_{k=1}^{nt} \nu^2(t_k)} \cdot \frac{nt - 1}{nt - nth} \tag{44}$$

Each iteration calculates a $\Delta\underline{\theta}$ value using $\underline{P}$ evaluated by Eq. (44), with $\nu(t_k)$ calculated from $\underline{\theta}$ at the end of the previous iteration.

If the measurement noise, σ^2, is unknown, it can be estimated using

$$\hat{\sigma}^2 = \frac{1}{nt - nth}(P\nu)^T(P\nu)\ . \tag{45}$$

The covariance of the parameter estimates is

$$Var(\hat{\theta}) = \frac{1}{nt - nth}\ (\overline{P}\nu)^T(\overline{P}\nu)[(PJ)^T(\overline{P}J)]^{-1} \tag{46}$$

where

$$\overline{P} = P\sqrt{1 - \rho^2}\ . \tag{47}$$

2.4.4 Spline Model Structure

The determination of a nonlinear, quasi-static aerodynamic (or hydrodynamic) model requires definition of a coefficient function having a general form

$$C = C(\alpha, \beta, \underline{\omega}', \underline{\delta}, R_e, F_r, M) \tag{48}$$

where α and β are relative flow angles, $\underline{\omega}'$ is a dimensionless angular rate vector, $\underline{\delta}$ is a control vector, and R_e, F_r, and M are the dimensionless numbers of Reynolds, Froude, and Mach. The model structure determination problem for identification of aerodynamic models usually refers to the problem of determining a mathematical form for this multivariable function.

Spline functions are effective ways to represent these coefficient functions. A one dimensional spline function is a piecewise polynomial function having certain continuity conditions between pieces. Figure 2.2 illustrates a one dimensional cubic spline. $C(\alpha)$ might represent pitch moment as a function of angle of attack. $C(\alpha)$ here is a cubic polynomial on each of the three regions indicated. The function is everywhere continuous and has continuous first and second derivatives. The points α_1, α_2, α_3, α_4 are called the knots of the spline.

The spline function has several properties which make it an effective interpolating function [40].

(1) The spline in Figure 2.2, for example, is uniquely determined once the values of the function at the four knots are known and certain end conditions are specified.

(2) The shape of the interpolating function is not overly sensitive to the function values at the knots. Small changes in these values do not cause overly large changes in interpolated function values between knots.

(3) The interpolating function $C(\alpha)$ has an optimal smoothness property. It is the unique function which interpolates the specific values at the knots, has the continuity conditions listed above, and has the minimum mean square curvature.

Spline function representation of nonlinear aerodynamic or hydrodynamic coefficient functions may be readily identified using either maximum likelihood, equation error or output error techniques. The analyst must specify the number of knots and their locations. The parameters to be identified are then the function values at the knots. The identification of the $C(\alpha)$ curve in Figure 2.2 would require the estimation of four parameters.

In Figure 2.2, the coefficients $C_1 - C_4$ are the function values at the knot locations $\alpha_1 - \alpha_4$. These coefficients are the parameters which will be estimated by the identification algorithm. The piecewise cubic polynomials $K_{A1} - K_{A4}$ provide cubic interpolation of $C_1 - C_4$ for α in the range $[\alpha_1, \alpha_4]$ and linear extrapolation for α outside this range.

Each of the piecewise cubic polynomials is defined over the entire range of $[-\infty < \alpha < +\infty]$. The function $C(\alpha)$ is a linear combination of the K_{Ai} basis functions. The definitions of K_{Ai} are such that

$$K_{Ai}(\alpha_j) = \begin{cases} 1 & i=j \\ 0 & i \neq j \end{cases}$$

This makes the coefficients in the linear combination equal to the C_i values. The array in Figure 2.2 defines the K_{Ai} functions over the five α regions.

The identification of spline functions is most effective when used with derivative free methods to minimize the negative log likelihood function. Such methods do not require the explicit calculation of the sensitivity of the spline function to changes in the parameters which define the spline. The only requirement is for the evaluation of the spline coefficients given function values at the knots, and for the evaluation of the function at intermediate points given the spline coefficients. Each iteration of the "direct analog" method requires the evaluation of the innovations (t_k) for nominal and for perturbed parameter values.

Methods exist for the use of multidimensional spline functions to represent smooth surfaces [41]. Intermediate methods are also useful. An intermediate method represents variation of a function in one dimension with a spline function and representation in other dimensions with other types of functions, such as low order polynomials.

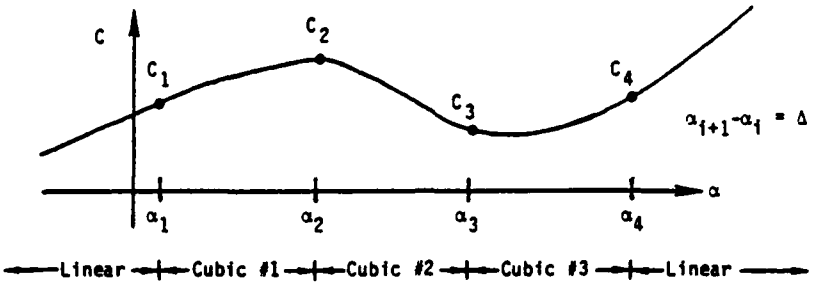

$$C = \sum_{i=1}^{4} C_i * K_{Ai}(\alpha_1,\alpha_2,\alpha_3,\alpha_4,\alpha)$$

C_i are coefficients to be identified.

	$\alpha \le \alpha_1$	$\alpha_1 \le \alpha \le \alpha_2$	$\alpha_2 \le \alpha \le \alpha_3$	$\alpha_3 \le \alpha \le \alpha_4$	$\alpha_4 \le \alpha$
K_{A1}	$1 - \frac{19}{15}\frac{(\alpha-\alpha_1)}{\Delta}$	$\frac{\alpha_2-\alpha}{\Delta} + \frac{4}{15}a$	$\frac{4}{15}b - \frac{1}{15}c$	$\frac{1}{15}d$	$-\frac{1}{15}\frac{(\alpha-\alpha_4)}{\Delta}$
K_{A2}	$\frac{8}{5}\frac{(\alpha-\alpha_1)}{\Delta}$	$\frac{\alpha-\alpha_1}{\Delta} - \frac{3}{5}a$	$\frac{\alpha_3-\alpha}{\Delta} - \frac{3}{5}b + \frac{2}{5}c$	$\frac{2}{5}d$	$\frac{2}{5}\frac{(\alpha-\alpha_4)}{\Delta}$
K_{A3}	$-\frac{2}{5}\frac{(\alpha-\alpha_1)}{\Delta}$	$\frac{2}{5}a$	$\frac{\alpha-\alpha_2}{\Delta} + \frac{2}{5}b - \frac{3}{5}c$	$\frac{\alpha_4-\alpha}{\Delta} - \frac{3}{5}d$	$-\frac{8}{5}\frac{(\alpha-\alpha_4)}{\Delta}$
K_{A4}	$\frac{1}{15}\frac{(\alpha-\alpha_1)}{\Delta}$	$-\frac{1}{15}a$	$-\frac{1}{15}b + \frac{4}{15}c$	$\frac{\alpha-\alpha_3}{\Delta} + \frac{4}{15}d$	$1 + \frac{19}{15}\frac{(\alpha-\alpha_4)}{\Delta}$

$$a = \frac{1}{\Delta^2}\left[\frac{(\alpha-\alpha_1)^3}{\Delta} - \Delta\,(\alpha-\alpha_1)\right] \qquad c = \frac{1}{\Delta^2}\left[\frac{(\alpha-\alpha_2)^3}{\Delta} - \Delta\,(\alpha-\alpha_2)\right]$$

$$b = \frac{1}{\Delta^2}\left[\frac{(\alpha_3-\alpha)^3}{\Delta} - \Delta\,(\alpha_3-\alpha)\right] \qquad d = \frac{1}{\Delta^2}\left[\frac{(\alpha_4-\alpha)^3}{\Delta} - \Delta\,(\alpha_4-\alpha)\right]$$

$$\Delta = \alpha_{i+1} - \alpha_i$$

Figure 2.2 Cubic Interpolating Polynomials

2.5 MODELING APPROACH

The approach selected for modeling nonlinear aerodynamic characteristics produces system identification results that can be used to validate preflight estimated aerodynamic models. The models are used for flight simulators and for making predictions of aircraft performance, stability and control characteristics. These aerodynamic models must account for the effect of a number of flight condition and aircraft configuration variables. The "art" in formulating the models is to represent the total aerodynamic coefficient by an incremental buildup, with each increment described by one or two independent variables. This process is illustrated by the following example for the rolling moment coefficient equation.

(1) Select the independent variables:

$$C_\ell = f(\alpha, \beta, P, R, \delta_R, \delta_A)$$

i.e., rolling moment coefficient is a function of angle of attack, sideslip, roll and yaw rate, rudder and aileron position.

(2) Partition independent variables into reasonable groups:

$$C_\ell = \Delta C_{\ell_{SIDESLIP}} + \Delta C_{\ell_{DYNAMIC}} + \Delta C_{\ell_{RUDDER}} + \Delta C_{\ell_{AILERON}}$$

(3) Select functional relationships for each group:

$$\Delta C_{\ell_{SIDESLIP}} = f(\alpha, \beta)$$

$$= C_{\ell_\beta}(\alpha) \cdot \beta$$

$$\Delta C_{\ell_{DYNAMIC}} = f(\alpha, P) + f(\alpha, R)$$

$$= C_{\ell_P}(\alpha)(Pb_w/2V_T) + C_{\ell_R}(\alpha)(Rb_w/2V_T)$$

$$\Delta C_{\ell}{}_{RUDDER} = f(\alpha, \delta_R)$$

$$= C_{\ell}{}_{\delta_R}(\alpha) \cdot \delta_R$$

$$\Delta C_{\ell}{}_{AILERON} = f(\alpha, \delta_A)$$

$$= C_{\ell}{}_{\delta_A}(\alpha) \cdot \delta_A$$

For this model formulation, each of the stability derivatives, (i.e., C_{ℓ_β}) is modeled as a nonlinear function of angle of attack. By using a cubic interpolation spline, as described in Section 2.4.4, the parameter identification algorithm solves for C_{ℓ_β} at specific values of angle of attack (i.e., the knots of the spline). This procedure is illustrated in Figure 2.3 which shows the identified variation of C with angle of attack. For the F-4S parameter identification study, C_{ℓ_β} was identified for α = 5°, 15°, 25°, and 35°. The lower four parts of Figure 2.3 illustrate the variation of the interpolation splines with angle of attack.

Because these interpolation splines are scaled by the appropriate value of C_{ℓ_β} (i.e., the $\alpha = 5^\circ$ spline is scaled by the value of C_{ℓ_β} for $\alpha = 5^\circ$), the summation of the four interpolation splines defines the value of C_{ℓ_β} for any value of angle of attack. It should also be noted that each interpolation spline has the value of C_{ℓ_β} when α equals its knot value, and it is zero for other knot values.

The spline formulation is suitable also for representing installed propulsion system performance models and test instrumentation calibration factors. More complicated models can be represented by a bicubic spline formulation.

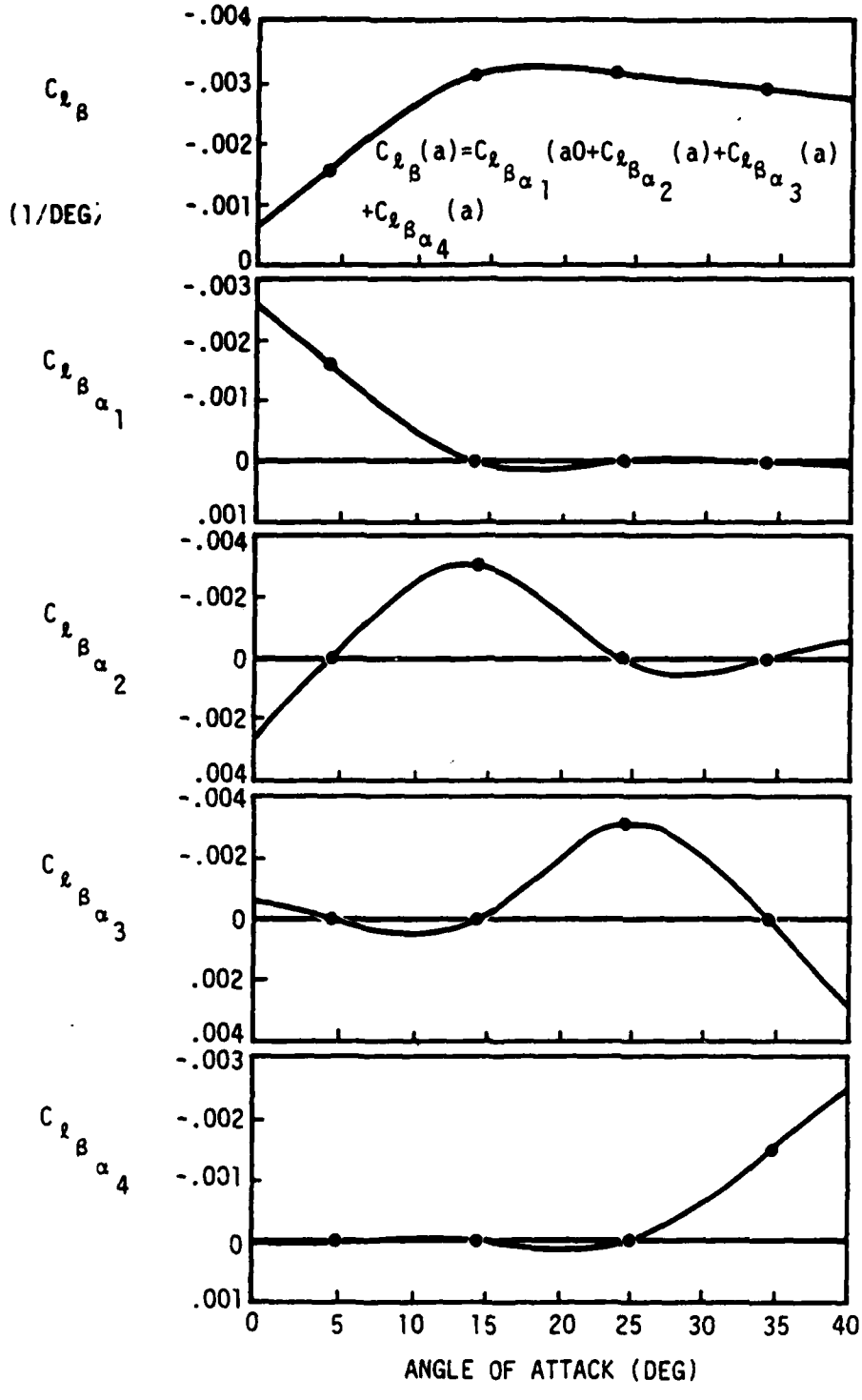

Figure 2.3 Illustration of Cubic Spline Model Formulation

III. FLIGHT TEST PROGRAM DESCRIPTION

This section describes the test aircraft, the flight test instrumentation system, and the test conditions evaluated for the F-4J identification program described by this report. The descriptions presented in this section are provided as background information for the discussions on model structure determination and parameter identification. This material is from Refs. 42 and 43.

3.1 TEST AIRCRAFT DESCRIPTION

The test aircraft, F-4S Bu No. 157286 (McAir No. 3846) was modified under McAir ECP 1049 R1, "F-4S Two Position Leading Edge Slat Retrofit Program." Major changes to distinguish this slatted F-4S model from previous F-4S aircraft are noted as follows:

(1) two position leading-edge slats;

(2) movable inboard leading-edge flaps;

(3) 42-unit angle-of-attack system;

(4) incorporated 12-pound overbalance weight to longitudinal control system; and

(5) J79-GE-10B smokeless combustor engines.

The basic motivation for adding leading-edge devices to the F-4 was to improve its high angle of attack aerodynamic characteristics. By forestalling separated wing flow with the leading-edge devices, it would be possible to expand the aircraft's maneuvering envelope and improve its handling qualities. Figure 3.1 illustrates some of the aerodynamic benefits of leading-edge devices by comparing slat on/off wind tunnel data [42].

The following subsections present a general description of the aircraft configuration, a tabulation of pertinent geometric characteristics, and mass properties.

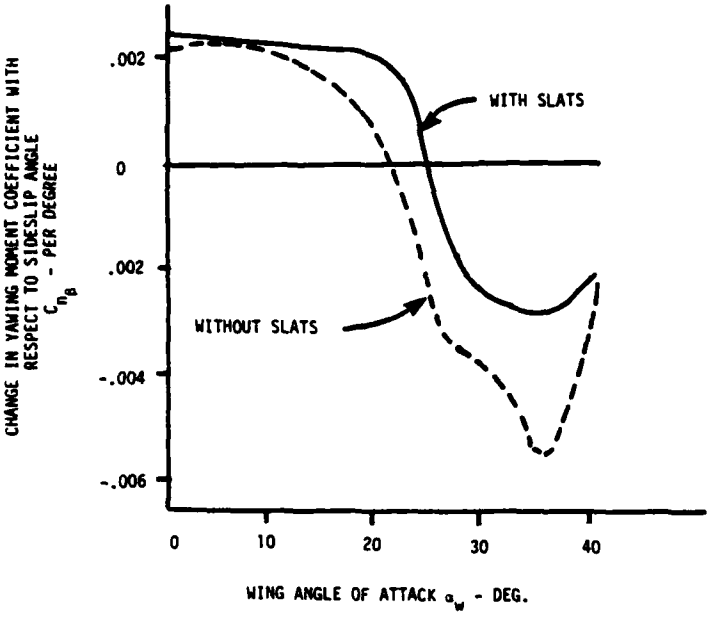

NOTES:

1. $\beta = 0^o$
2. $M = .2$
3. $\delta_s = 0^o$
4. $cg = 33\% \bar{c}$

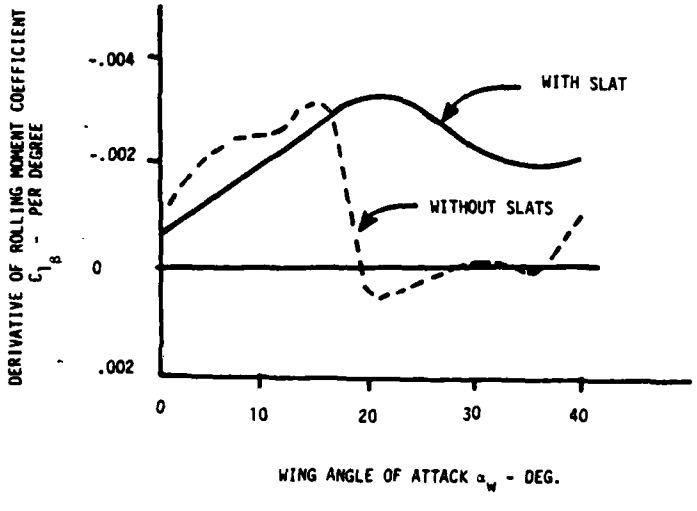

3.1.1 Aircraft Configuration

The slat equipped F-4J is a two-place, all-weather fighter capable of performing as a missle-launching or cannon-firing interceptor or an intermediate and long-range attack bomber. General configurational features of the F-4S are illustrated by an in-flight photograph (Figure 3.2) of the test aircraft. The aircraft is powered by two General Electric J79-10B turbojet engines with automatically controlled external compression air inlets. The basic design is characterized by a low aspect ratio wing swept back 45° at the 25 percent chord line, and an all-movable slotted leading-edge stabilator with 23-1/4° of negative dihedral. Lateral control is provided by a spoiler-aileron combination. Directional stability and control are provided by a vertical fin-rudder combination. The following paragraphs provide functional description of the wing leading and trailing-edge high lift devices.

The F-4S flap/slat system is an integrated system that provides for automatic slat configuration changes during in-flight maneuvering and selective flap/slat configurations for take-off and landing. Each wing has two leading-edge slats (one on the inboard wing panel and one on the outboard folding-wing panel), one leading-edge flap mounted adjacent to the fuselage, one trailing-edge flap which incorporates boundary layer control, and one aileron with droop capability (Figure 3.3). The entire system is electrically selected through solenoid-operated selector valves and hydraulically actuated using the utility hydraulic system.

The leading-edge slats are designed to operate a two-position system: slats out (extended) for the high-lift, maneuvering configuration and slats in (retracted) for the clean-cruise configuration. The slats consist of inner and outer sections, each outer section having two segments to minimize the effects of outer wing bending. Both segments of the outer section are positioned by a single hydraulic actuator and the inner section is positioned by another hydraulic actuator. All four slat actuators are powered by the utility hydraulic system and all slat sections move simultaneously when actuated. The inner slat section translates between the retracted and

Figure 3.2 Test Aircraft

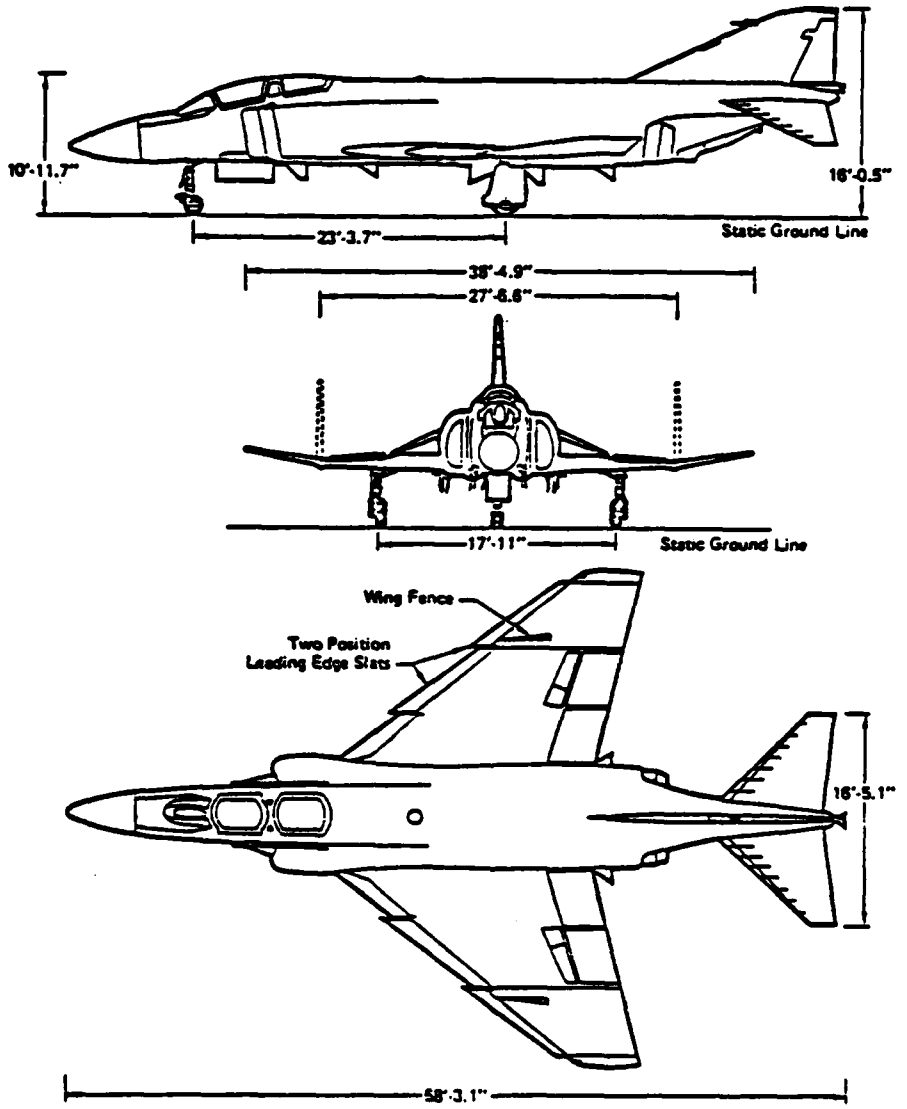

Figure 3.3 F-4S Three View: Slats Extended

extended positions and the outer slat section pivots between the retracted and extended positions. All slat sections are mechanically locked in both retracted and extended positions by overcenter linkages.

The leading-edge flaps are designed to operate as a two-position system: flaps down for take-off, slow flight, and landing; and flaps up for the clean-cruise configuration. Each leading-edge flap is positioned by a hydraulic actuator. Each flap is held in the extended position by hydraulic pressure and locked in the retracted position by overcenter linkages. Leading-edge boundary layer control has been removed from the slat-modified F-4J.

The trailing-edge flaps are designed to operate as a three-position system: flaps up for the clean-cruise configuration; flaps one-half for the take-off configuration; and flaps down for the slow flight and landing configuratiion. Each trailing-edge flap is positioned by a hydraulic actuator. Each flap is held in the extended position by hydraulic pressure and locked in the retracted position by internal locks in the hydraulic actuating cyliner. Trailing-edge flap boundary layer control is operative only when the flaps are in the full down position.

Each aileron droops (deflects 16-1/2° down) whenever one-half or full flaps are selected. This is accomplished by utilizing an aileron droop cylinder which is repositioned by an electromechanical droop aileron actuator. Both aileron systems continue to function as originally designed when drooped, except that the aileron neutral point is 16-1/2° lower.

Flap/slat control is provided by the existing switch in the front cockpit. The switch is airfoil in shape and has newly labeled positions, from top to bottom, of UP-NORM, 1/2-OUT, and DN-OUT. When the switch is in the UP-NORM position, all flaps are fully raised and the slats operate automatically as a function of angle of attack (provided that aircraft weight is off the landing gear). As long as aircraft weight is off the gear, the slats are extended when AOA exceeds 11.5 units and retracted when AOA decreases to 10.5 units. With aircraft weight on the landing gear, the slats retract if UP-NORM is selected regardless of AOA value as a safety feature (to prohibit inadvertent extension or retraction of the slats on the deck due to AOA vane movement).

Two airspeed retraction switches are provided to protect the slats, flaps, and ailerons from structural damage if they are inadvertently left extended above their structural airspeed limits. The slats airspeed switch retracts the slats when accelerating through an airspeed of approximately 585 KCAS. The flaps' airspeed switch retracts the flaps and ailerons when accelerating through an airspeed of approximately 237 KCAS. If the slats or flaps are retracted by their respective airspeed switches, they will return to the selected flap/slat switch position when the airspeed is reduced below specific limits.

3.1.2 Aircraft Geometry

General information on the geometric and mass characteristics of the test aircraft are presented in this section. These data are required for the solution of the equations of motion and in the reconstruction of nondimensional aerodynamic force and moment coefficients from flight measurements. Dimensions of the F-4S are shown in Figure 3.3, and the required reference geometry is defined below.

- wing area, $S_w = 530$ ft^2
- wing span, $b_w = 38.67$ ft
- wing mean aerodynamic chord, $\bar{c}_w = 16.04$ ft

Moment arms for calculating thrust moments and the displacements between the c.g. and sensor locations are presented. The latter set of geometry is required to reconstruct equivalent c.g. measurements since the equations of motion are defined in terms of c.g. quantities. (The equations which are used to define equivalent c.g. measurements are presented in Section IV.) The location of the c.g., sensors, and the thrust reaction point are expressed in terms of a fuselage station (FS), a water line (WL), and a butt line (BL) in inches. Moment arms are then defined in terms of axial (ℓ_x), lateral (ℓ_y), and vertical displacements (ℓ_z) from the c.g. in feet. The following sign convention is used: $\ell_x > 0$ ahead of the c.g., $\ell_y >$ to the right of the c.g., and $\ell_z > 0$ below the c.g. The following set of data defines the c.g. location and the location and moment arms for the

accelerometer package, nose boom α and β vanes and the net thrust reaction point.

c.g. Location

FS = 261 + 1.92 X_{cg} (where X_{cg} = c.g. location in percent $\overline{c}_w$)

WL = 28

BL = 0

Accelerometer Package

FS = 347.62

WL = 12.75

BL = 4.25 (right)

$\ell_{x_{ACC}} = -7.22 + .16\ X_{cg}$

$\ell_{y_{ACC}} = .35$

$\ell_{z_{ACC}} = 1.27$

Noseboom α Vane

FS = - 65.5

WL = 8.02

BL = - 8.5 (left)

$\ell_{x_\alpha} = 27.21 + 16\ X_{cg}$

$\ell_{y_\alpha} = -.71$

$\ell_{z_\alpha} = 1.67$

Noseboom β Vane

FS = - 70.15

WL = - .48

BL = 0

$\ell_{x_\beta} = 27.60 + 16\ X_{cg}$

$\ell_{y_\beta} = 0$

$\ell_{z_\beta} = - 2.38$

Net Thrust Reaction Point (Used for Phase I)

FS = 313.5

WL = 32.4

BL = 23.8 left and right

$\ell_{x_{TN}} = - 4.38 + .16\ X_{cg}$

$\ell_{y_{TN}} = \pm 1.98$

$\ell_{z_{TN}} = - .37$

Gross Thrust Reaction Point (Phases II and III)

FS = 518

WL = 13

BL = ±23

Inlet Ram Force Reaction Point

FS = 162

WL = 30

BL = ±35

3.2 TEST INSTRUMENTATION

The airborne data acquisition system used for the flight test program included a three-axis rate gyro, a vertical gyro, a directional gyro, engine RPM and fuel flow measurements, a three-axis linear accelerometer, position and force transducers, and a test airdata system. The airdata system uses a noseboom which has a pitot-static head for the measurement of impact pressur, static pressure and temperature. The noseboom also has vanes for measurements of angle of attack and sideslip.

Figure 3.4 shows test aircraft body axis inertias and product of inertia as a function of gross weight. These data have been derived for

- zero fuel weight = 33,243 lbs
- no armament
- tank 7 fuel
- flight test pod
- gear up

3.3 TEST FLIGHT CONDITIONS

3.3.1 Phase I

Ten of the Phase I flight conditions were selected for system identification processing. These flight conditions are listed in Table 3.1 and their selection was based on having one test condition for each type of control input. Aircraft weight and center of gravity location, run time, and initial-minimum-maximum values for pressure altitude, equivalent airspeed, Mach number, and angle of attack are tabulated in Table 3.2 for each flight condition. All test conditions are for subsonic flight ($M < .6$) along the minimum speed boundary of the operational envelope.

When the Phase I test conditions were flown, a number of test points were flown back to back. After each run, the pilot dropped the nose to regain airspeed and then retrimmed for the next test point. Because the nose dropped

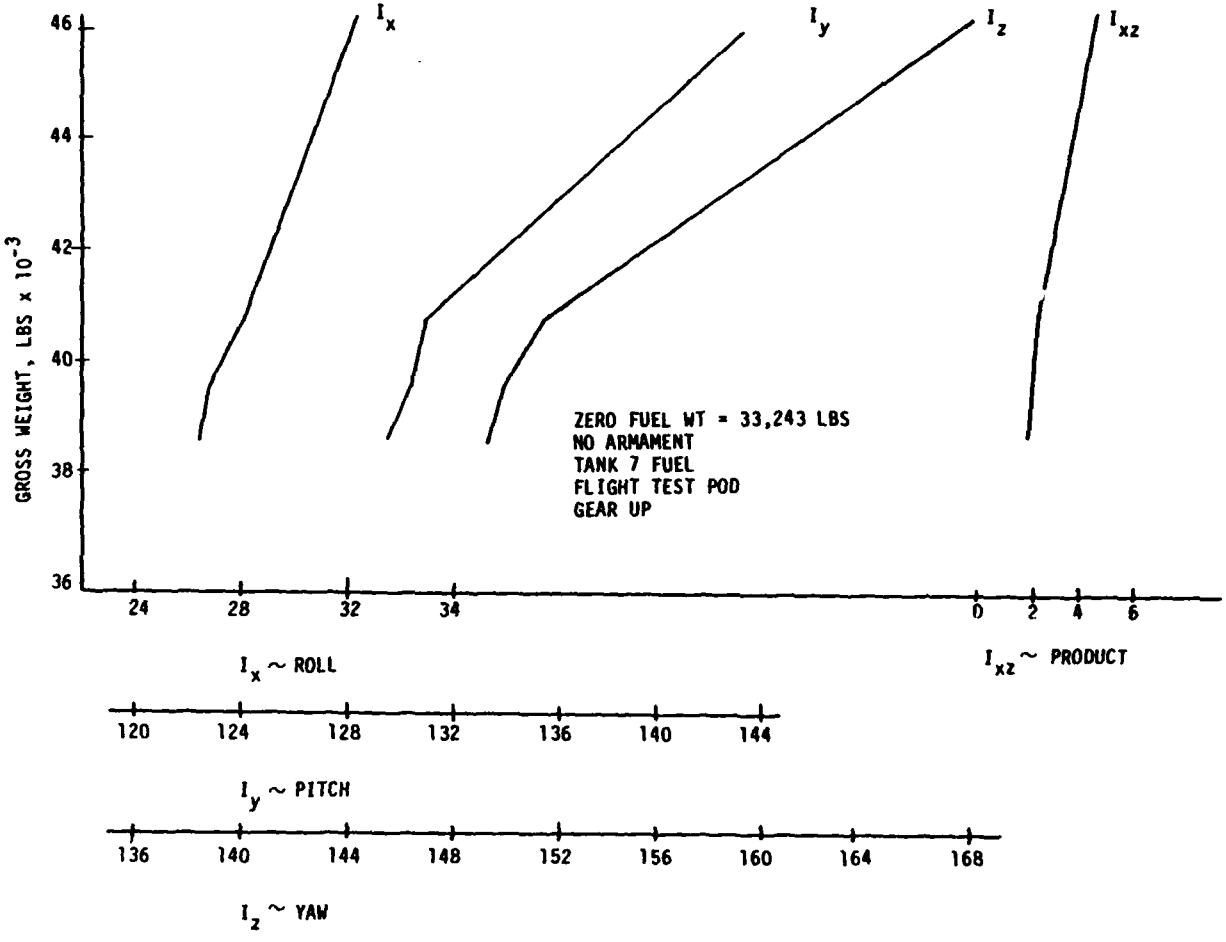

Figure 3.4 F-4S Inertia ~ Slug-Ft^2 x 10^{-3}

Table 3.1

Flight Conditions Processed for Model Structure Determination

FLIGHT TEST NUMBER	TEST INPUT	COMMENTS
1004-5	Full Aft Stick	α_{MAX} 47°; Moderate Pitch-up Rate
1004-11	Full Aft Stick with Simultaneous Lateral Stick Doublet	α_{MAX} 52°; Rapid Pitch-up Rate; Sustained Oscillation for $\alpha > 40°$
1005-7	Moderate Aft Stick with Continued Series of Lateral Stick Doublets	Oscillatory α in $15° < \alpha < 40°$ Range
1005-10	Moderate Aft Stick with Simultaneous Pedal Doublet	Oscillatory α in $15° < \alpha < 30°$ Range
1006-4	Full Aft Stick at Slow Application Rate with 1-1/2 Pedal Doublets	$\alpha_{MAX} \approx 53°$
1006-5	Moderate Stick with Repeated Pedal Doublets	Oscillatory α in $15° < \alpha < 34°$
1006-8	Simultaneous 3-Axis Doublets with Repeated Lateral-Directional Doublets at end of Maneuver	Oscillatory α in $9° < \alpha < 34°$ Range
1007-5	Full Aft Stick with Full Lateral Stick 2 Sec Command	$\alpha_{MAX} \approx 42°$; Moderate Pitch-up Rate
1009-5	Full Aft Stick with 4 Sec Lateral Command	$\alpha_{MAX} \approx 57°$; Moderate Pitch-up Rate
1010-7	Full Aft Stick with 2 Sec Pedal Command	$\alpha_{MAX} \approx 55°$; Moderate Pitch-up Rate

Table 3.2

Flight Condition Summary for Phase I Flight Test

				ALTITUDE (ft x 10^{-3})			AIRSPEED (KEAS)			MACH NUMBER			α (UNITS)		
RUN NO.	RUN TIME (SEC)	W (LBS)	cg (% $\bar{c}_w$)	h_o	h_{MAX}	h_{MIN}	V_{e_o}	$V_{e_{MAX}}$	$V_{e_{MIN}}$	M_o	M_{MAX}	M_{MIN}	α_o	α_{MAX}	α_{MIN}
1004-5	19.0	41,500	31.2	38.5	38.5	37.7	168	168	91.5	.54	.54	.29	16.9	39.5	16.6
1004-11	70.1	36,200	28.7	39.1	39.2	28.2	153	153	67.8	.49	.49	.22	17.8	41.4	17.8
1005-7	29.7	40,000	31.1	40.7	41.1	39.9	190	190	146.0	.61	.61	.47	15.4	38.2	11.5
1005-10	17.4	37,100	28.6	41.7	41.7	41.4	177	177	137.0	.57	.57	.44	16.2	35.5	16.1
1006-4	22.5	42,600	31.8	38.8	38.8	37.3	162	162	80.9	.52	.52	.26	16.6	41.4	16.5
1006-5	12.5	41,700	30.8	39.4	39.4	38.9	170	171	147.0	.54	.55	.47	17.2	33.4	12.5
1006-8	24.4	39,400	30.6	40.5	40.5	39.6	179	180	147.0	.57	.57	.47	14.7	34.3	10.5
1007-5	12.9	37,400	28.9	39.8	39.9	38.8	167	167	130.0	.53	.53	.41	14.9	37.3	14.9
1009-5	25.5	41,200	30.7	38.9	38.9	37.9	179	179	63.0	.57	.57	.20	14.7	41.5	14.5
1010-7	31.1	39,400	30.6	39.9	39.9	38.4	174	174	63.0	.56	.56	.20	14.8	41.4	14.8

through vertical and the airplane rolled over on its back during the recovery maneuver, this phase of the flight record was not used for system identification. When data files were established for each flight, the final time was selected by one of the following conditions:

- $|\phi| < 120^{\circ}$
- $\theta < -20^{\circ}$
- stick position has been pulled beyond $\delta_S > 10^{\circ}$ and then pushed through trim

3.3.2 Phase II

Data for the second phase were obtained from a flight which took place on 27 March 1980. The flight test plan for this flight (W/O-7) was prepared jointly by NATC and SCT personnel.

The flight test program was conducted in a clean configuration with the throttles fixed for each maneuver and with flight near and beyond stall. Test conditions were generally initiated from wing level, constant altitude flight with $\alpha = 10^{\circ}$ and $M \approx .6$. For some test conditions, the pilot-applied variable aft stick to maneuver the aircraft through the desired angle-of-attack test range. For some of the stall entry conditions, lateral stick and/or pedal doublets were combined with the longitudinal stick command. Other flight conditions included single-axis and multi-axis sequenced doublet inputs. These inputs were made by the pilot and were not intended to be repeatable nor precise with regard to their spectral characteristics, but were generally effective in creating large-amplitude motions. The overall test goal was to force the aircraft through a broad range of test conditions.

A summary of flight test conditions from flight W/D-7, which were used for the identification study, is presented in Table 3.3.

3.3.3 Phase III

Three flights in the F-4S were flown for Phase III in order to update the existing F-4S simulation data base. Test techniques used include variable frequency sweep inputs in all three axes for small amplitude maneuver analyses

Table 3.3

Flight Condition Summary for Phase II Flight Test

MANEUVER	MANEUVER DESCRIPTION	TAPE/FILE	DURATION (SEC)	h_o (FT)	M RANGE	α RANGE (DEG)	β RANGE (DEG)
1	Stall with Lateral Doublets	M01431/4	58	30K	.3/.5	3/42	-20/18
2	Stall with Pitch Doublets	M01431/3	74	30K	.35/.45	5/35	-13/13
3	Stall with Rudder Doublets	M01431/5	87	30K	.32/.36	6/42	-22/15
4	Pitch Doublets	M01431/6	44	37K	.4/.49	2/40	-2/3
5	Aileron Doublets	M00599/3	42	30K	.4/.45	8/25	-5/7
6	Rudder Doublets	M00599/4	57	30K	.49/.52	-8/25	-20/25
7	1G Sequential Doublets	M00599/5	53	30K	.45/.60	0/33	-15/10

and stall and departure maneuvers with three-axis doublets. Two flights were flown in the cleaning loading in configurations Cruise (CR), Take-off (TO), and Power Approach (PA) to update the existing clean-loading simulation. One flight was flown in a high stability index loading and the same configurations to extend the simulation capability to include store loadings. This unit stability index number has been assigned to a particular weapon or piece of suspension equipment as a measure of the destabilizing effect of that item. The high stability index tests were performed to give quantitative estimates of the performance, stability, and control of the A/C in that particular loading. Table 3.4 presents a summary of the Phase III test conditions.

Table 3.4

Phase III Flight Test Conditions

FLIGHT	RECORD	CONFIGURATION	MANEUVER
2	4	TO	LONG. SINE LOW AOA
2	9	TO	LONG. SIN MED AOA
2	11	TO	RUDDER SINE MED AOA
3	30	PA	LONG. SINE LOW AOA
3	32	PA	RUDDER SINE LOW AOA
3	35	PA	LONG. SINE HIGH AOA
3	36	PA	RUDDER SINE HIGH AOA
3	46	CR (M = .7)	LONG. + AILERON + RUDDER SINE LOW AOA
3	47	CR (M = .8)	LONG. SINE LOW AOA
3	48	CR (M = .9)	LONG. SINE LOW AOA
10	7	HSI TO	LONG. SINE LOW AOA
10	9	HSI TO	LONG. SINE MED AOA
10	11	HSI TO	LONG. SINE HIGH AOA
10	19	HSI PA	LONG. SINE LOW AOA
10	20	HSI PA	LONG. SINE MED AOA
10	21	HSI PA	LONG. SINE HIGH AOA
12	20	HSI CR (M = .7)	LONG. SINE LOW AOA
12	23	HSI CR (M = .8)	LONG. SINE LOW AOA

IV. FLIGHT TEST DATA ANALYSIS AND PREPROCESSING

The analysis and preprocessing of flight test data is a major element of the integrated system identification procedure. The overall objectives of this task are to evaluate the suitability of the flight test data for identifying aerodynamic characteristics and to develop a complete set of kinematically consistent measurements. Completeness is required to ensure that all parameters of interest can be identified. Measurement consistency has a significant impact on parameter identification accuracy since unaccounted-for errors will bias parameter estimates.

This task involves five steps:

(1) flight data evaluation;
(2) error correction;
(3) data filtering;
(4) data reconstruction; and
(5) instrument calibration.

These steps are briefly reviewed below.

4.1 FLIGHT DATA EVALUATION AND ERROR CORRECTION

The flight test data is first transferred from magnetic tapes to binary disk files. For each flight maneuver, all relevant data channels are plotted for evaluation.

Each channel is inspected for sign errors, data dropout, and wild points. Sign and units conversions are performed, if necessary. Wild points are removed using an interactive computer program that searches for adjacent data points differing by more than a threshold specified by the user. Data dropout problems can be solved in two ways: either the particular variable is reconstructed from other measurements or if the data loss is of short duration, the maneuver is split into two shorter ones.

The second part of the flight test data evaluation concerns the quality and completeness of the measurement set. The need for smoothing the data and/or reconstructing missing or noisy measurements must be assessed. In

addition, the frequency content of the maneuver is evaluated to ensure that all dynamic modes of interest are properly excited. Based on this evaluation, several different maneuvers (e.g., pitch, roll, and yaw sssp's) are combined to improve the identification accuracy.

In addition, cross plots of the independent variables are generated to define regions where the nonlinear models can be identified. Figure 4.1 illustrates an independent variable cross plot which has been generated from Phase II flight test data. This crossplot is used to show that aerodynamic model terms which are a function of α and β should be identifiable for $10^\circ < \alpha < 30^\circ$ and $|\beta| < 10^\circ$.

4.2 DATA FILTERING

A Fast Fourier Transform (FFT) is used to smooth the data by removing high-frequency components. The FFT algorithm can also be used to generate smooth derivatives for any desired variable. This is particularly useful to generate variables such as $\dot{P}$ or $\dot{\phi}$ which are not usually measured.

To be effective, the filtering process should remove most of the high-frequency noise without affecting the information content in the frequency range of interest. Consequently, the choice of the FFT cutoff frequency for each measurement is based on the following criteria:

- The cutoff frequency must be at least four times greater than the highest frequency of interest (i.e., the highest dynamic mode affected by that particular measurement).
- The difference between the original and filtered signal should appear like white noise.

Figure 4.2 illustrates the effect of different cutoff frequencies on the roll-rate signal. The difference between the original roll-rate signal and the filtered signal (with a cutoff frequency of 4 Hz) is shown in Figure 4.3, together with the corresponding curves for α, β, and ϕ. The proper choice of cutoff frequency is even more critical when the FFT capability to generate derivatives is used as shown in Figure 4.4 (roll acceleration generated from the roll-rate signal of Figure 4.2).

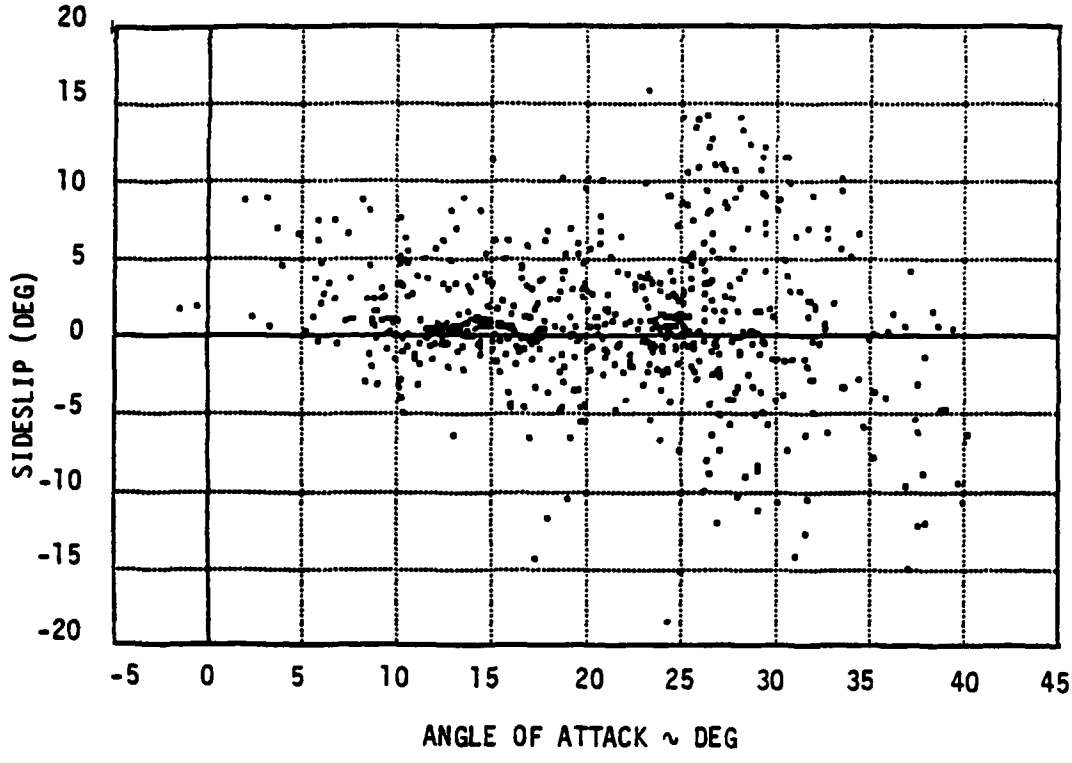

Figure 4.1 Angle of Attack/Sideslip Test Data Crossplot

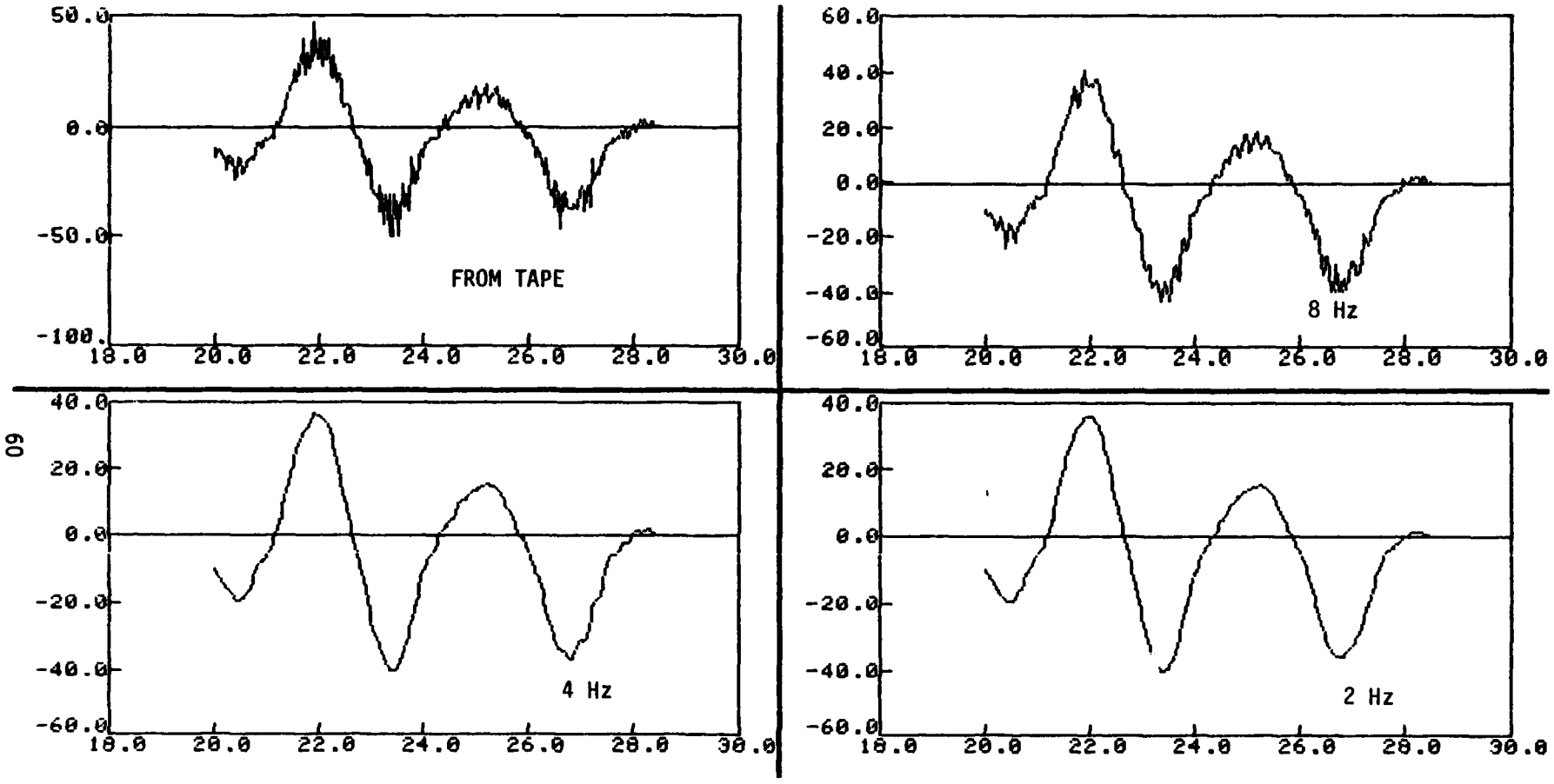

Figure 4.2 Effect of Cutoff Frequency on P

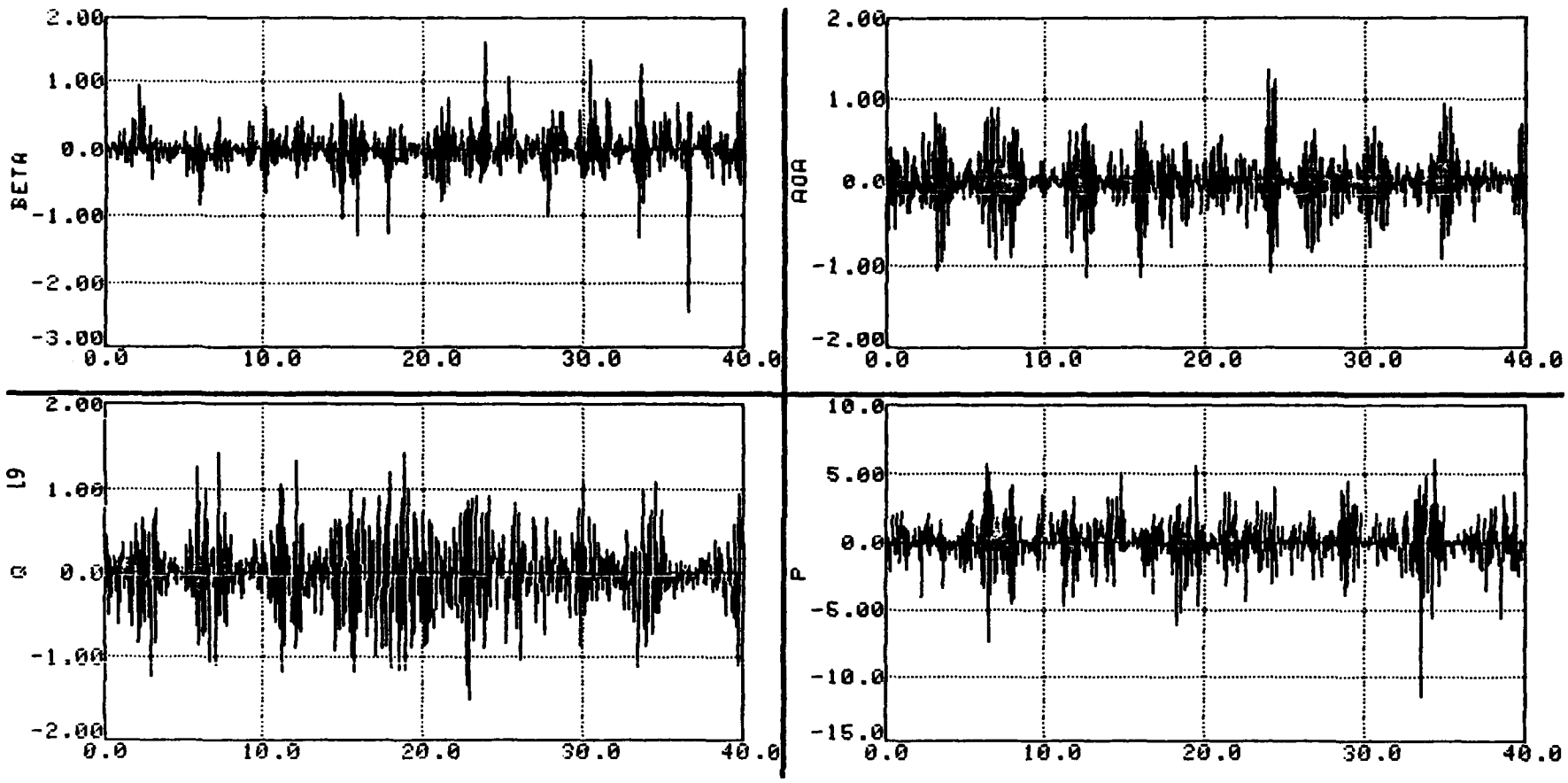

Figure 4.3 Difference Between Original and Filtered Signals (4 Hz)

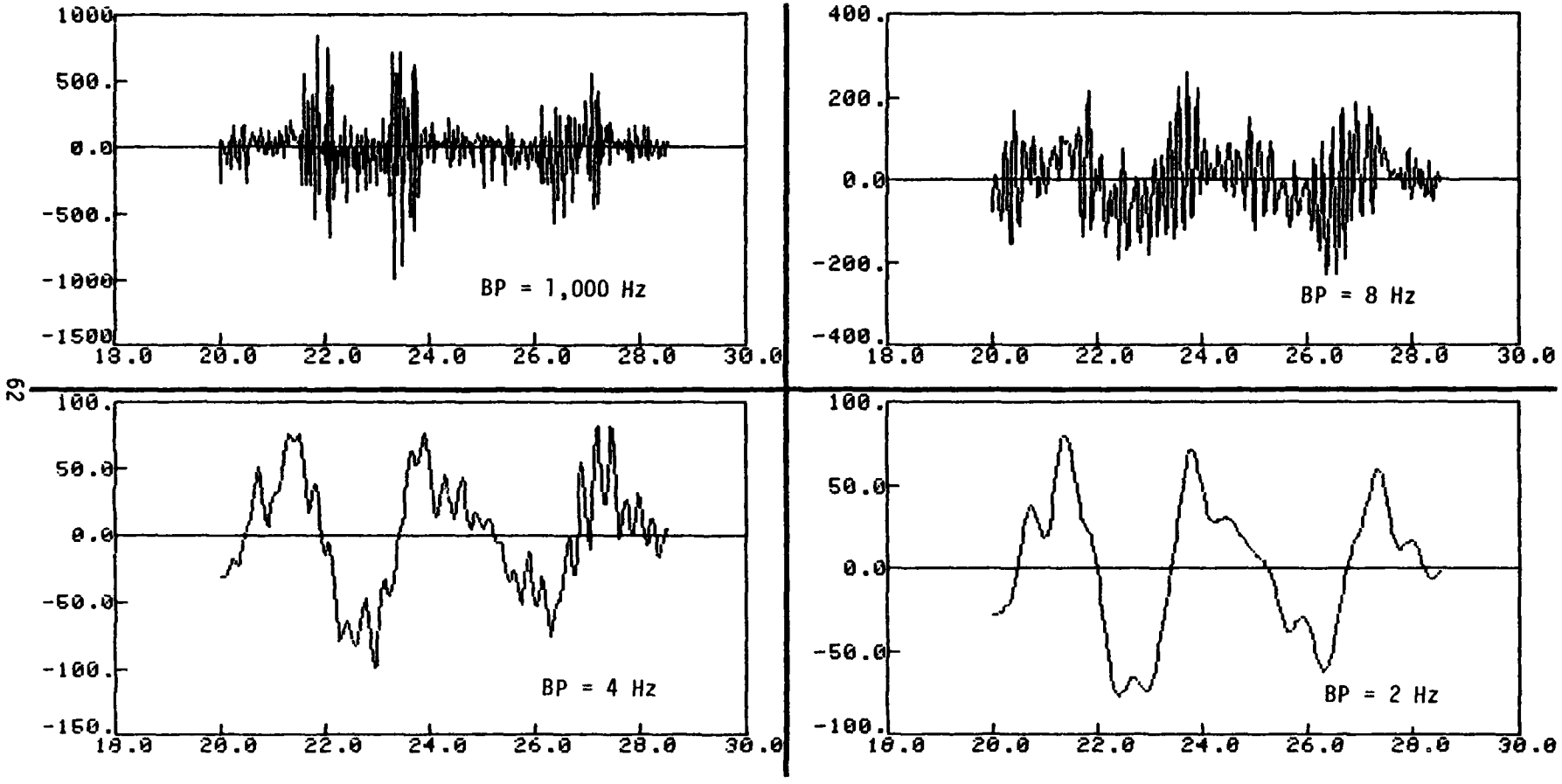

Figure 4.4 Effect of Cutoff Frequency on $\dot{P}$

4.3 DATA RECONSTRUCTION

Data reconstruction is required for variables that are not measured at all or not measured directly, and for recorded measurements that cannot be used due to instrumentation or data acquisition problems.

For the F-4S flight test data analysis, the following measurements were reconstructed:

(1) The roll rate signal was saturated at 60 deg/sec and was reconstructed from the roll angle derivatives (ϕ) generated by the FFT algorithm:

$$P = \dot{\phi} - (Q \sin\phi + R \cos\phi) \tan\theta$$

(2) The angular accelerations were generated by the FFT algorithm from the angular rates. The equations for accelerometer location correction contain terms in $\dot{P}$, $\dot{Q}$, and $\dot{R}$ and these derivatives must be supplied as input when the corresponding states (P, Q, and R) are not propagated.

(3) Velocity components at the center of gravity (U, V, and W) were reconstructed from the nose-boom measurements (V_T, α, and β). For example,

$$V_{NB} = V_T \sin\beta$$

$$V = V_{NB} + P \cdot \ell_z - R\ell_x$$

where

ℓ_x, ℓ_z = nose boom location relative to the c.g. These reconstructed velocities are used:

(a) To obtain the initial conditions for the propagation (i.e., integration) of u, v, and w.

(b) To enable identification of only a subset of the parameters. For example, to identify only longitudinal characteristics (e.g., $C_D(\alpha)$ and $C_L(\alpha)$), u and w are propagated while the reconstructed values are used for v. As a result, $C_D(\alpha)$ and $C_L(\alpha)$ can be identified without any a priori knowledge of lateral/directional characteristics such as C_{y_β}.

(4) Mass and inertia characteristics were reconstructed from measurements of the fuel quantity in each of the aircraft's eight fuel tanks. The curves relating fuel quantity to incremental change in mass and inertia were provided by the NATC. The reconstructed variables were: m, I_x, I_y, I_z, I_{xz}, X_{cg}, Y_{cg}, and Z_{cg}.

4.4 INSTRUMENT CALIBRATION

The instrumentation system errors are identified so that sensor signals will be kinematically consistent. Otherwise bias, scale factors and time delays in the sensor signal will appear as errors in the identified aerodynamic parameters. Kinematic consistency is determined by comparing the angular positions ϕ, θ and ψ to the integrals of the Euler rates which are reconstructed from the body rates P, Q and R. Similarly, velocities (U, V and W) are compared to the integrals of the accelerations. Bias, scale factors and time delays are identified so as to reduce the comparison errors.

For example, pitch rate-gyro calibration:

$$\Delta\theta = \theta_m - \int_{t_o}^{t_1} [Q \cos \phi_m - R \sin \phi_m]dt$$

$$Q = (Q_m - b_q)/(1 + k_q) \quad \text{and} \quad R = (R_m - b_r)/(1 + K_r)$$

where:

Q, R = true pitch and yaw rates

Q_m, R_m = measured pitch and yaw rates

b_q, b_r = pitch and yaw rate biases

k_q, k_r = pitch and yaw rate scale factors

θ_m, ϕ_m = measured pitch and roll attitudes

$b_{(\ )}$ and $k_{(\ )}$ are identified by the SCIDNT program so as to minimize $\Delta\theta$. Identification of the time delay is a built-in capability of SCIDNT and is done by shifting the Q_m input until $\Delta\theta$ achieves a minimum.

The accelerometers, angles of attack and sideslip and airspeed sensors are identified in a similar way using the kinematic equations relating A_x, A_y and A_z to α, β, V_T and h_p. For example, vertical accelerometer calibration:

$$a_{z_{aa}} = (a_{z_m} - b_{az})/(1 + K_{az})$$

$$a_{z_{cg}} = a_{z_{aa}} + (\dot{Q} - P\,R)\ell_{x_a} - (\dot{P} + R\,Q)\ell_{y_a} + (Q^2 + P^2)\ell_{z_a}$$

$$W = \int (U \cdot Q - V \cdot P + g \cos\theta \cos\phi + a_{z_{cg}})\, dt$$

$$W_{NB} = W + P\ell_y - Q\ell_x$$

$$\Delta\alpha = \alpha_m - \tan^{-1}\left(\frac{W_{NB}}{U_{NB}}\right)$$

b_{az} and K_{az} are identified by SCIDNT so as to minimize $\Delta\alpha$.

It should be noted that in the actual process, all three rate gyros and all three accelerometers are calibrated simultaneously, and all relevant measurements are used. As a result of the coupling between the state variables, additional terms (e.g., a bias on the vertical gyro: b_ϕ) and cross terms (e.g., K_{QP} and K_{azx}) can be identified.

When several maneuvers are combined together and processed simultaneously, it is also necessary to identify maneuver-dependent terms for those parameters that are time varying, such as the gyro biases (b_ϕ, b_θ, and b_ψ) and rate-gyro biases (b_P, b_Q, and b_R).

The complete list of instrument calibration terms and equations is contained in Appendix A, and Figure 4.5 presents the instrumentation calibration model which was identified from Phase II flight test data.

- NOSEBOOM VANE

  $\alpha_{meas} = 1.102\hat{\alpha} + .06$ deg

- NOSEBOOM VANE

  $\beta_{meas} = 1.061\hat{\beta} - .63$ deg

- DYNAMIC PRESSURE: See Figure 4.5

- ACCELEROMETER
  - AXIAL: BIAS = .01 f_{ps}^2
  - LATERAL: BIAS = .50 f_{ps}^2
  - VERTICAL: BIAS = -2.10 f_{ps}^2

- VERTICAL GYRO
  - ROLL ALTITUDE: Vertical Alignment: $-.63^0 < \phi_\varepsilon < 1.36^0$*
  - PITCH ALTITUDE: Vertical Alginment: $.43^0 < \theta_\varepsilon < .23^0$*

- RATE GYRO
  - ROLL: Defective:
  - PITCH: Bias: $-.34^0/Sec < b_q < -.05^0/Sec$*
    Scale Factor: -.052
  - YAW: Bias: $.38^0/Sec < b_r < .58^0/Sec$*
    Misalignment from Vertical: 1.5^0

* Dependent on Maneuver

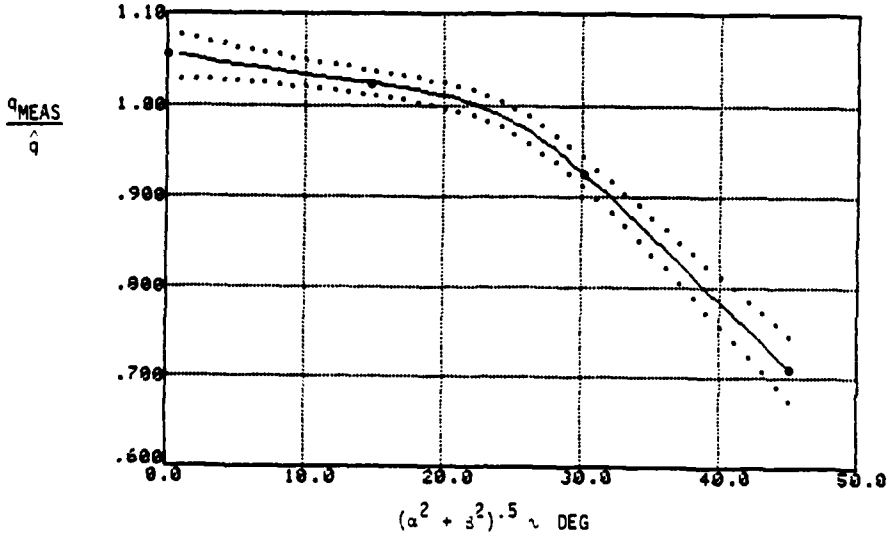

Figure 4.5 Identified Instrumental System Calibration Factors (Phase II)

V. SYSTEM IDENTIFICATION RESULTS

This section presents the aerodynamic and propulsion model data which were identified from both the Phase II and Phase III flight test programs. This data base, along with the mathematical model presented in Appendix A, comprise a simulation of the F-4S.

5.1 LONGITUDINAL CHARACTERISTICS AND EXTERNAL STORE EFFECTS

5.1.1 General

This section presents the F-4S longitudinal characteristics at low to medium angles of attack. The incremental effect of external stores is also shown. Longitudinal aerodynamic models were identified for the following configurations:

- Take-Off (TO) - slats and landing gear extended, trailing edge flaps deflected 30 deg, and inboard leading edge flaps deflected 30°.
- Power Approach (PA) - slats and landing gear extended, trailing edge flaps deflected 60°, inboard leading edge flaps deflected 30°.
- Cruise (CR) - landing gear and flaps retracted, slats extend and retract automatically. Two CR models were identified for Mach 0.7 and Mach 0.8.

Two models were estimated for each configuration:

- A clean or low stability index (LSI) loading.
- A high stability index (HSI) loading with numerous external stores.

External store incremental effect was derived as the difference between the HSI and the LSI models.

5.1.2 Instrumentation Considerations

Phase III flight test maneuvers were processed for this phase. Both the LSI and HSI flights had instrumentation problems, which were solved as follows.

(1) For the LSI flights, air temperature was not recorded, and a cold standard day model for temperature was used. This impacts the air density, Mach number, and $\sqrt{\theta_{T2}}$ computations. $\sqrt{\theta_{T2}}$ is used as a correction factor for the thrust model.

(2) For the HSI flights, the engine fuel flow and flight control system (FCS) gyro data were not recorded. Since fuel flow is needed in the gross thrust model, it was calculated from engine RPM. Figures A.3 and A.4 in Appendix A show the corrected RPM to corrected fuel flow curves used in the analysis. This rleationship is only valid for power settings less than mil power. Since the FCS vertical and rate gyros data were not available, alternative sources of these measurements were explored. The measurements could not be adequately calibrated by using instrumentation pod bank angle, roll rate, or pitch rate. However, the airdata, noseboom, and inertial measurements could be calibrated when roll rate, bank angle, yaw rate, heading, and sideslip were assumed zero and the derivative of pitch angle used as pitch rate. This approach is valid since the maneuvers processed for the longitudinal models have negligible lateral-directional excitation. Table 5.1 summarizes the sources used for these troublesome measurements.

The instrumentation problems necessitated identification of two LSI aero models. The first and more accurate model is based on the FCS and fuel flow data, and the second model, LSI*, is based on the instrumentation pod pitch attitude and calculated fuel flow. The LSI* model is needed to determine store effects by comparison with the HSI model. The LSI* model may also be used in the future if fuel flow is not known.

Table 5.1

Measurement Sources for LSI, LSI*, and HSI Analysis

MEASUREMENT	SOURCE FOR LSI ANALYSIS	SOURCE FOR LSI* AND HSI ANALYSIS
ROLL RATE	FLIGHT CONTROL SYSTEM (FCS) DATA	ASSUMED ZERO
PITCH RATE	FCS	SET TO $\dot{\theta}$
YAW RATE	INSTRUMENTATION POD	ASSUMED ZERO
BANK ANGLE	FCS	ASSUMED ZERO
PITCH ATTITUDE	FCS	INSTRUMENTATION POD
HEADING	INSTRUMENTATION POD	ASSUMED ZERO
FUEL FLOW	RECORDED FLIGHT DATA	CALCULATED FROM RPM
AIR TEMPERATURE	ASSUMED STANDARD DAY -15°C	RECORDED FLIGHT DATA

5.1.3 Results

The longitudinal aerodynamic characteristics are presented as follows.

(1) A summary of the data processing accuracy is presented in Figure 5.1. The root mean squared (rms) errors for each measurement (Q, a_x, a_z, α_{NB}, $\bar{q}$, and h_p) and each maneuver are shown.

(2) A more detailed presentation of identified model accuracy is given in Figures 5.2 to 5.4. Each figure is a time history plot for one of the three configurations (TO, PA, and CR). Both the actual recorded test data and the estimated measurements derived from the identified aerodynamic models are shown.

(3) The identified aerodynamic coefficients for the TO, PA, CR/M = 0.7, and CR/M = 0.8 are shown in Figures 5.5 through 5.10, 5.11 through 5.16, 5.17 through 5.22, and 5.23 through 5.28, respectively. Each figure presents the variation of the aerodynamic coefficient versus wing angle of attack and the corresponding external store incremental effect. The estimation uncertainty is shown by the $\pm 2\sigma$ bounds.

The lift and pitching moment coefficients due to pitch rate are shown in Tables 5.2 and 5.3. All of the results are in the stability axis system and are referenced to c.g. = 33 percent and $\delta_s = 0$.

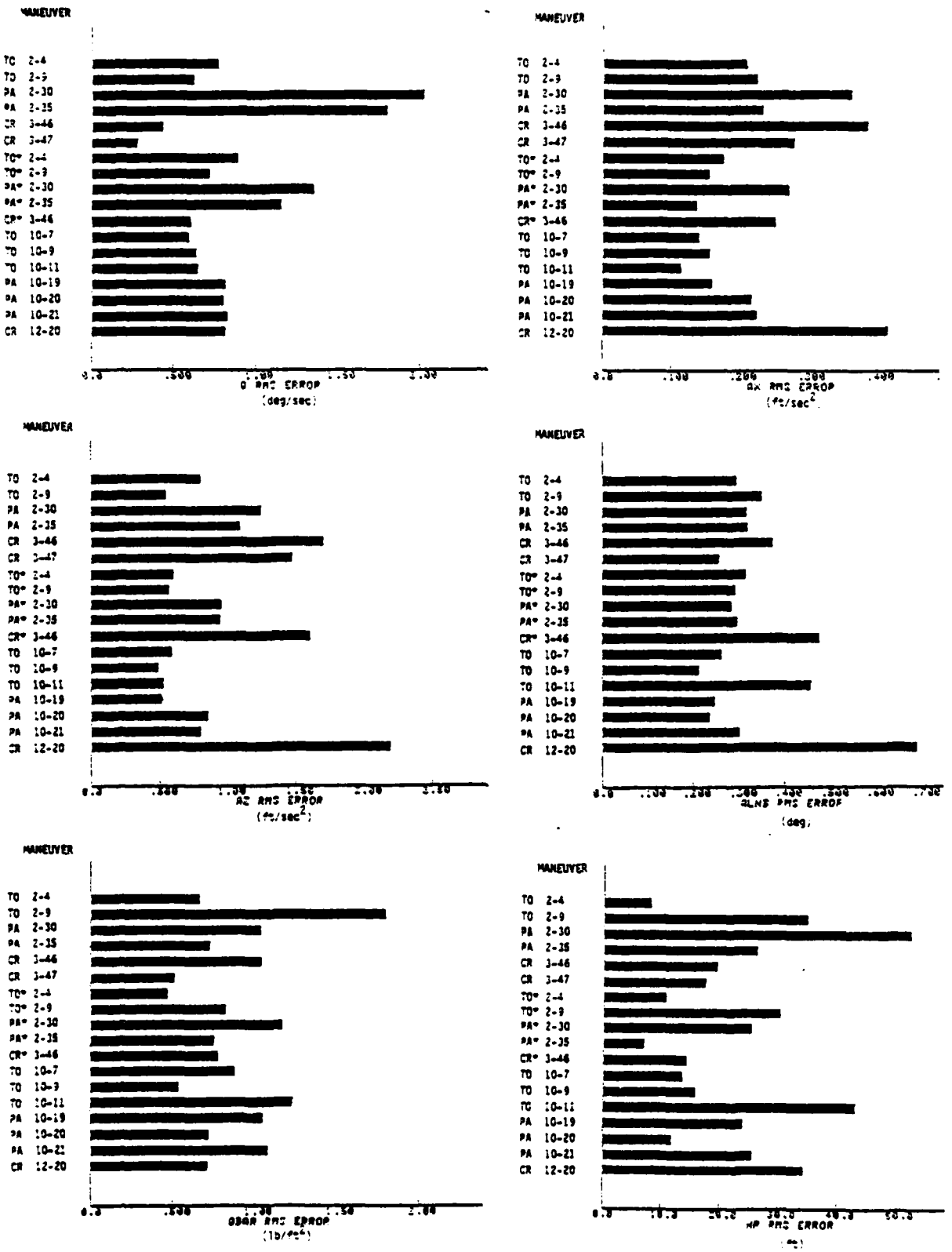

Figure 5.1 Root Mean Square Measured Errors

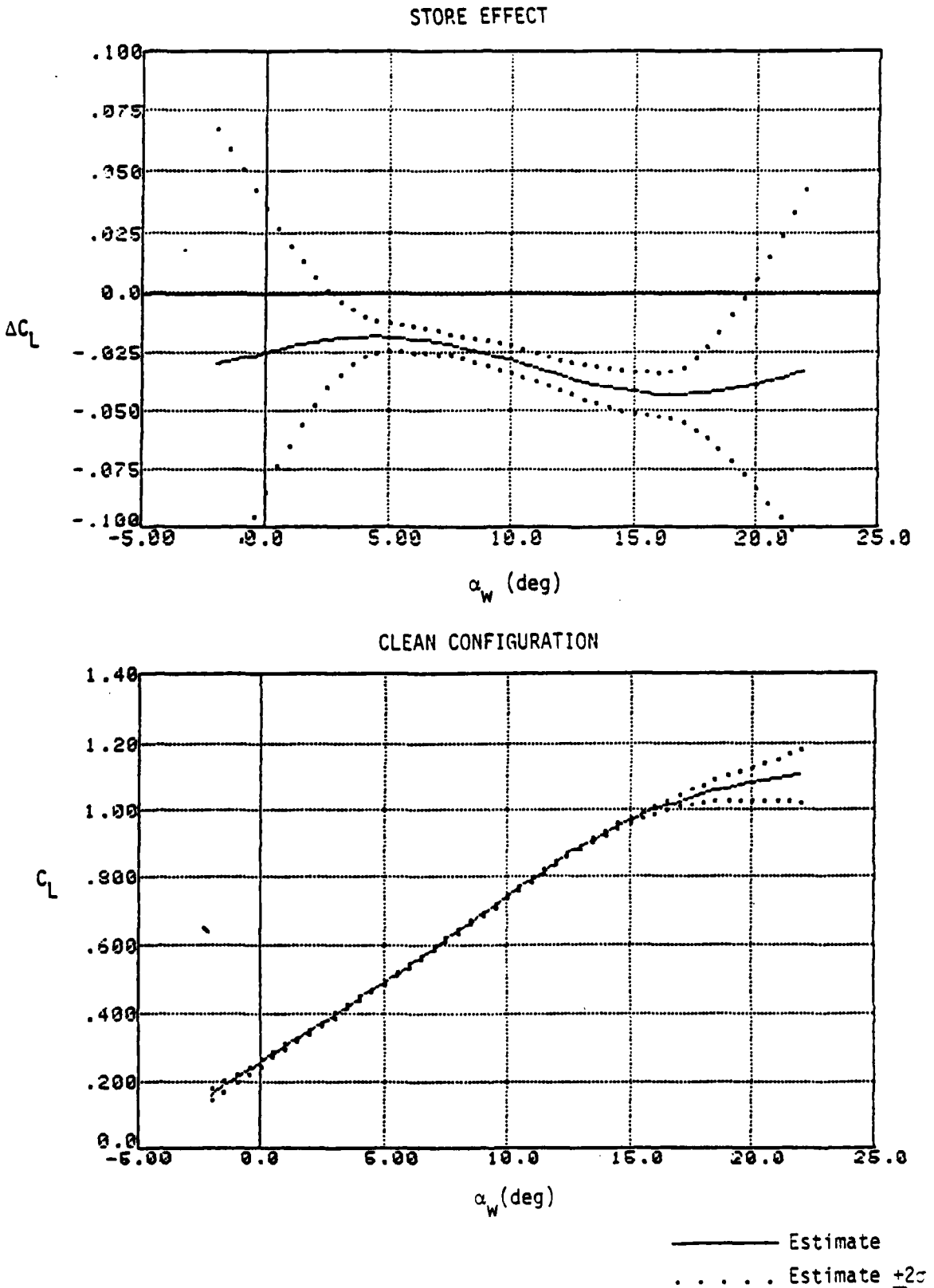

Figure 5.1 Lift Coefficient - Takeoff

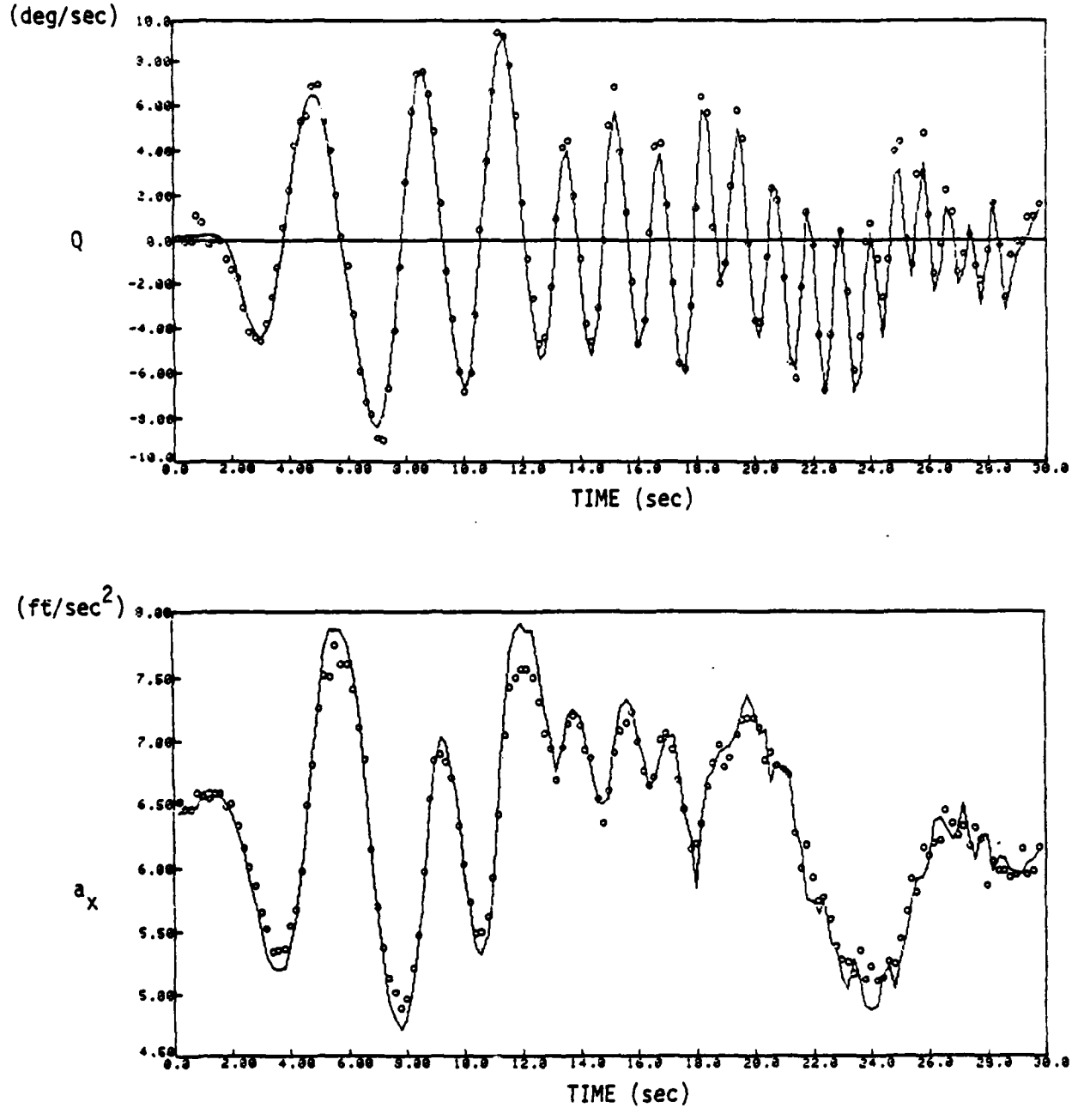

Figure 5.2 Time History Plot - Takeoff (HSI)

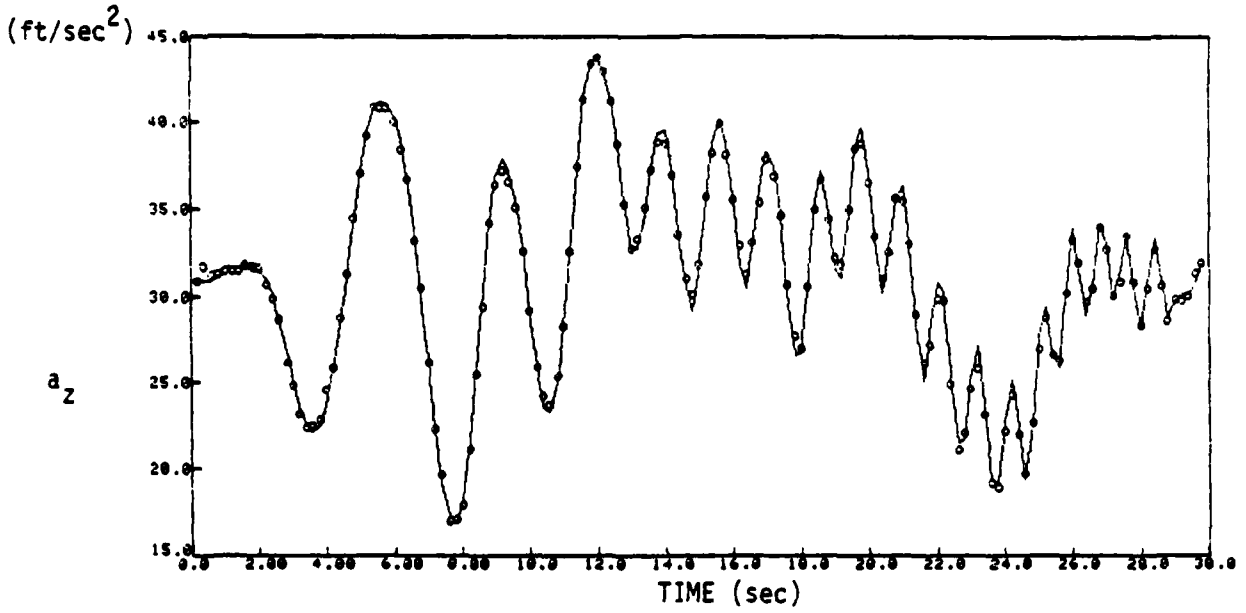

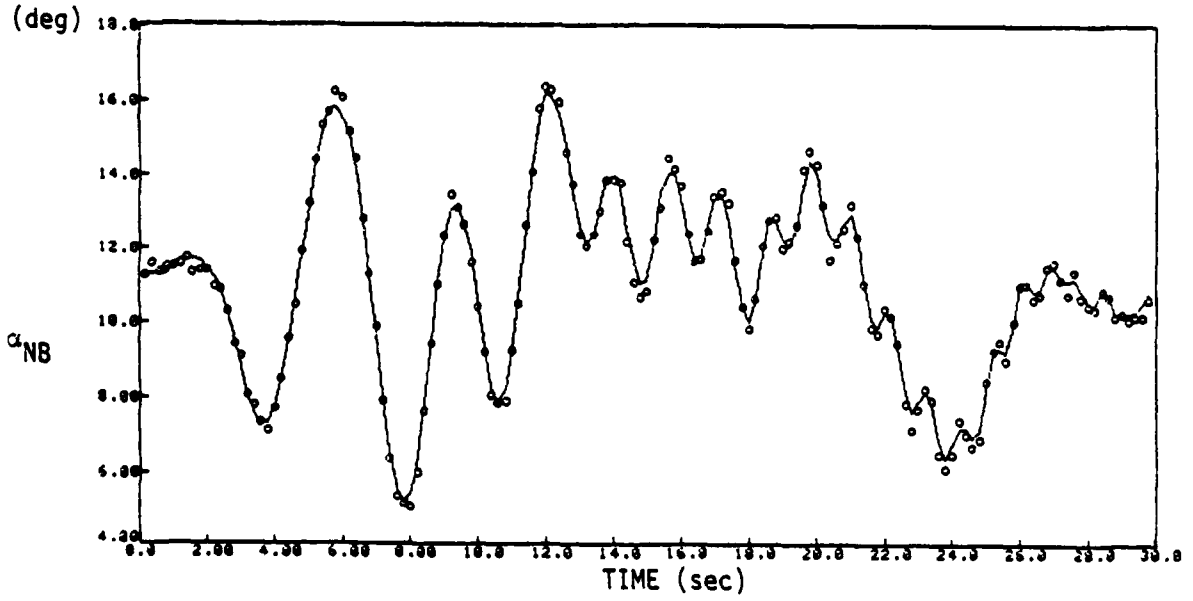

——— Estimate from Identified Aerodynamic Model

o o o o o Flight Test Data

Figure 5.2 Time History Plot - Takeoff (HSI) (Cont'd)

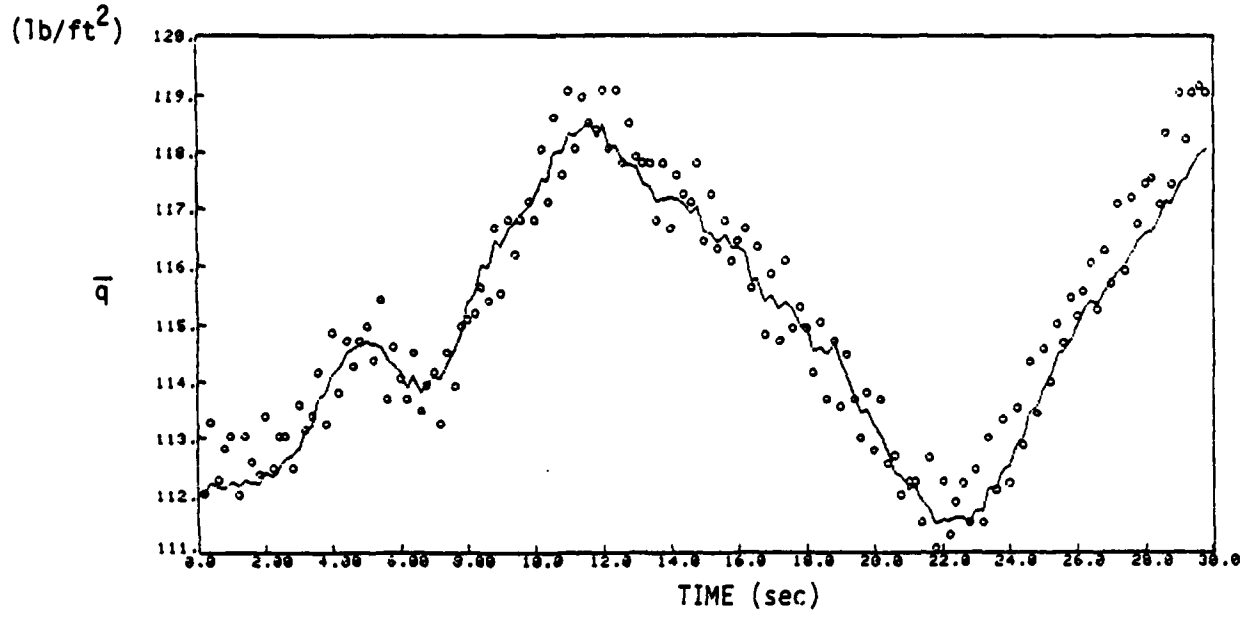

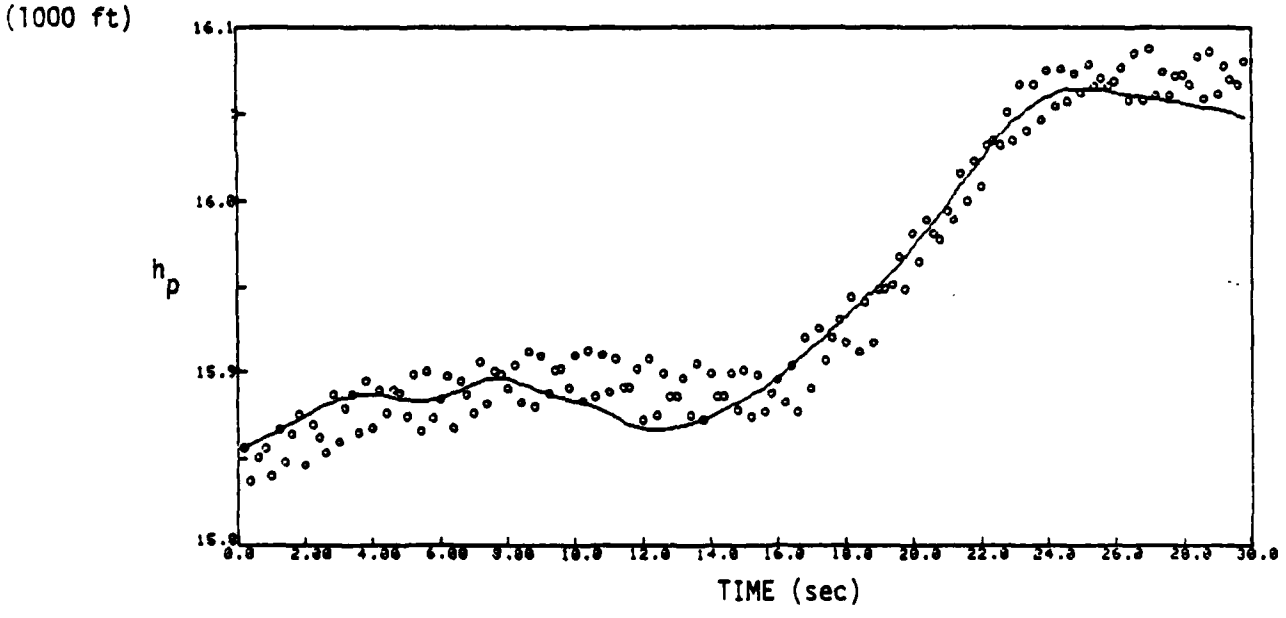

——— Estimate from Identified Aerodynamic Model

o o o o o Flight Test Data

Figure 5.2 Time History Plot - Takeoff (HSI) (Cont'd)

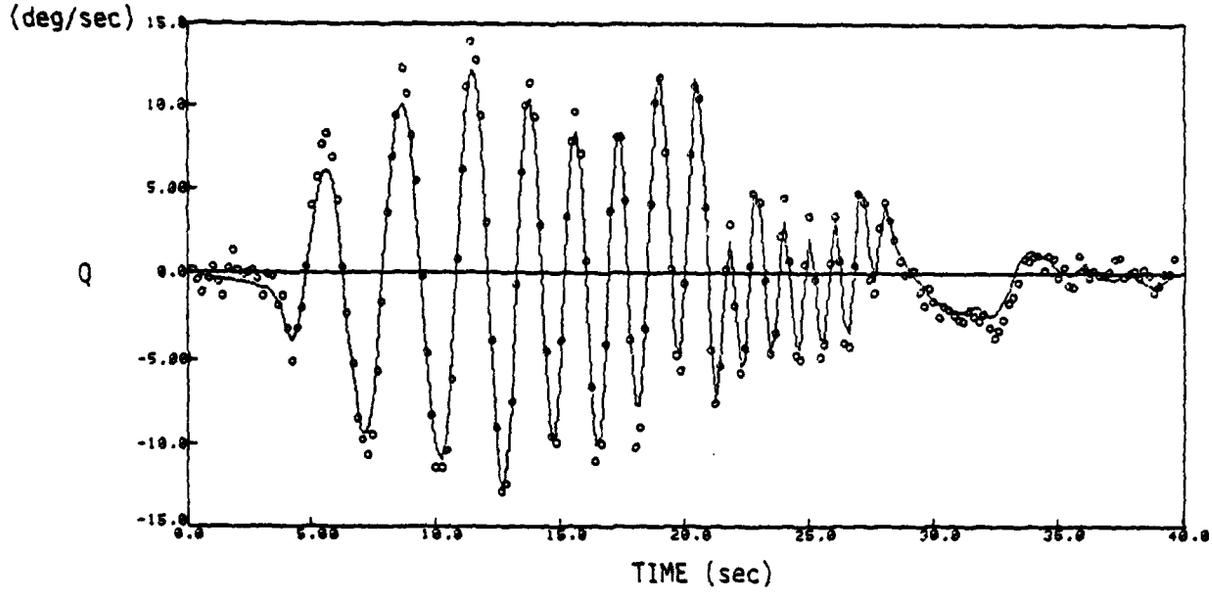

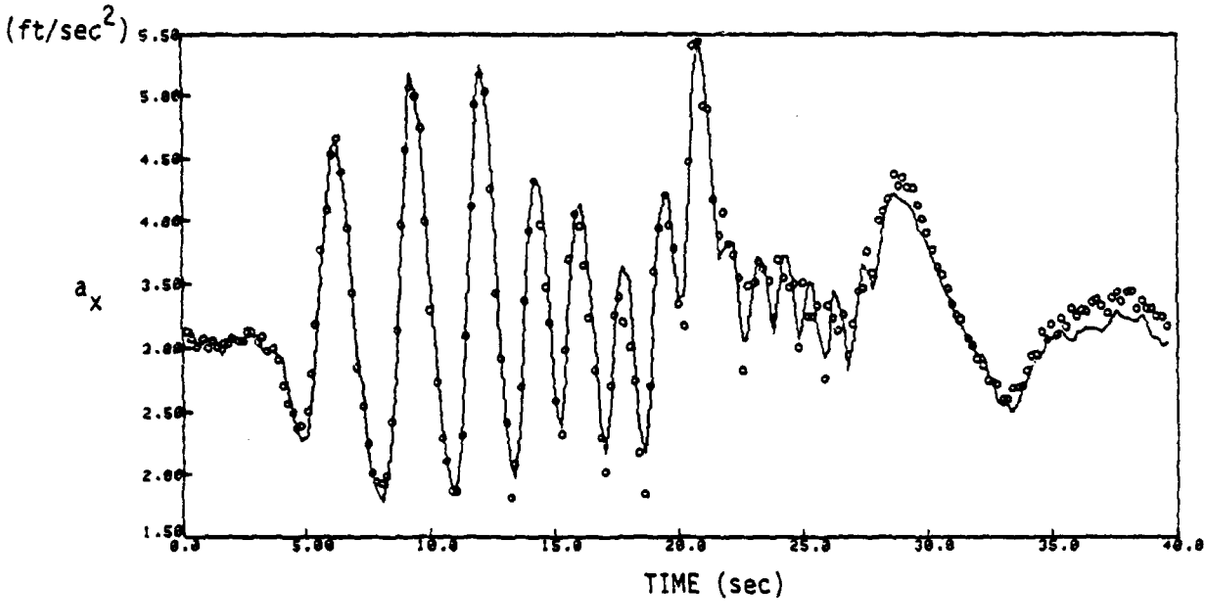

——— Estimate from Identified Aerodynamic Model

o o o o o.o Flight Test Data

Figure 5.3 Time History Plot - Power Approach (HSI)

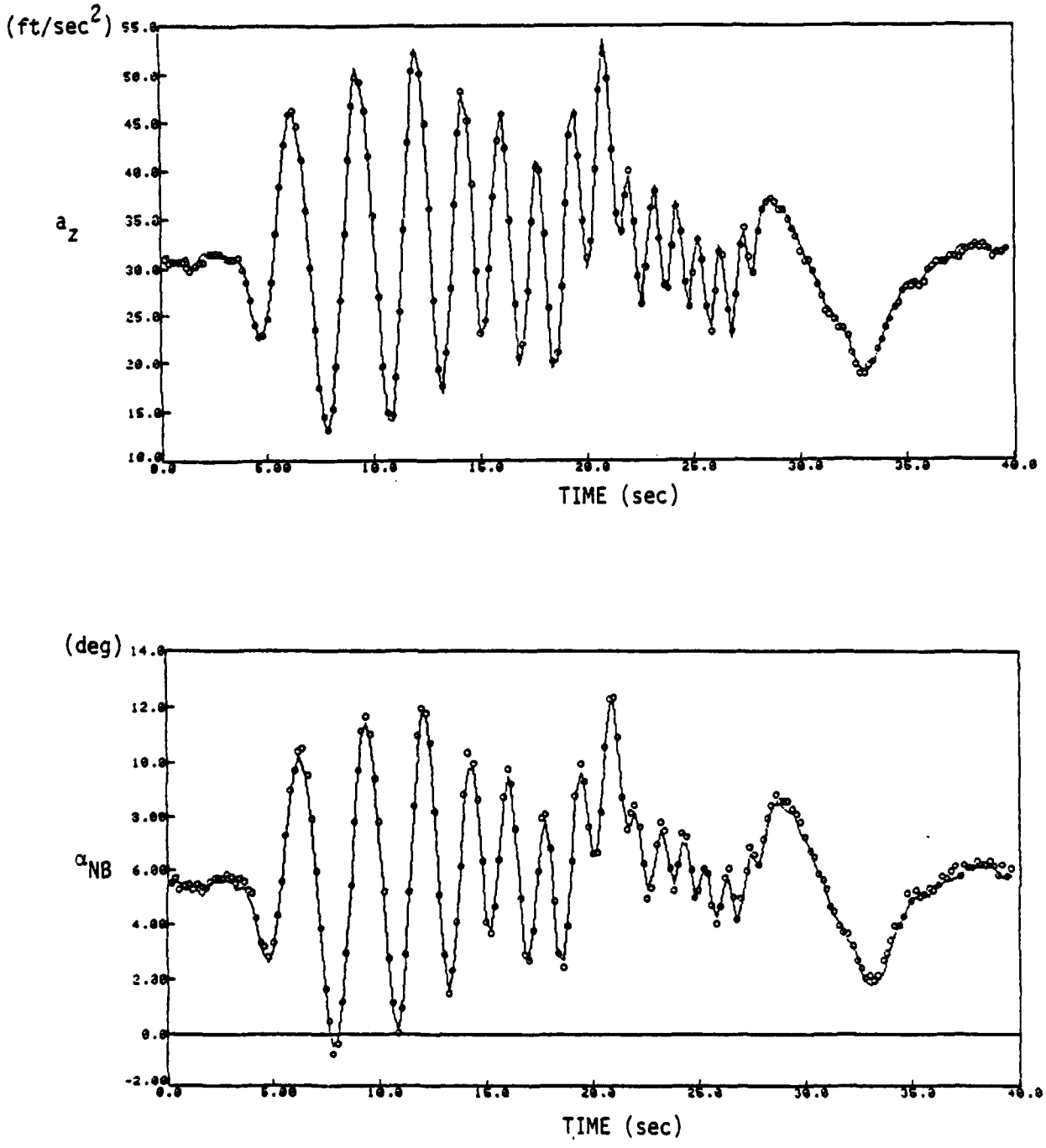

Figure 5.3 Time History Plot - Power Approach (HSI) (Cont'd)

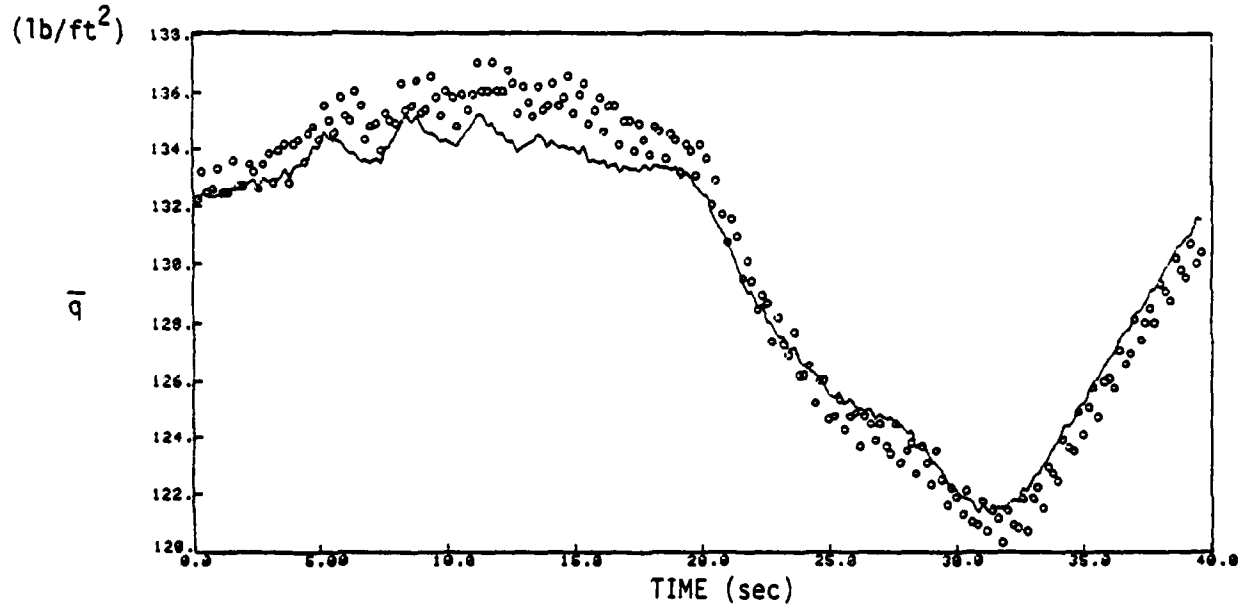

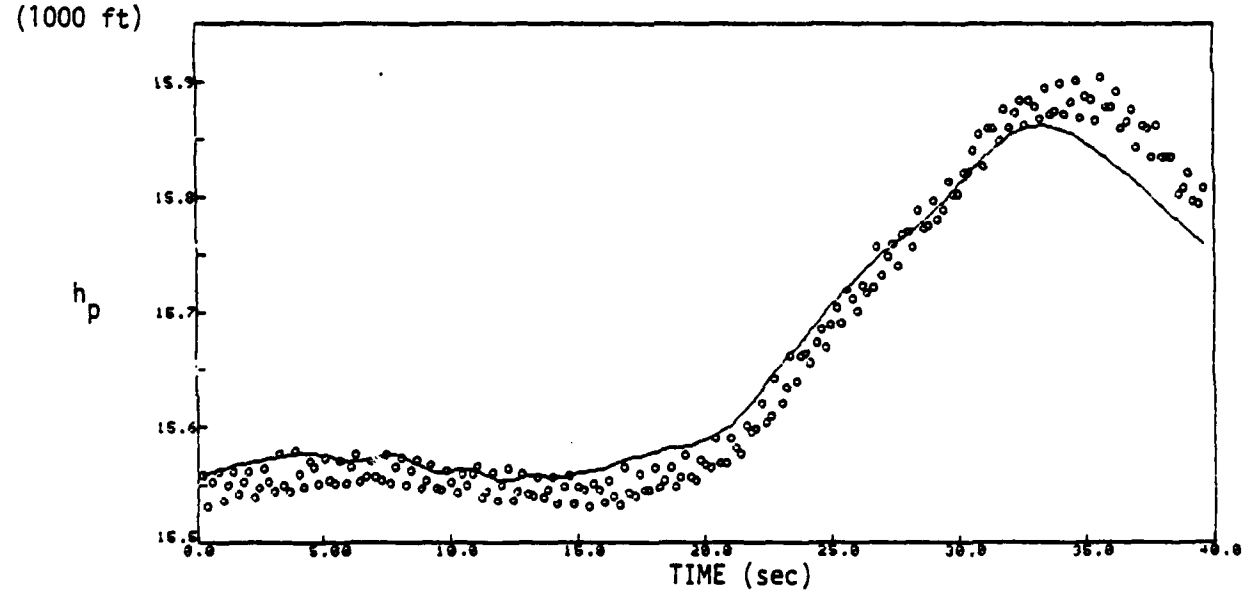

——— Estimate from Identified Aerodynamic Model

o o o o o Flight Test Data

Figure 5.3 Time History Plot - Power Approach (HSI) (Cont'd)

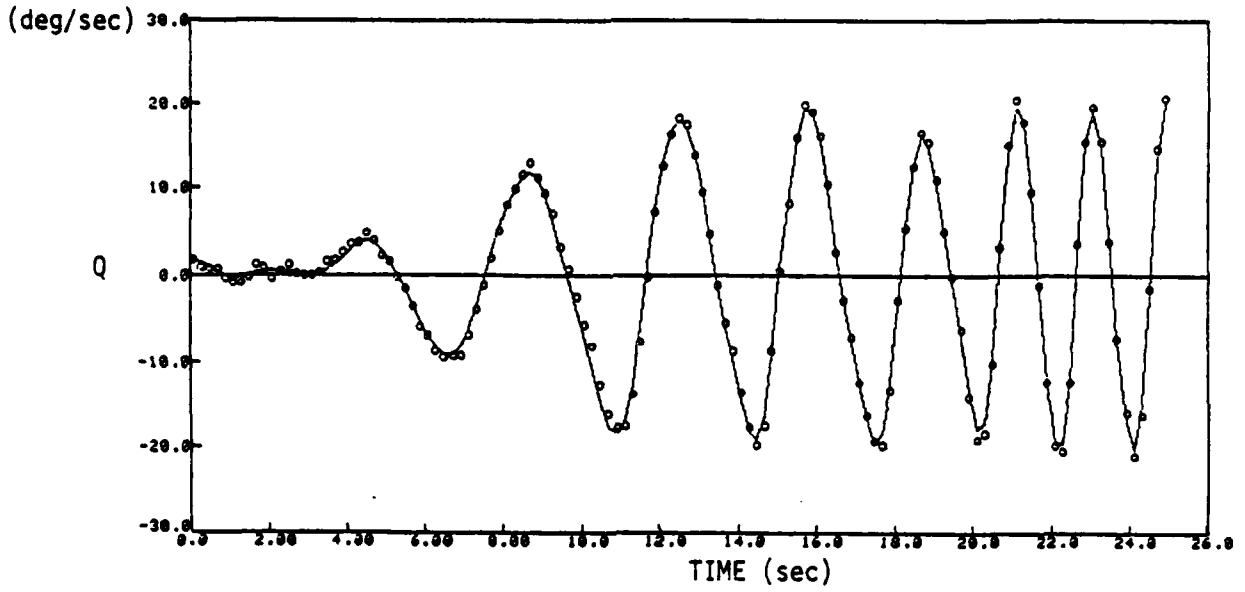

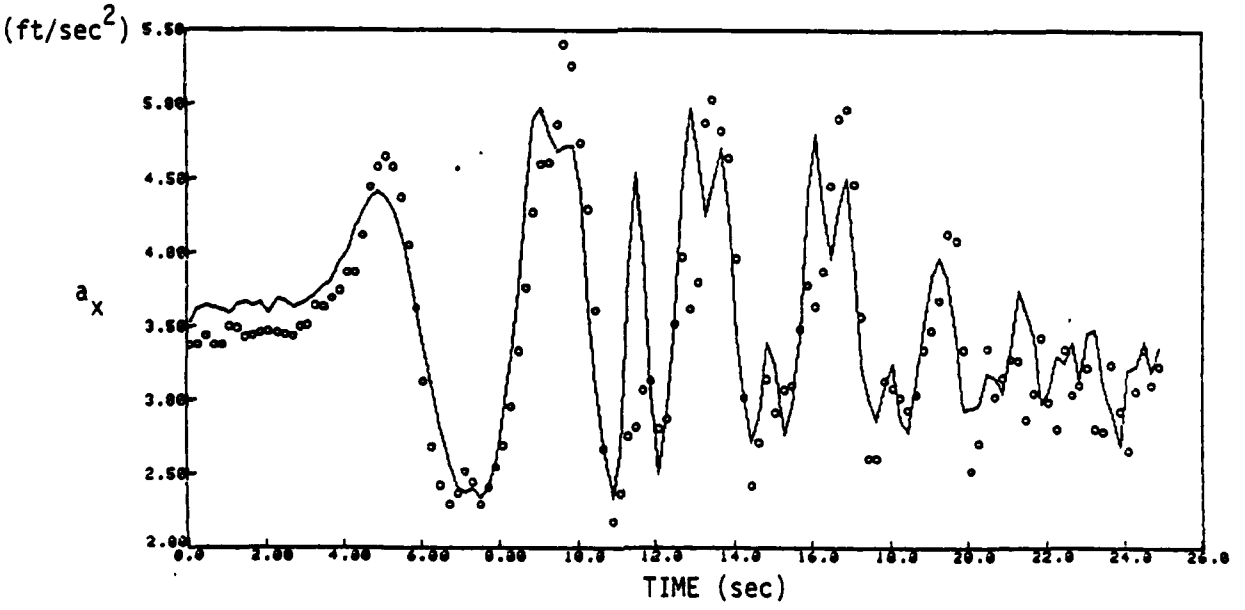

——— Estimate from Identified Aerodyanmic Model

o o o o o Flight Test Data

Figure 5.4 Time History Plot - Cruise (HSI)

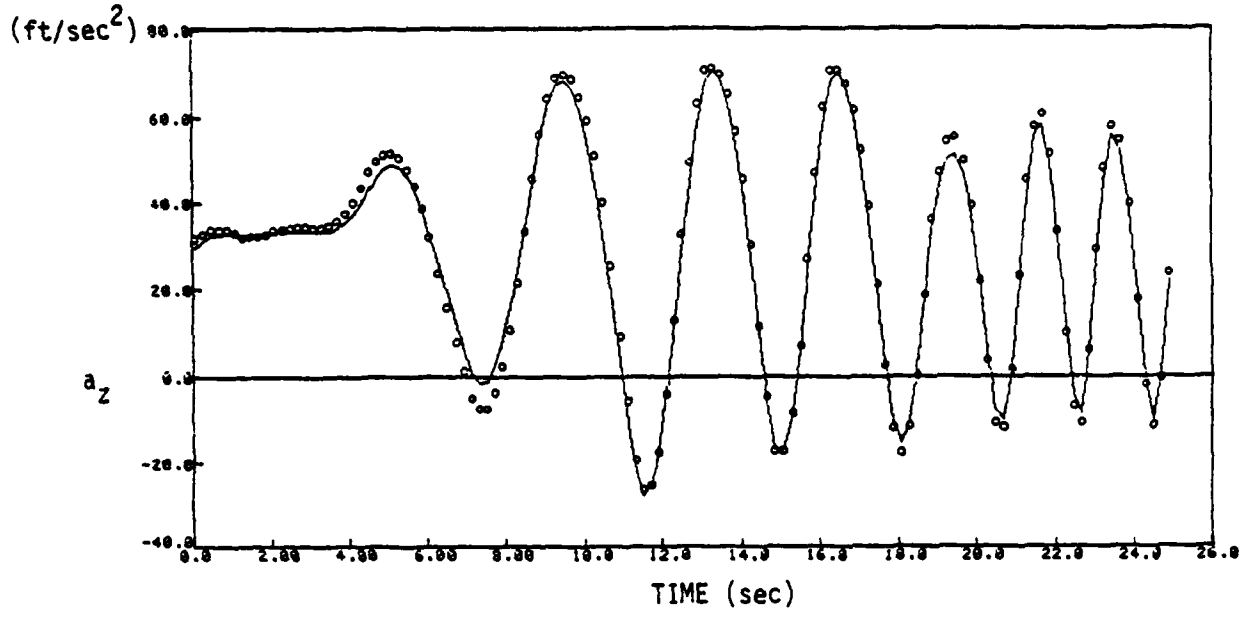

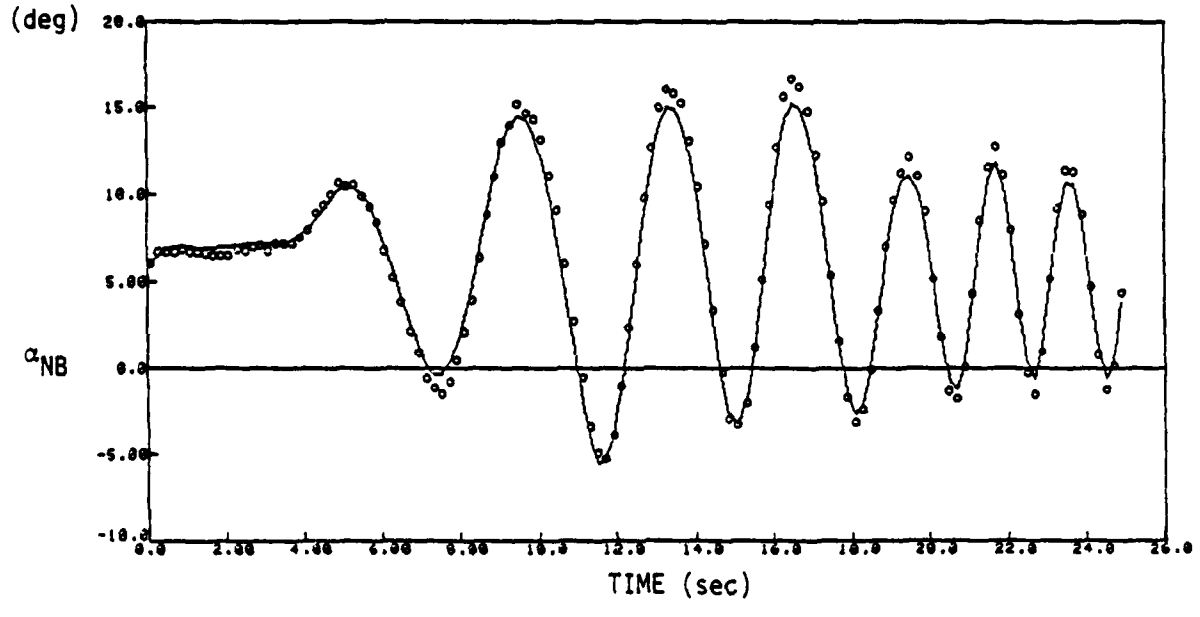

——————— Estimate from Identified Aerodynamic Model

o o o o o Flight Test Data

Figure 5.4 Time History Plot - Cruise (HSI) (Cont'd)

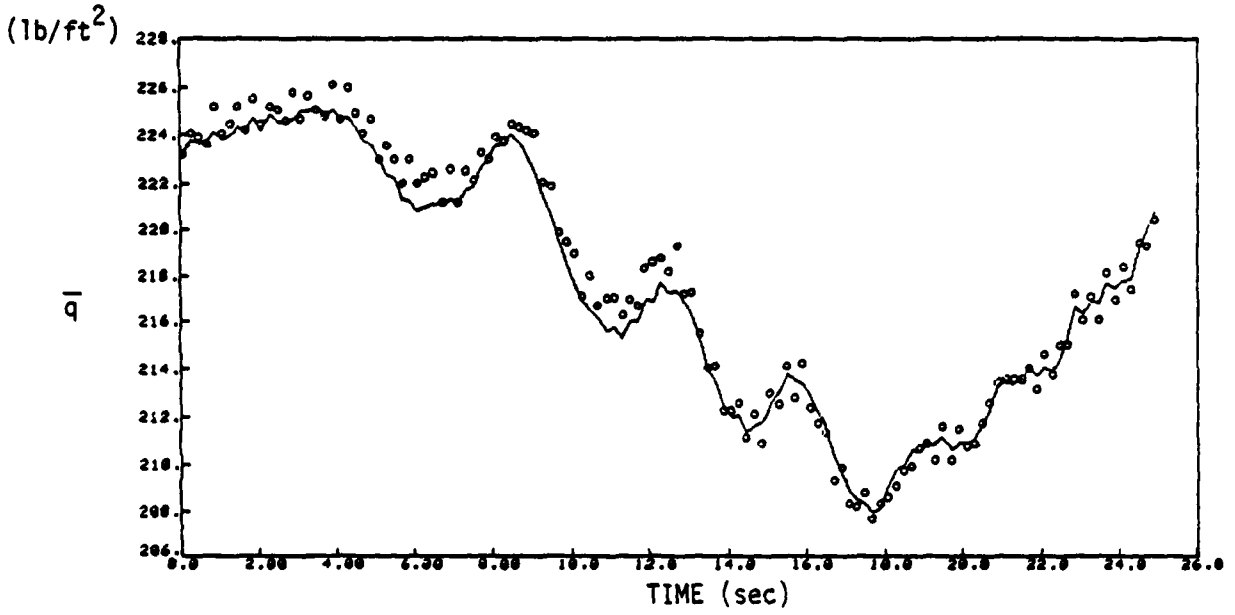

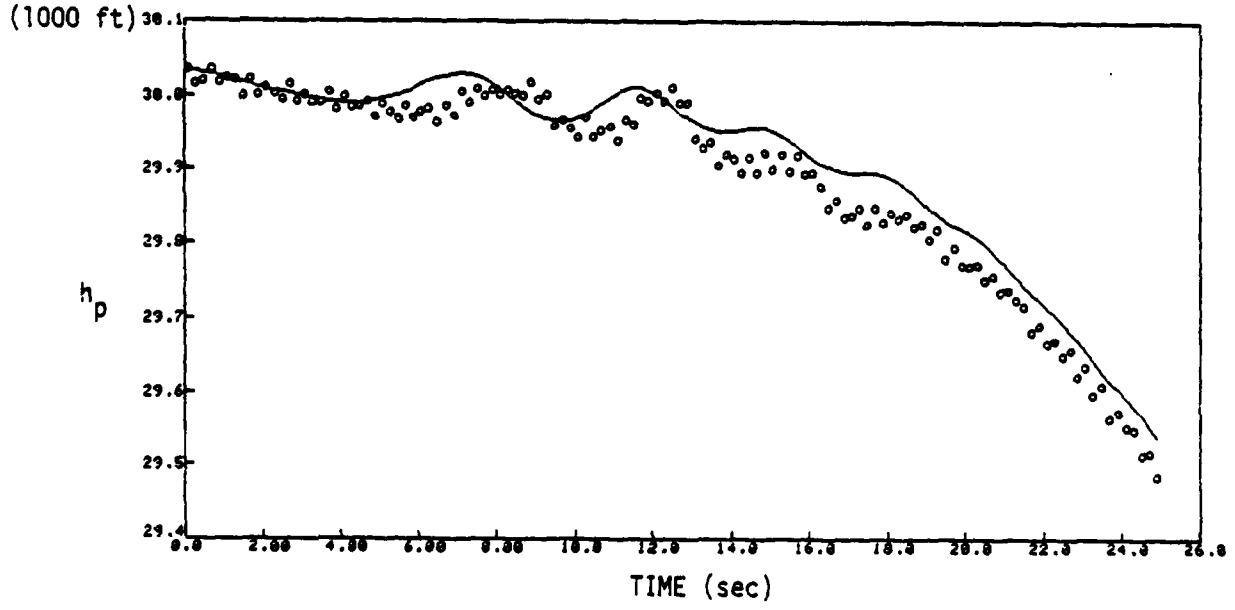

——— Estimate from Identified Aerodynamic Model

o o o o o Flight Test Data

Figure 5.4 Time History Plot - Cruise (HSI) (Cont'd)

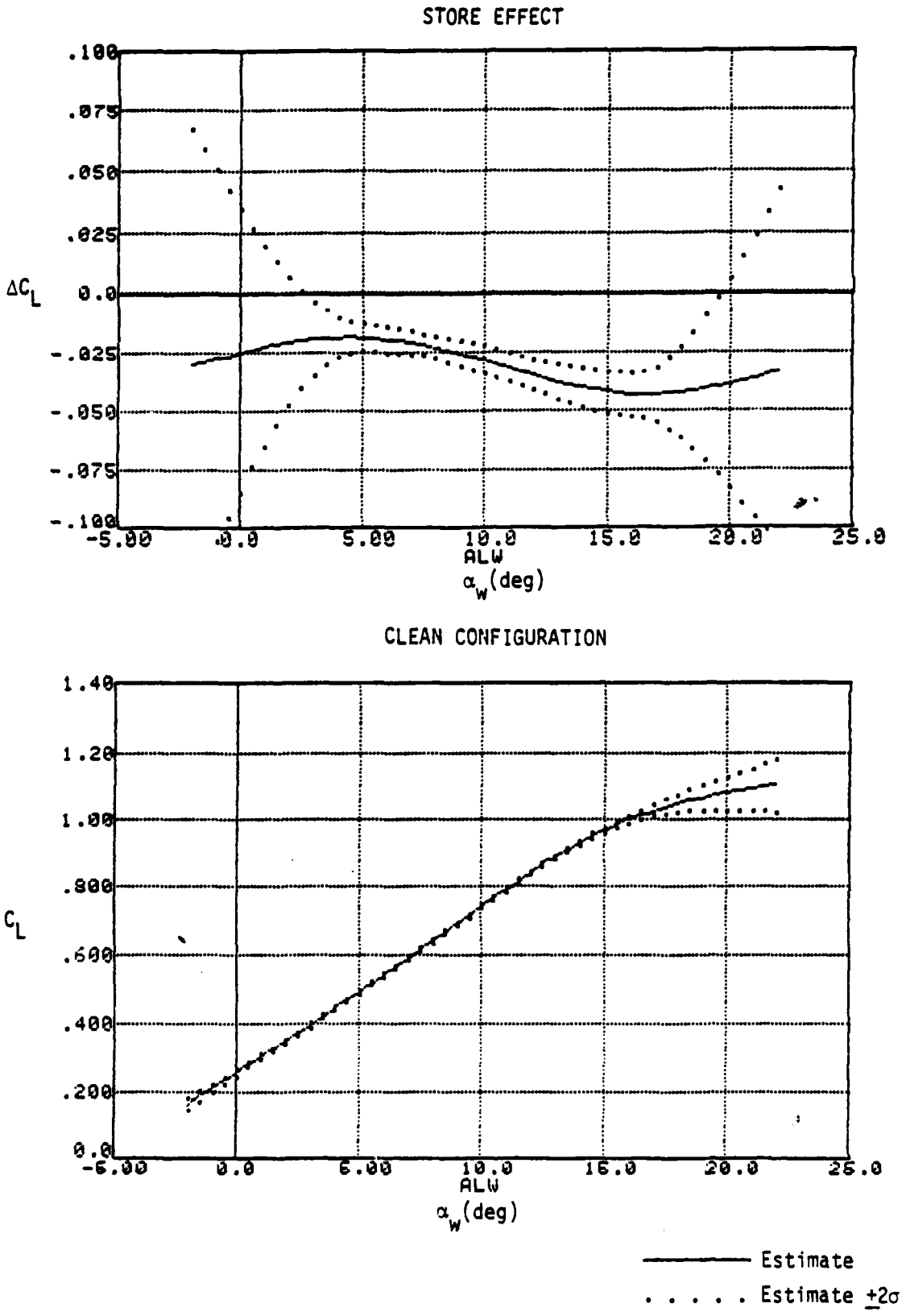

Figure 5.5 Lift Coefficient - Takeoff

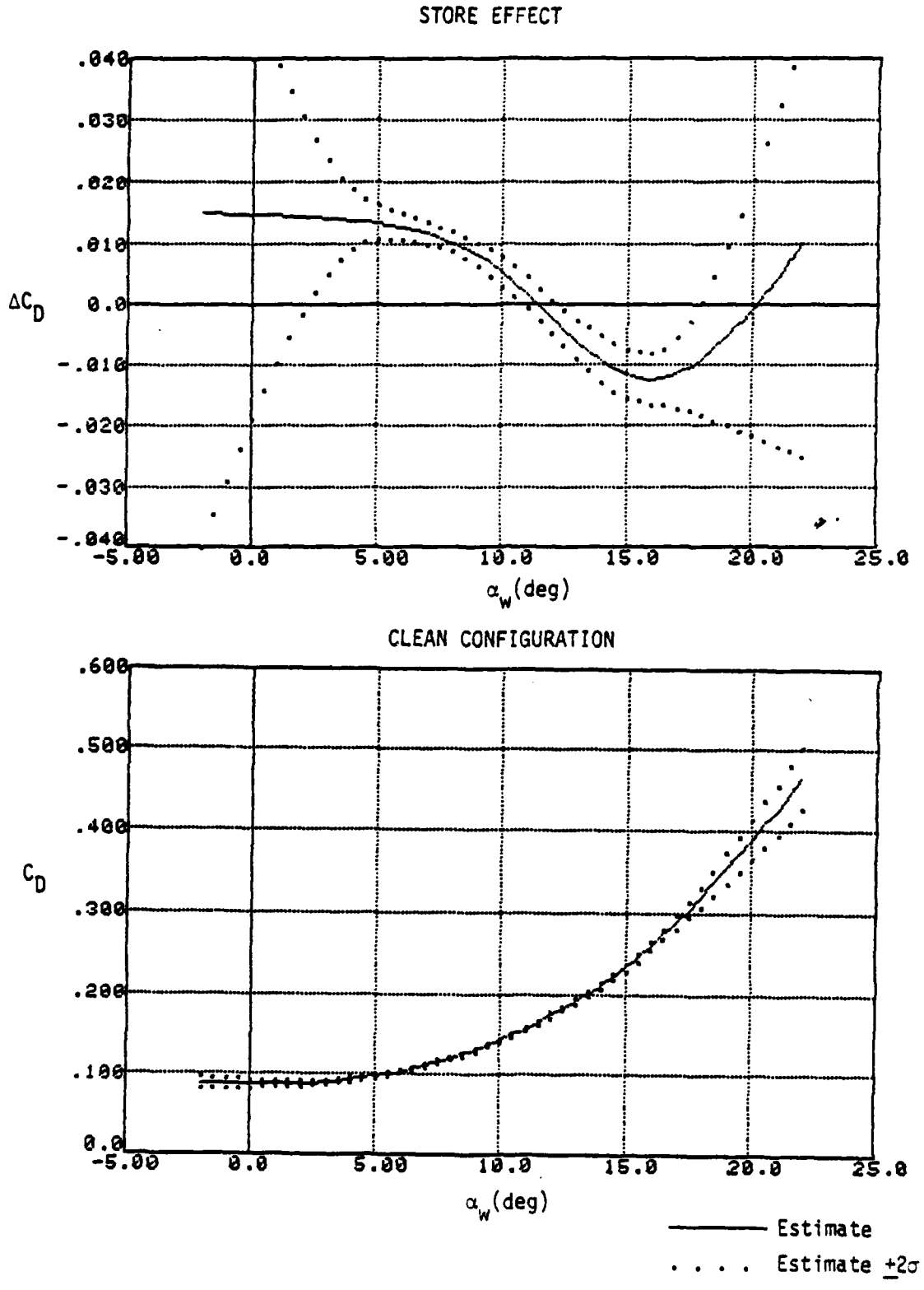

Figure 5.6 Drag Coefficient - Takeoff

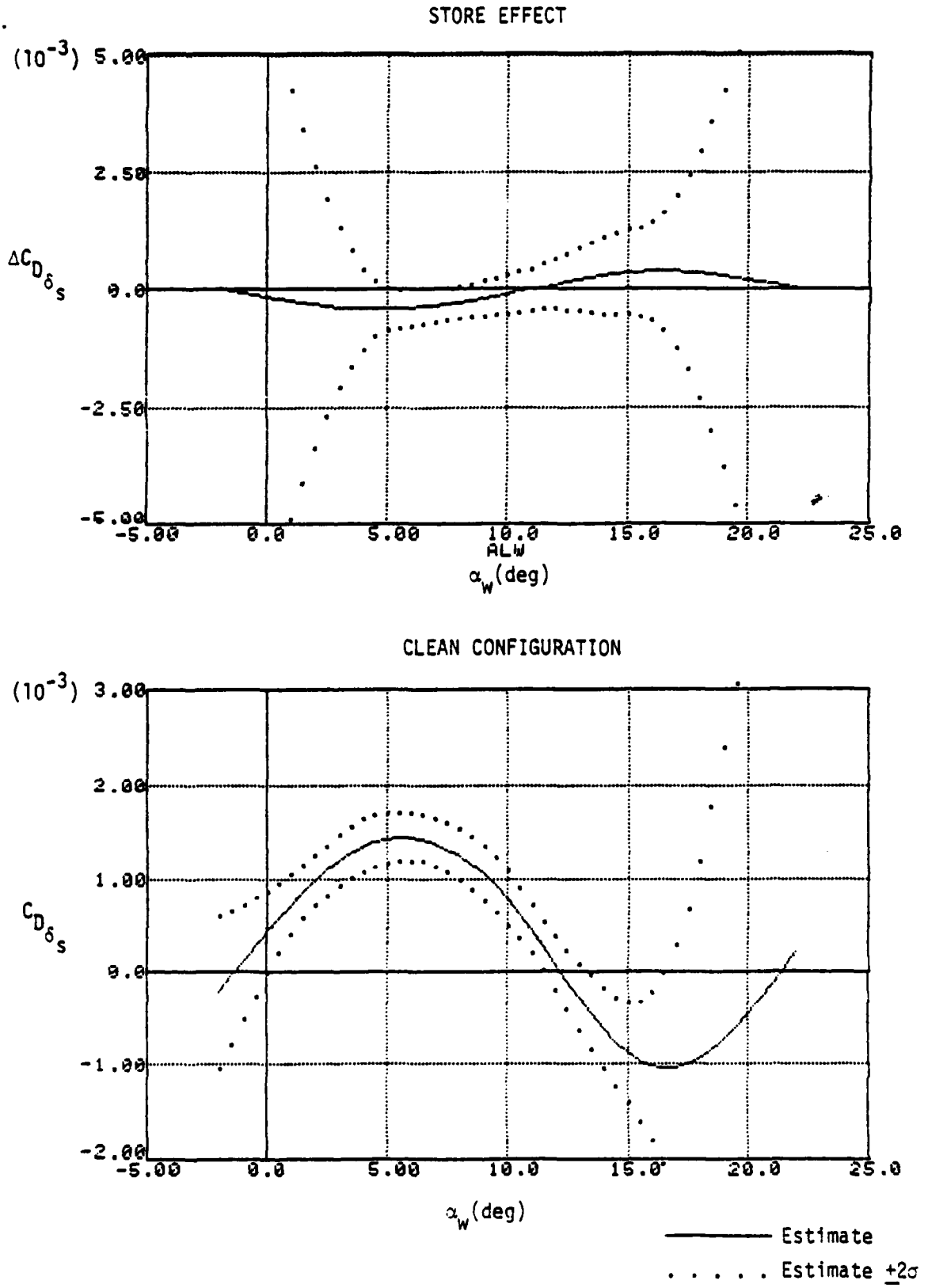

Figure 5.7 Drag Coefficient due to Stabilator - Takeoff

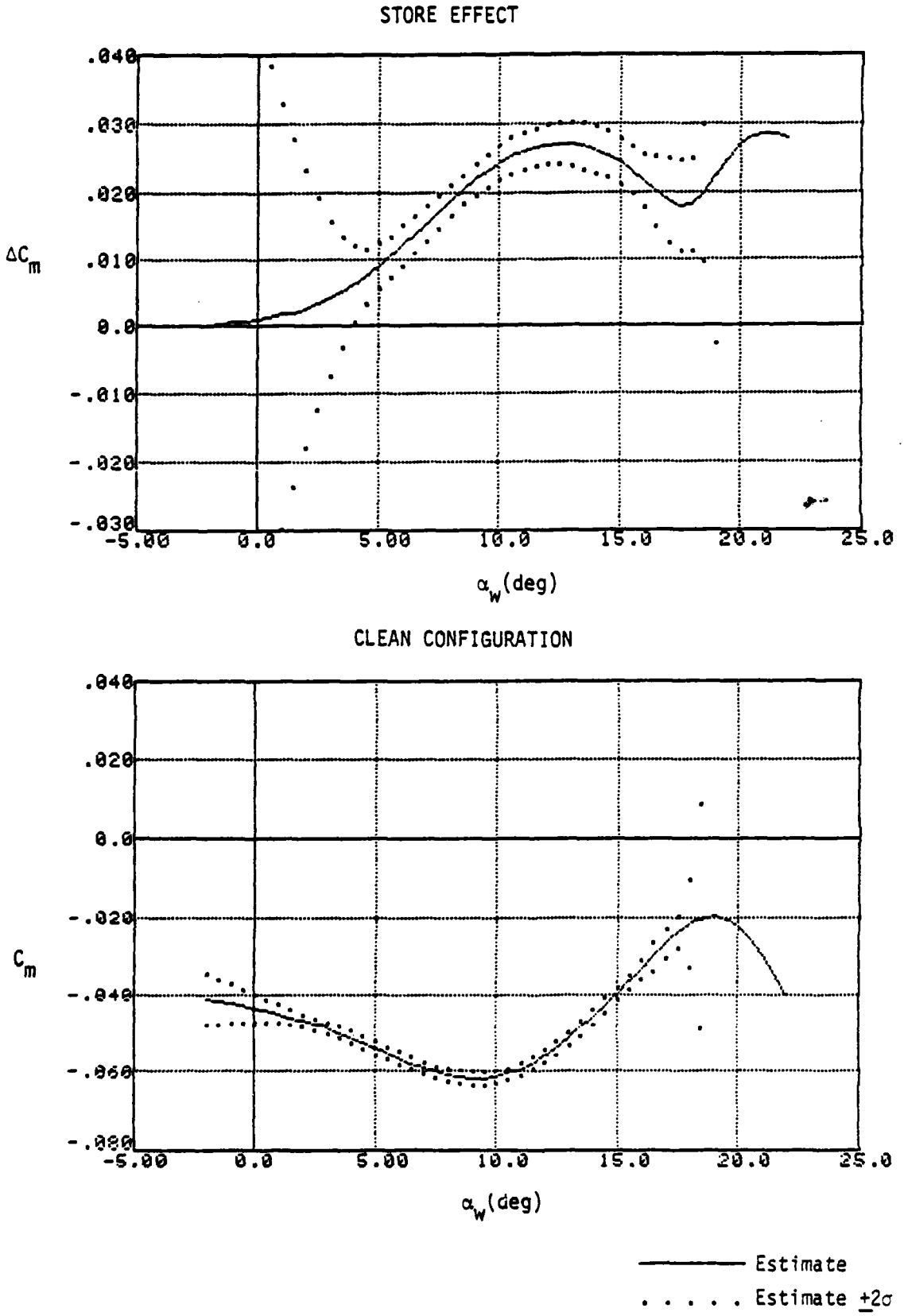

Figure 5.8 Pitching Moment Coefficient - Takeoff

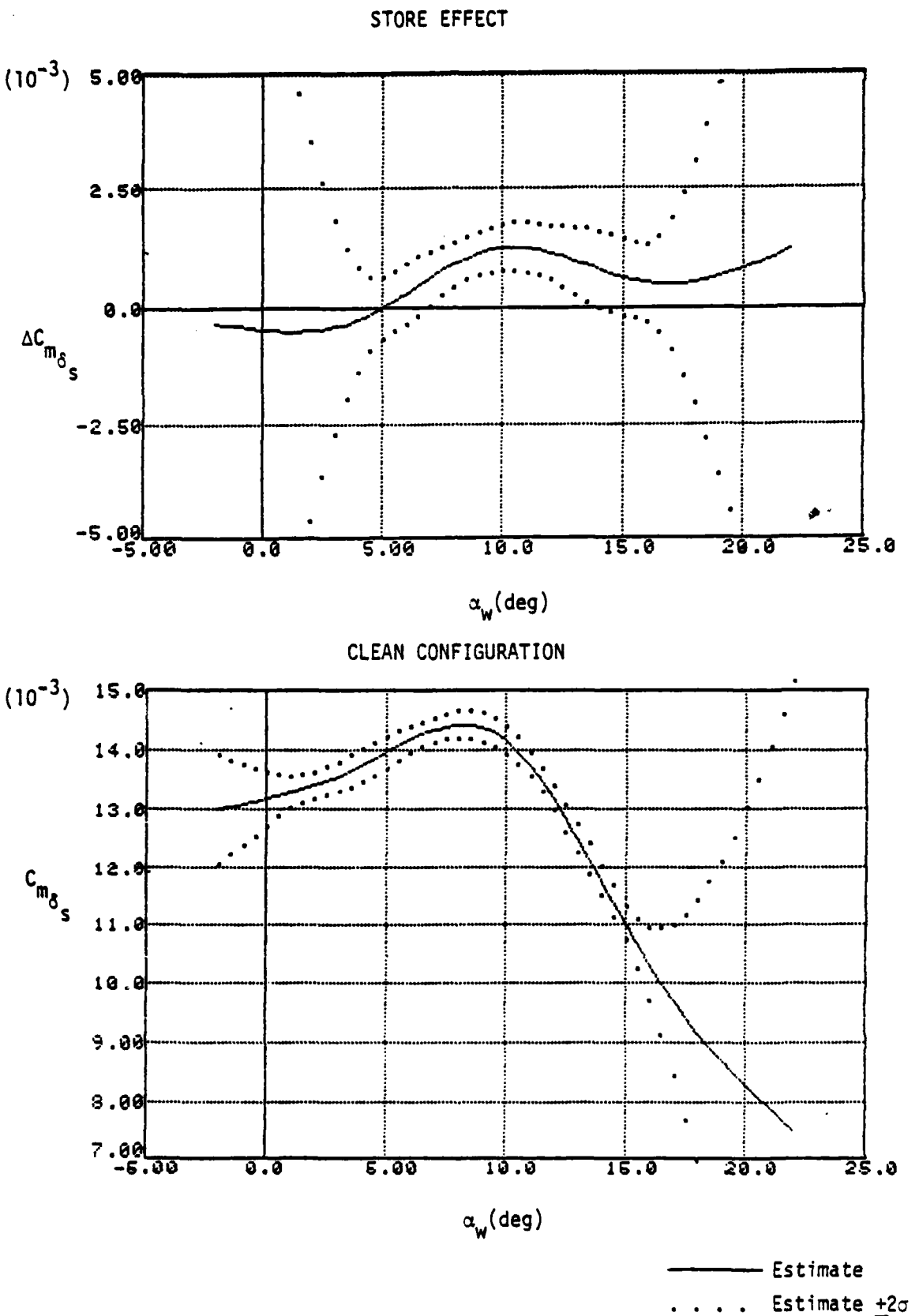

Figure 5.9 Pitching Moment Coefficient due to Stabilator - Takeoff

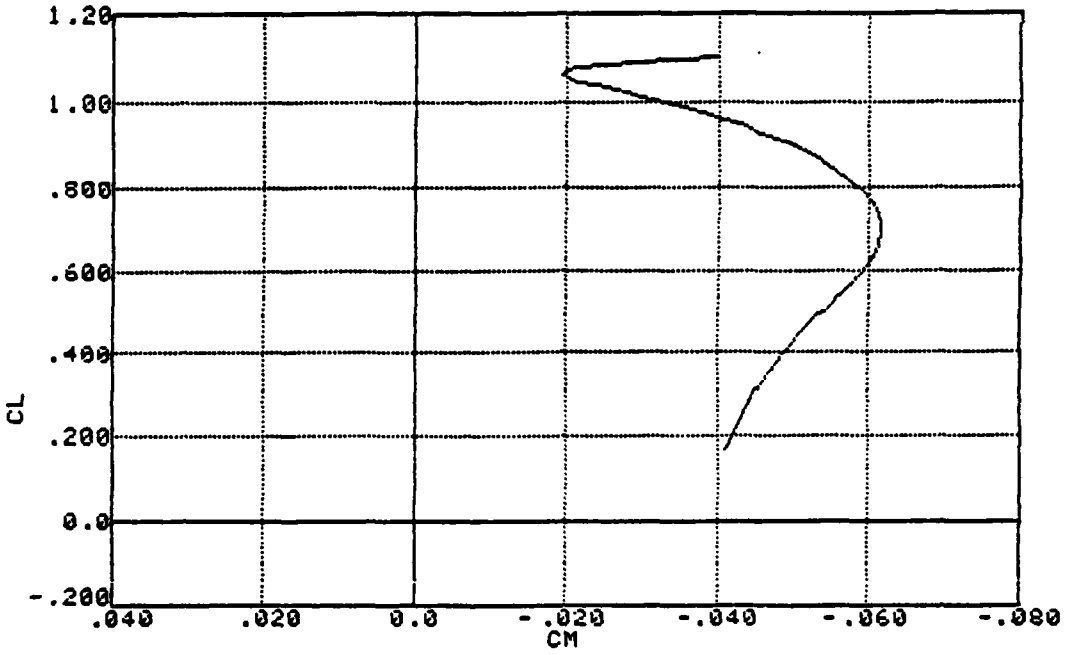

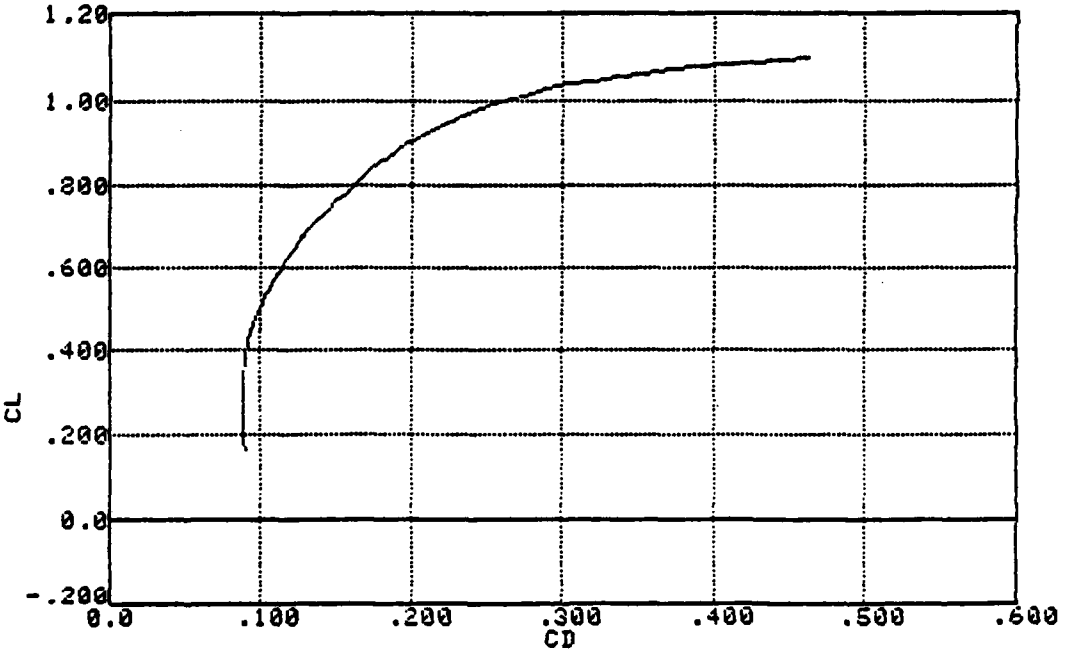

Figure 5.10 C_D and C_m versus C_L - Takeoff

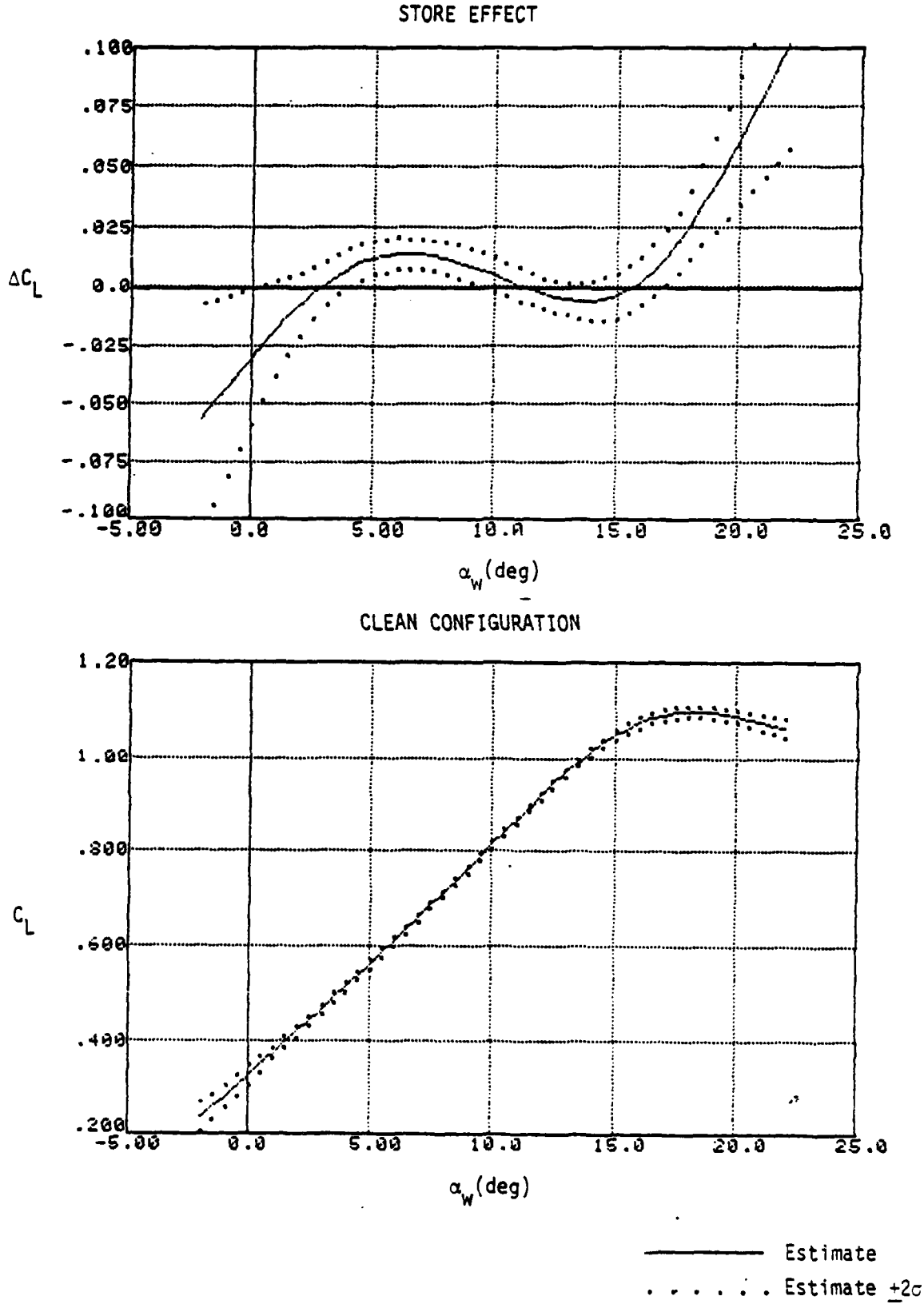

Figure 5.11 Lift Coefficient - Power Approach

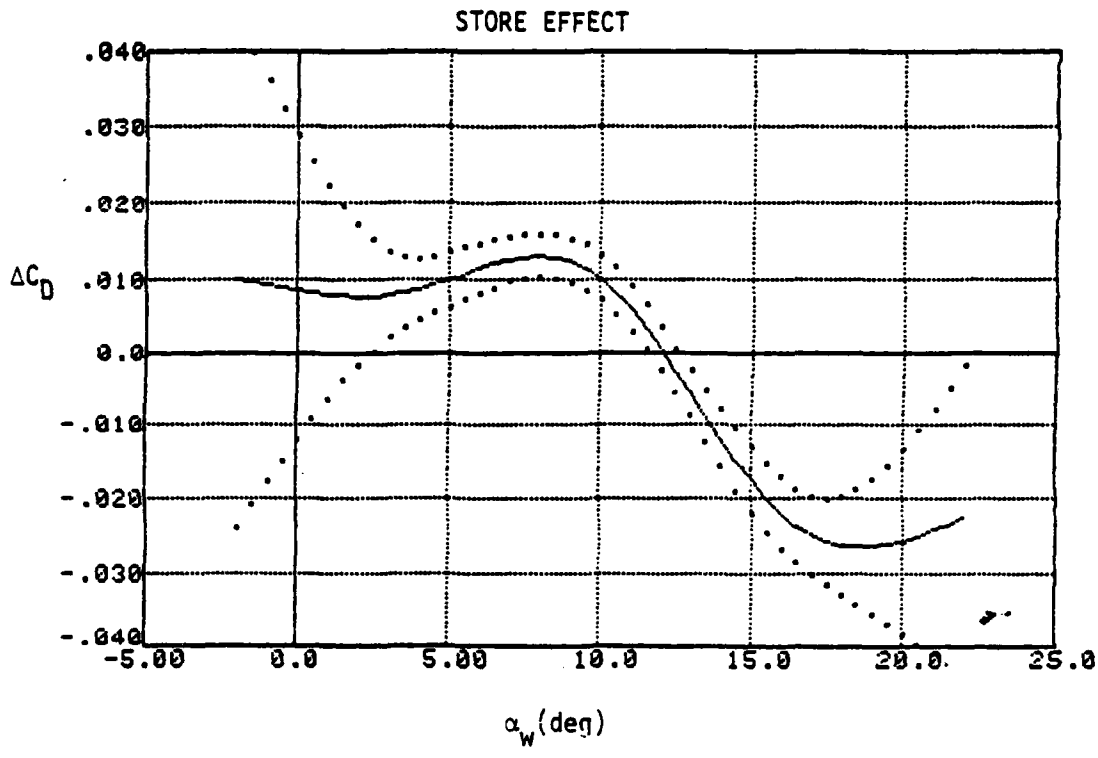

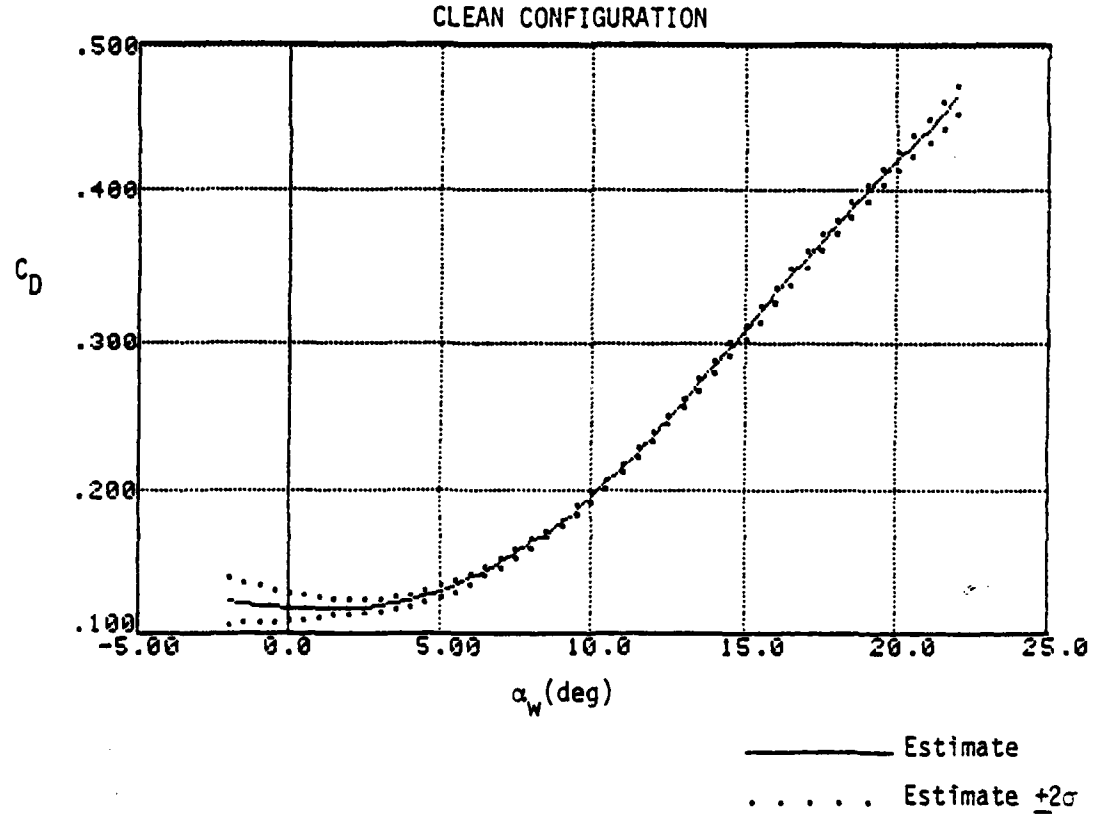

Figure 5.12 Drag Coefficient - Power Approach

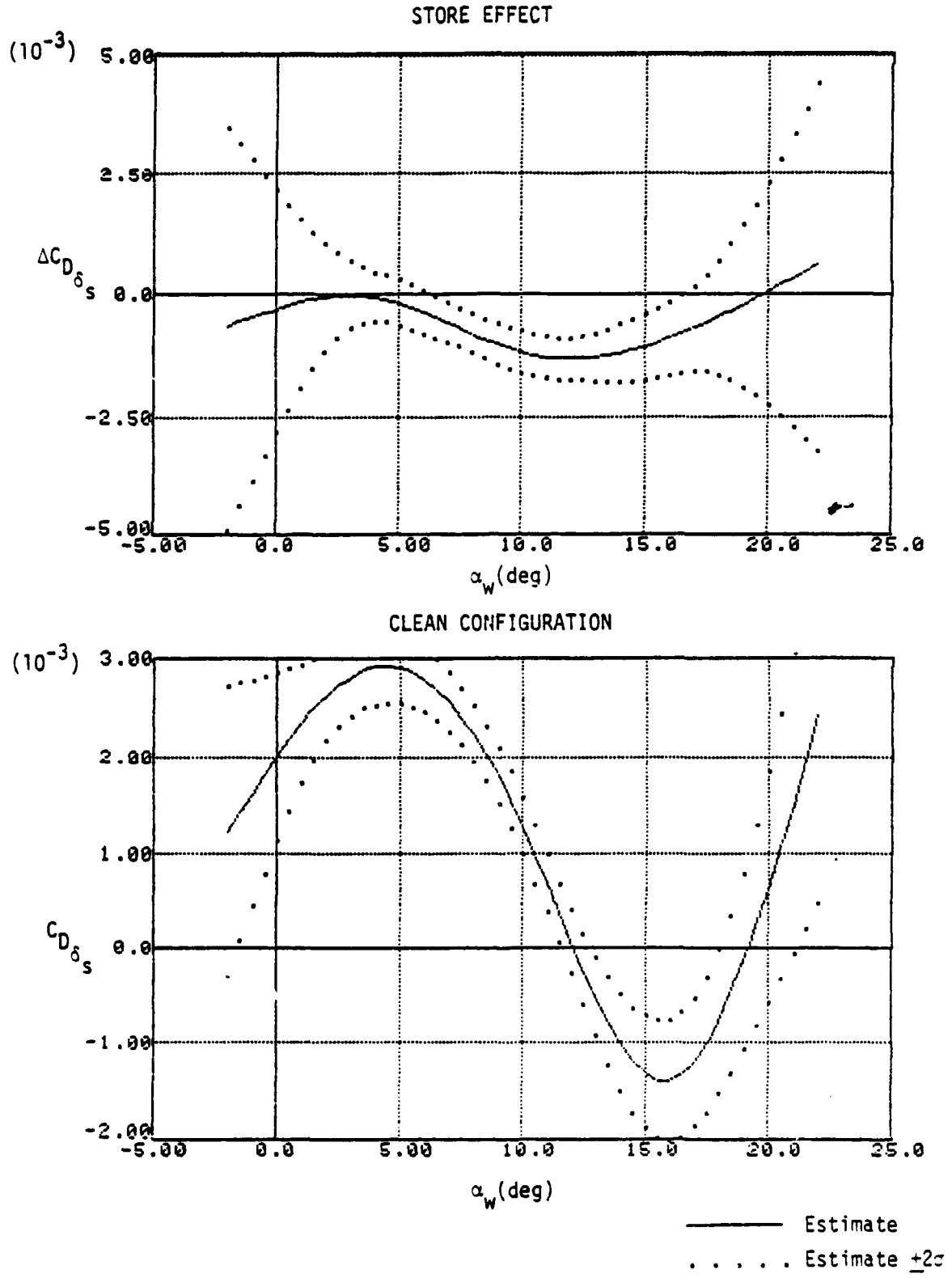

Figure 5.13 Drag Coefficient due to Stabilator - Power Approach

AD-A146 289 NONLINEAR SYSTEM IDENTIFICATION METHODOLOGY DEVELOPMENT 2/2
BASED ON F-4S FLI..(U) SYSTEMS CONTROL TECHNOLOGY INC
PALO ALTO CA J H VINCENT ET AL. DEC 83
UNCLASSIFIED N00421-81-C-0289 F/G 14/2 NL

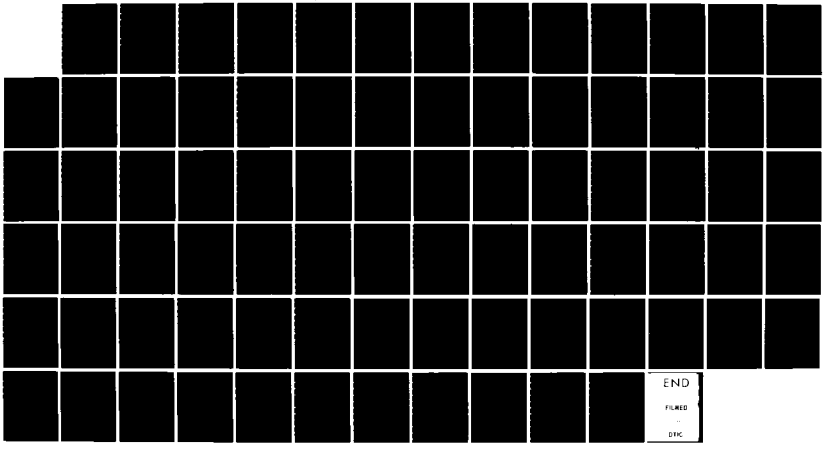

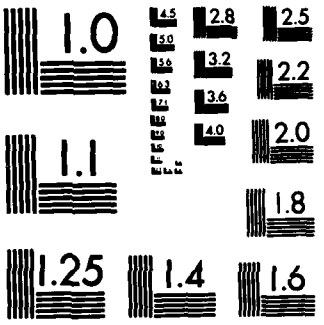

MICROCOPY RESOLUTION TEST CHART

STORE EFFECT

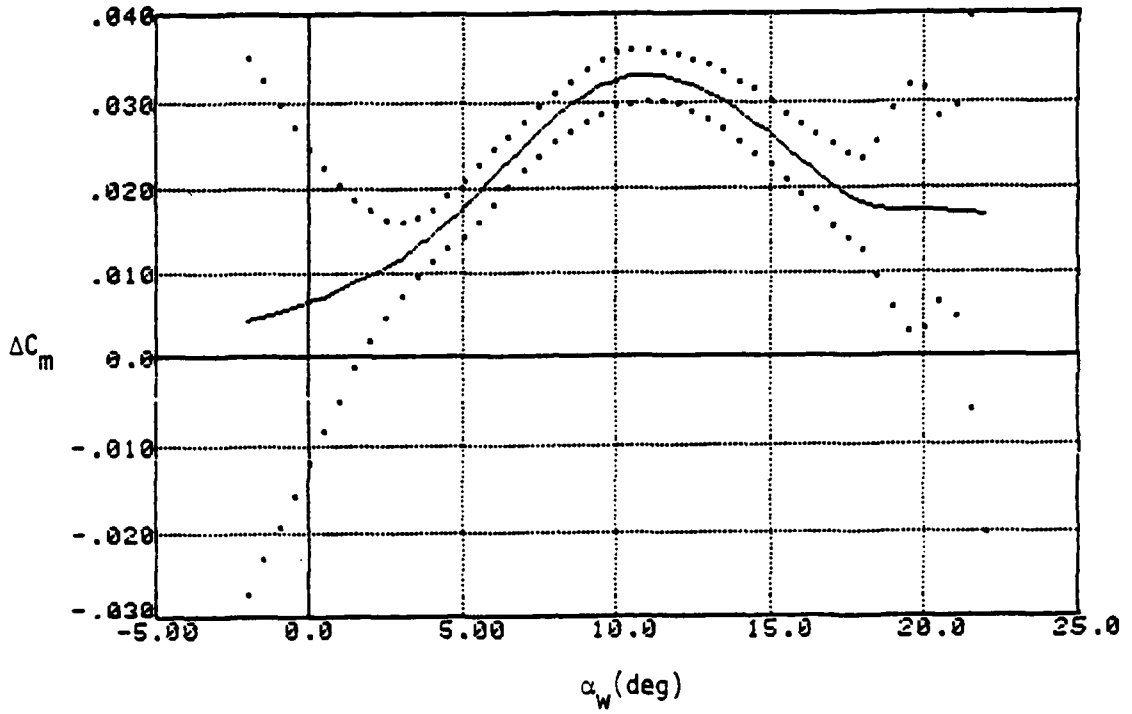

CLEAN CONFIGURATION

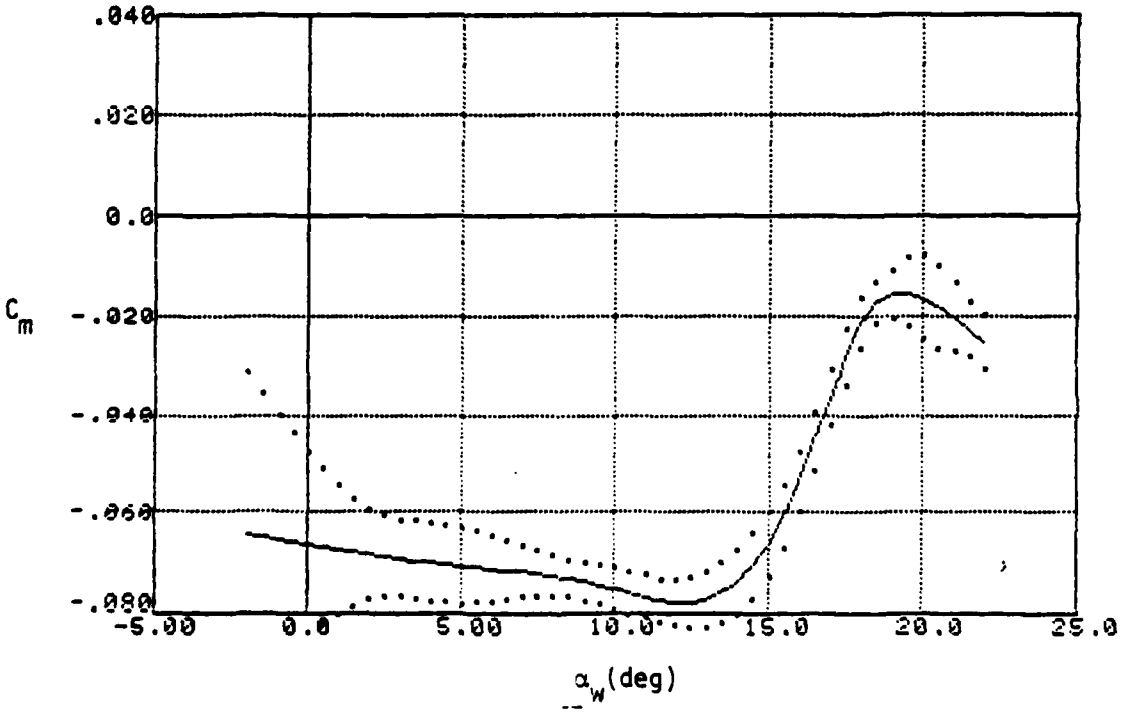

Estimate

Estimate ±2σ

Figure 5.14 Pitching Moment Coefficient - Power Approach

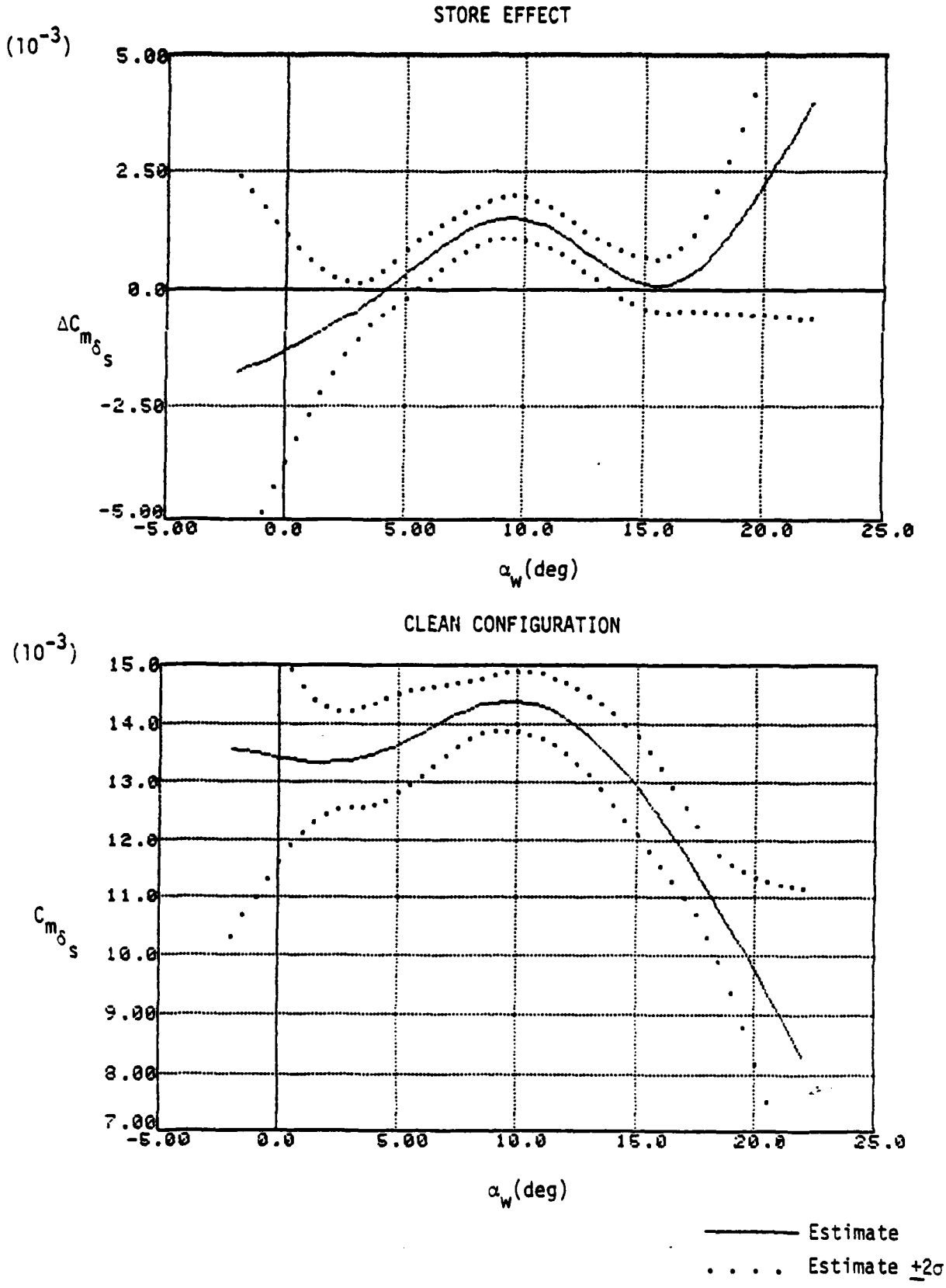

Figure 5.15 Pitching Moment Coefficient due to Stabilator - Power Approach

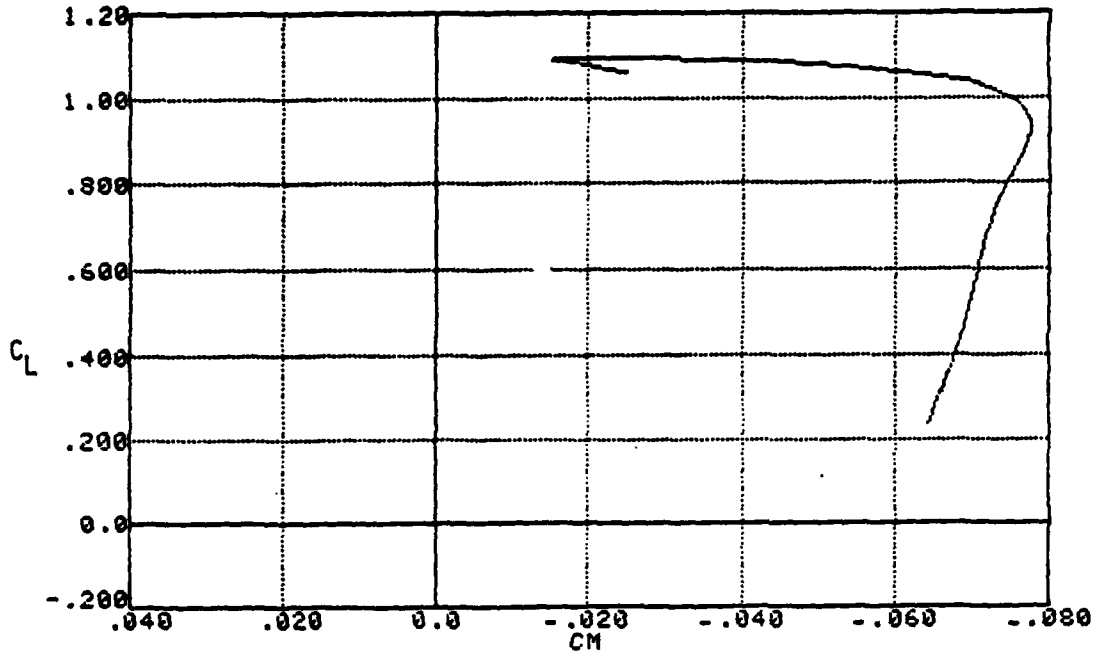

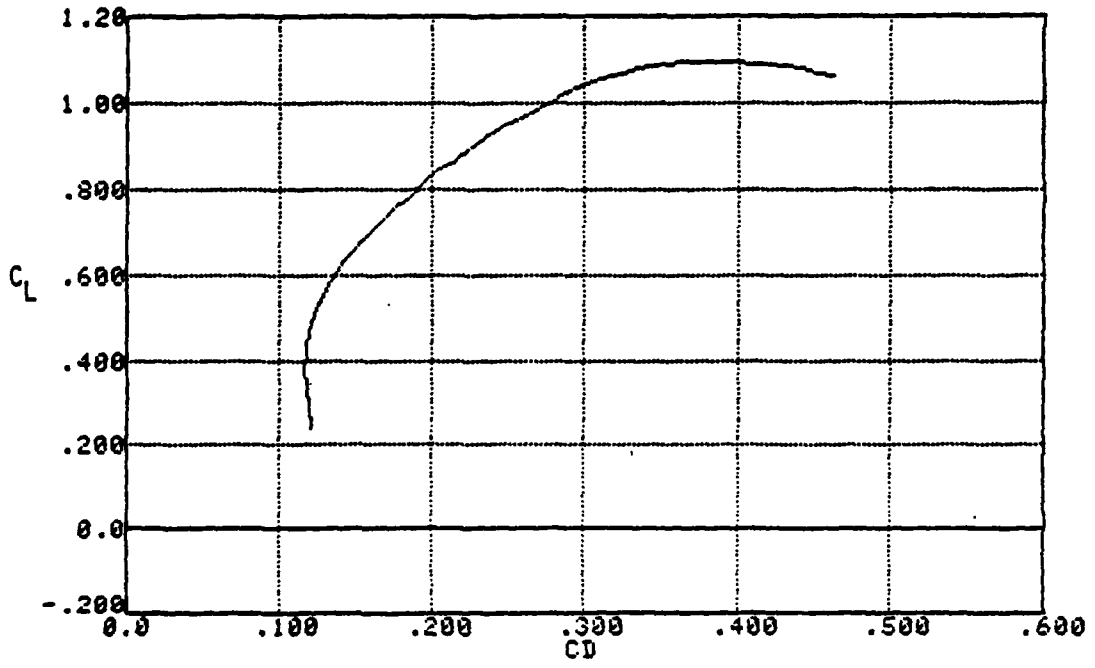

Figure 5.16 C_D and C_m versus C_L - Power Approach

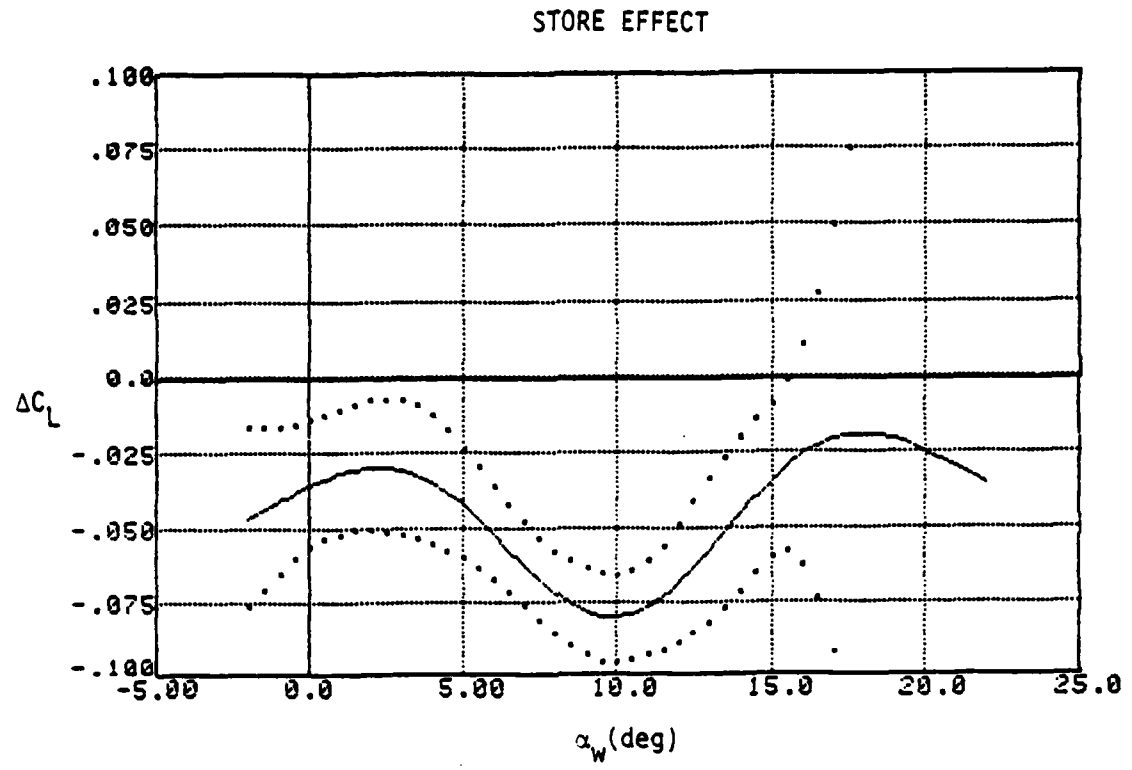

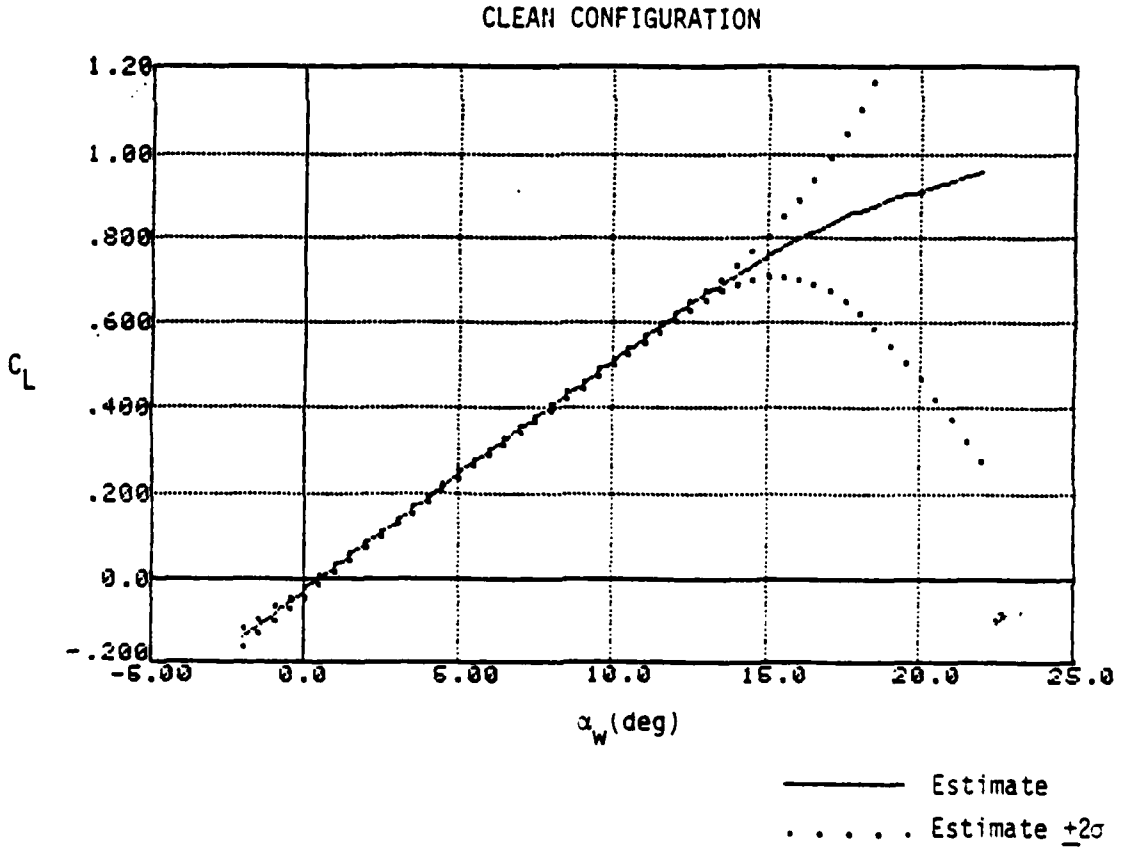

Figure 5.17 Lift Coefficient - Cruise (M = .7)

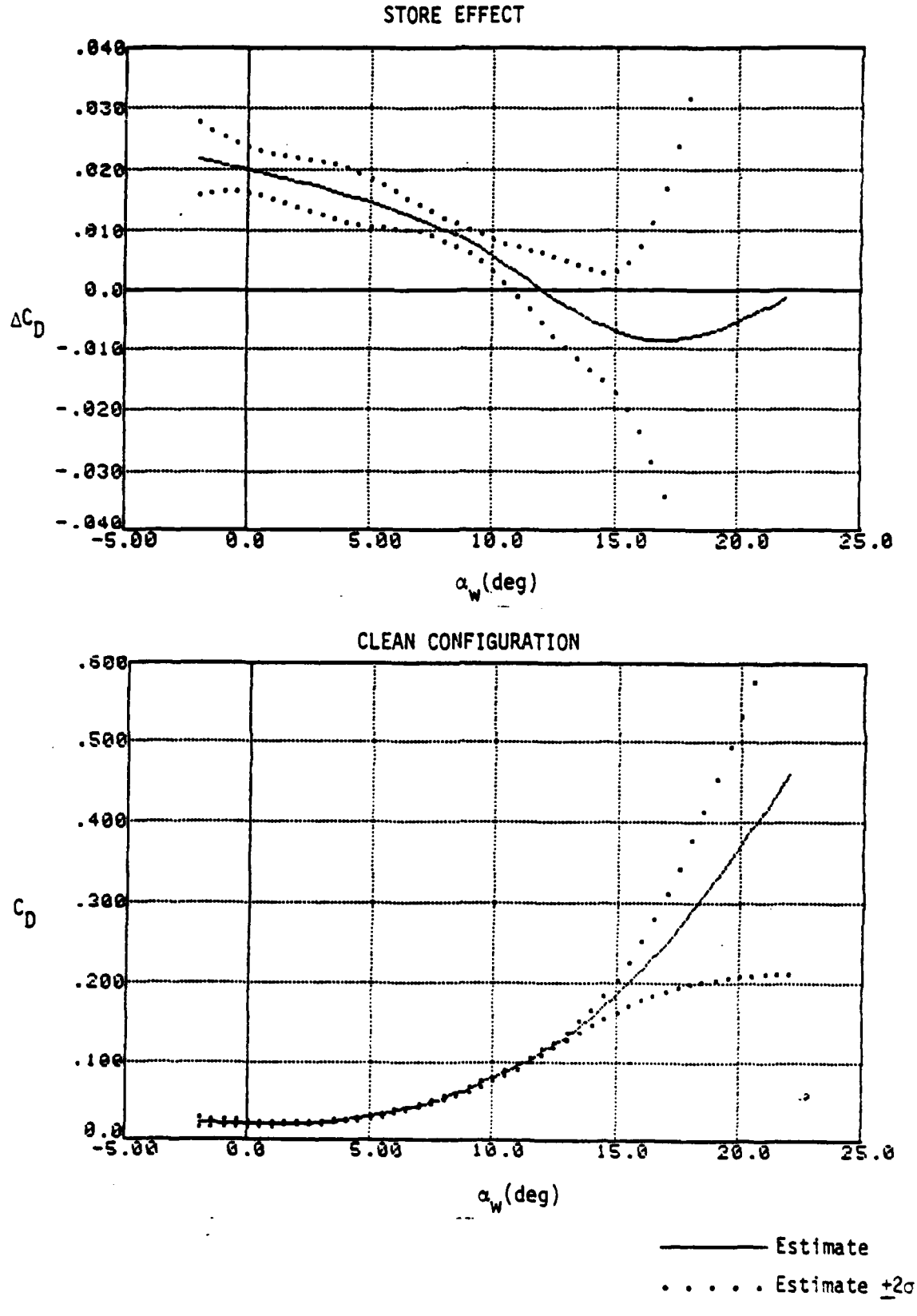

Figure 5.18 Drag Coefficient - Cruise (M - .7)

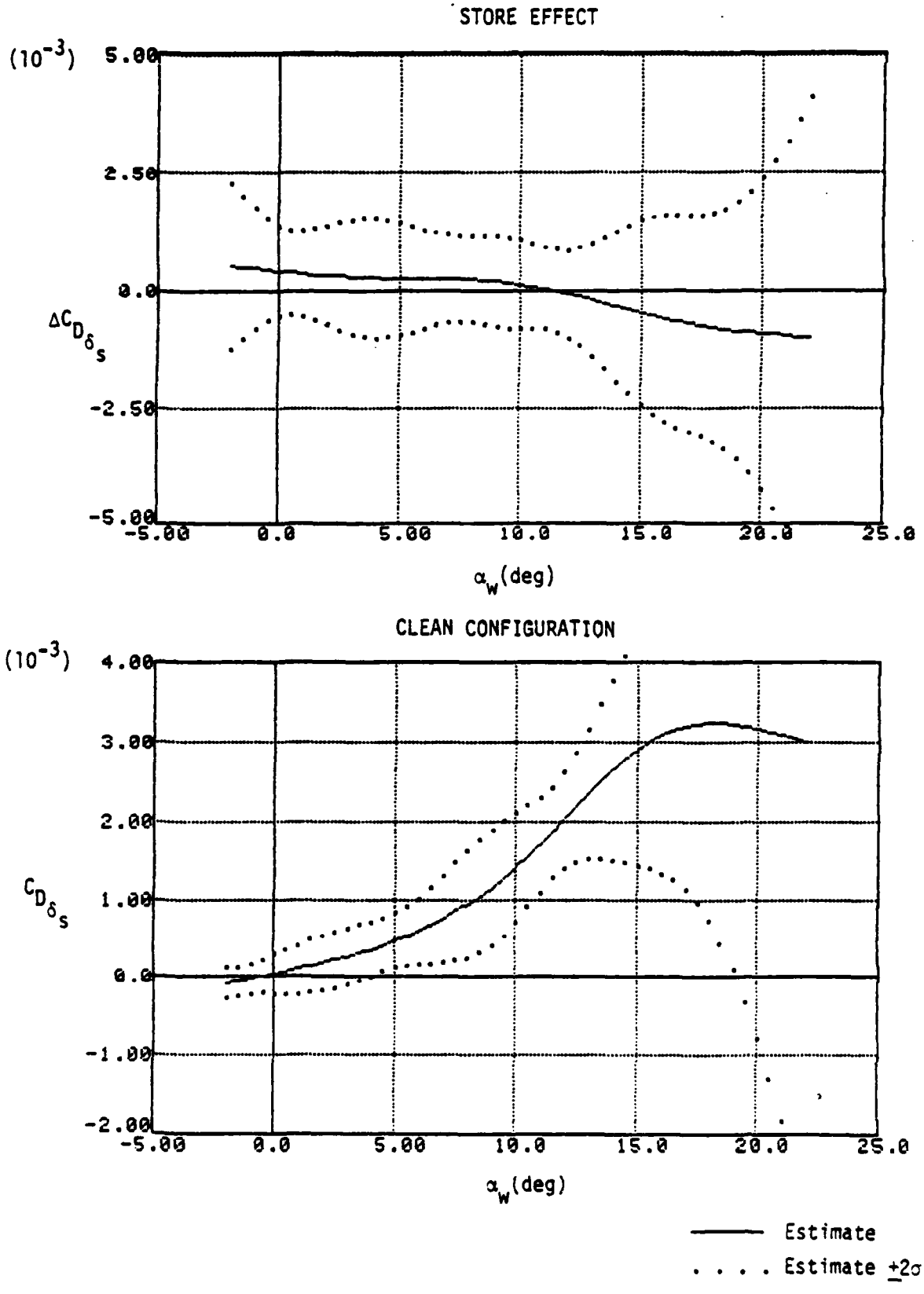

Figure 5.19 Drag Coefficient due to Stabilator - Cruise (M = .7)

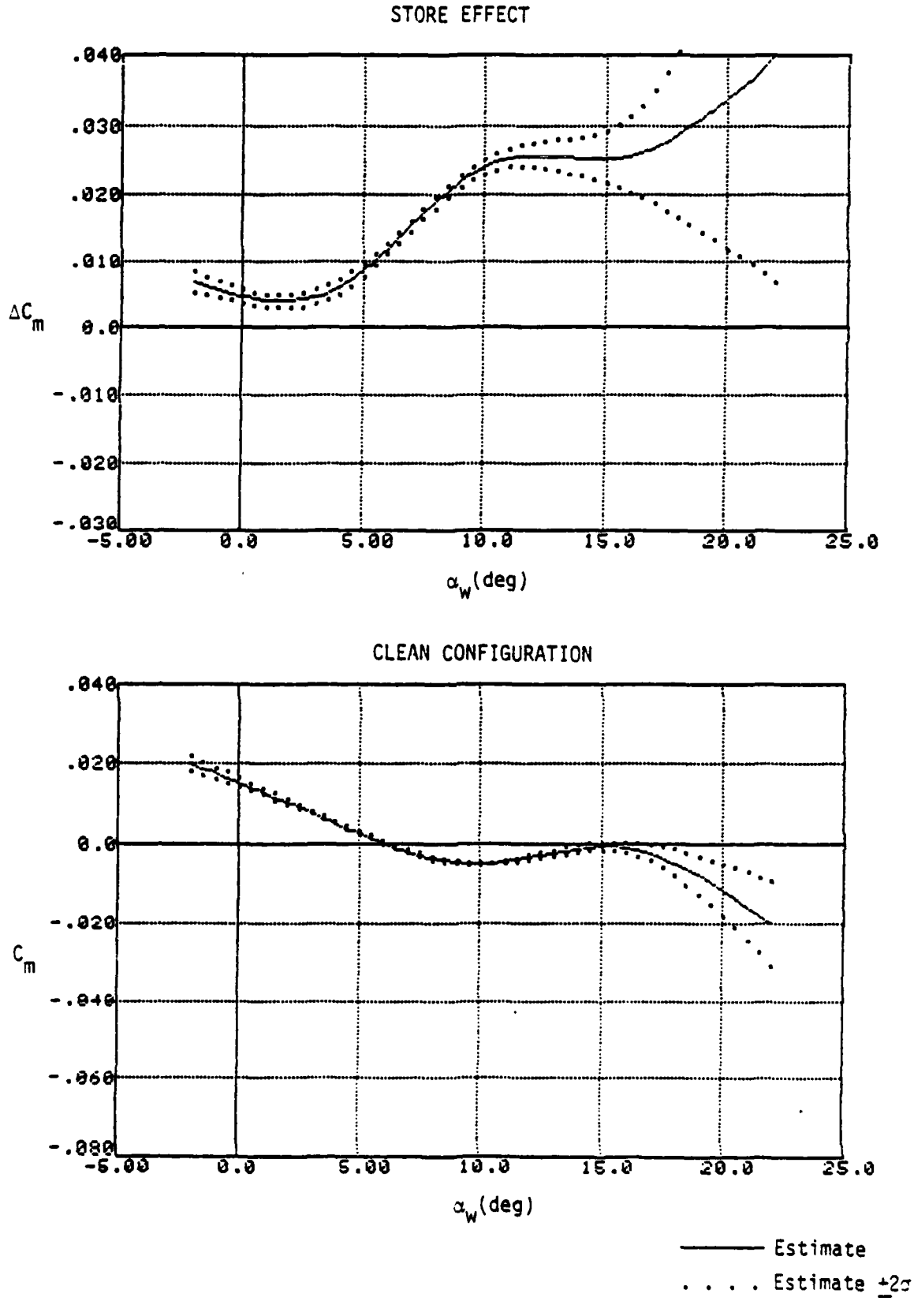

Figure 5.20. Pitching Moment Coefficient - Cruise (M = .7)

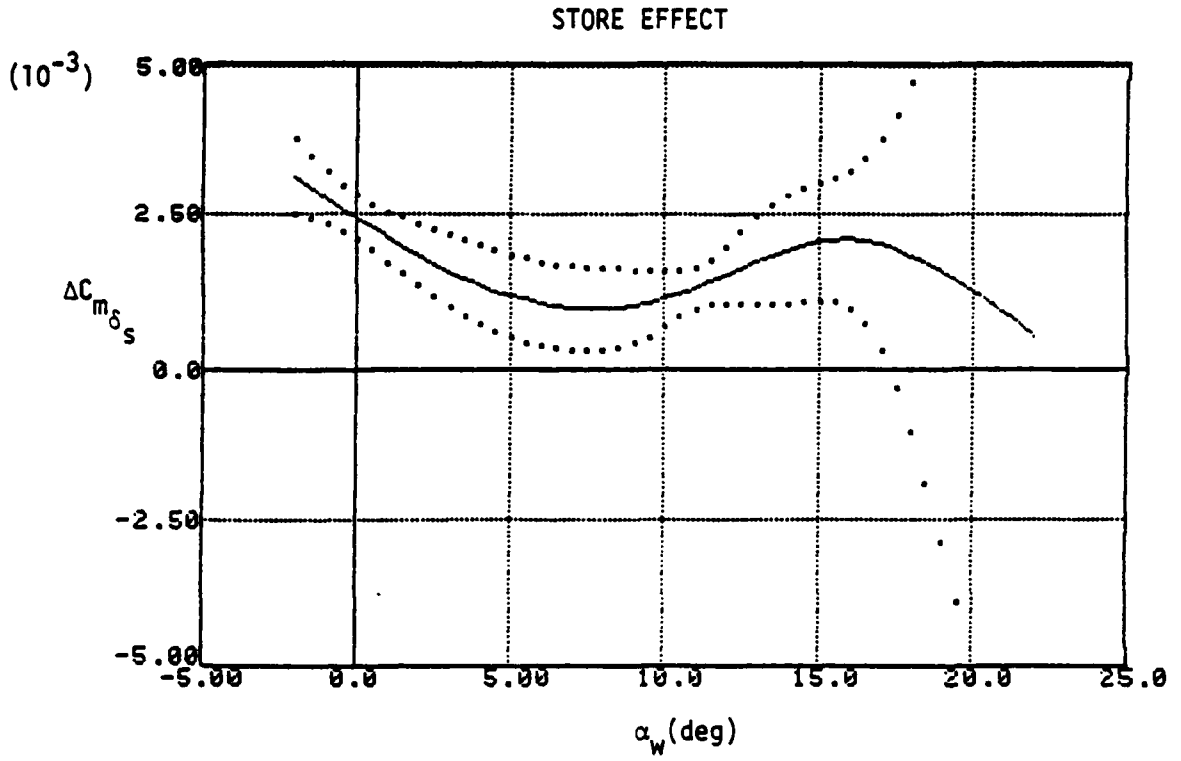

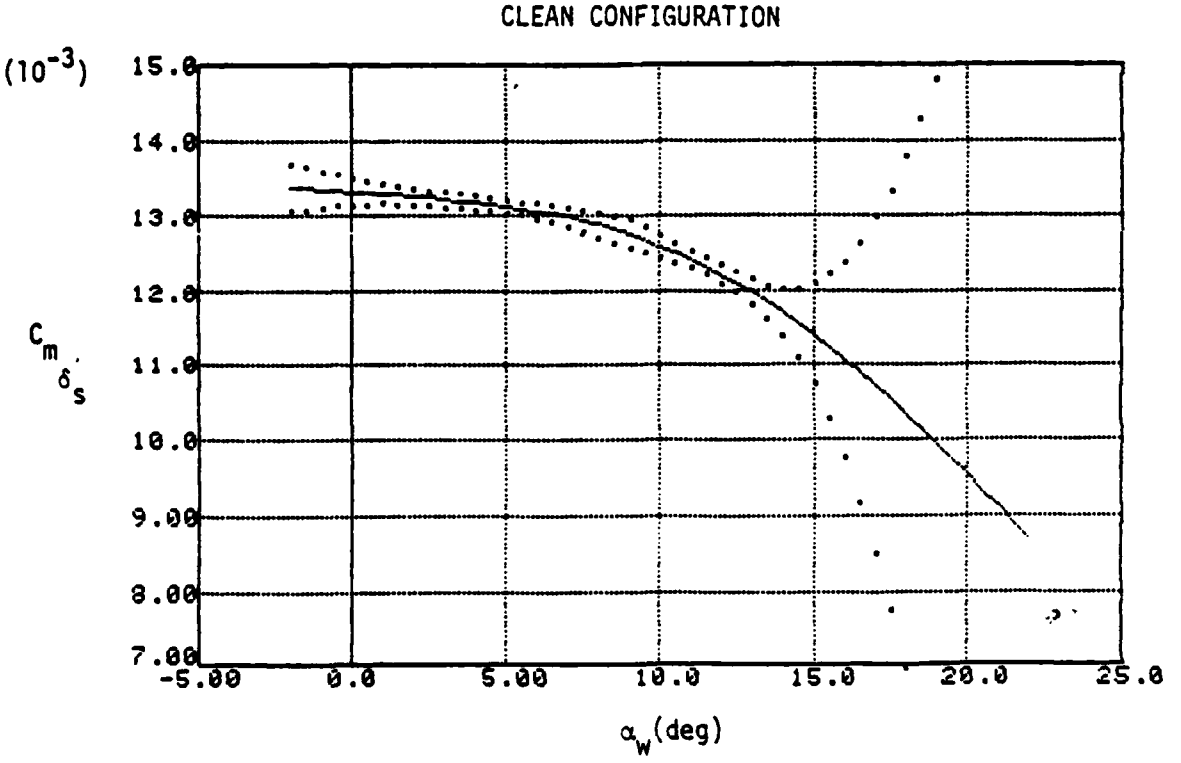

Figure 5.21 Pitching Moment Coefficient due to Stabilator - Cruise (M = .7)

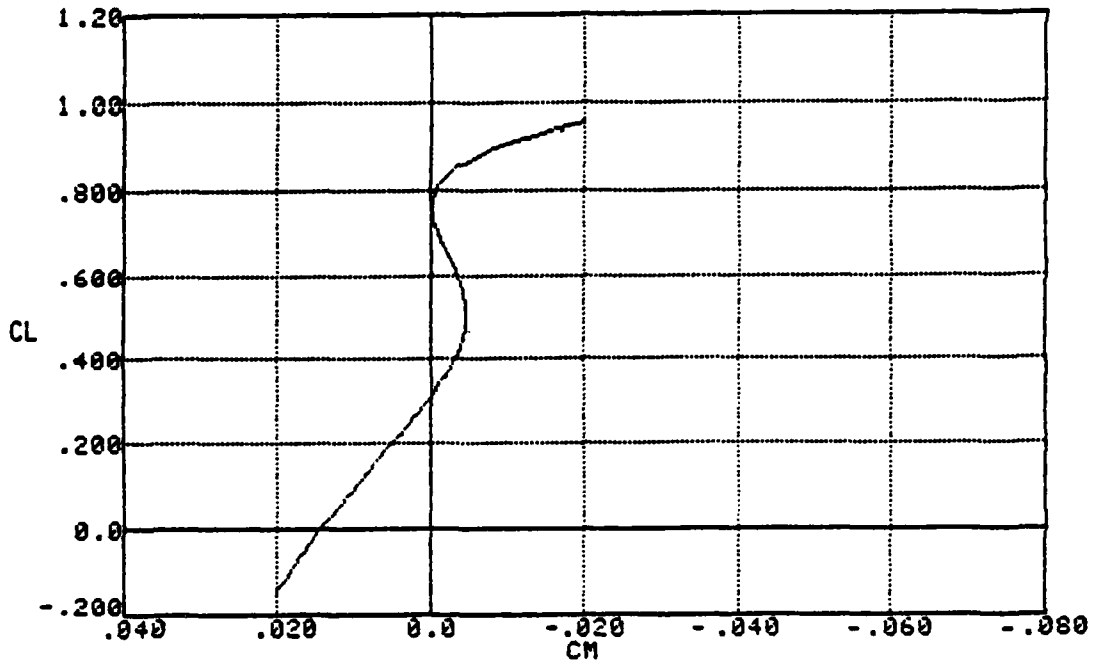

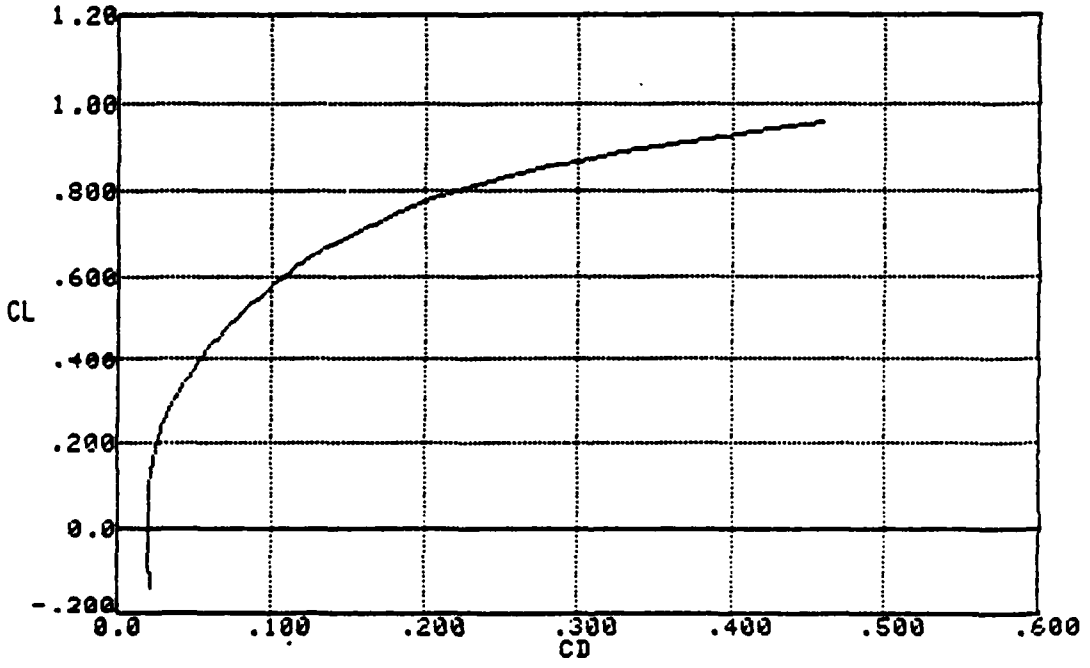

Figure 5.22 C_D and C_m versus C_L - Cruise (M = .7)

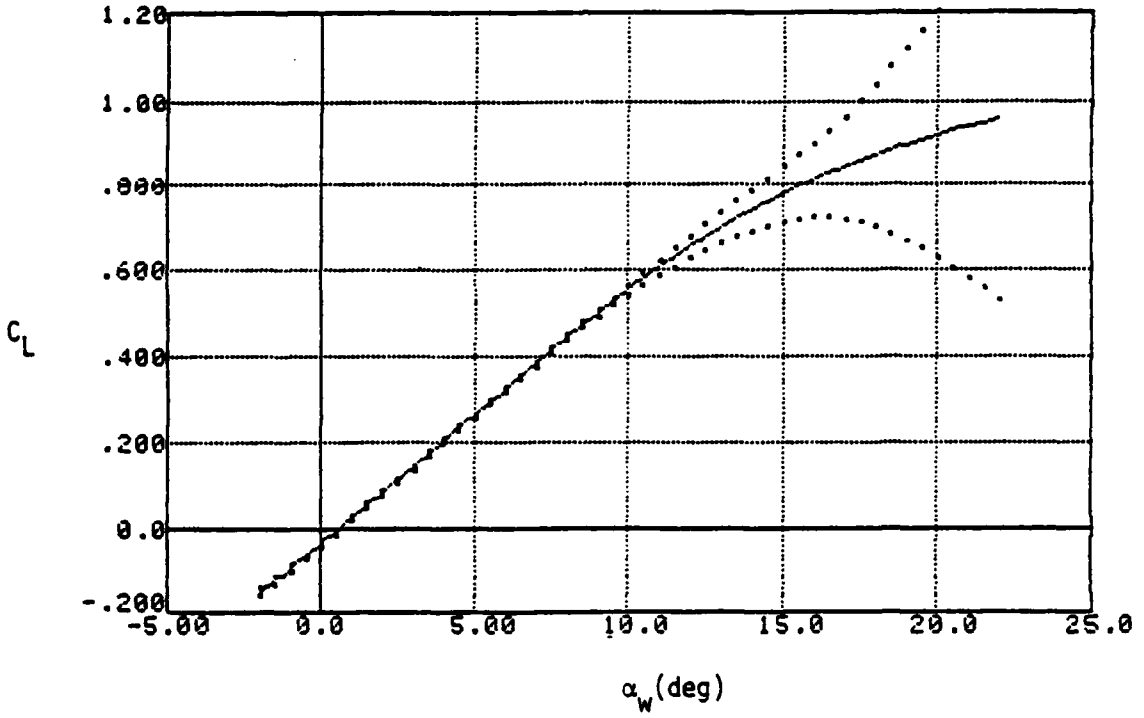

Figure 5.23 Lift Coefficient - Cruise (M = .8)

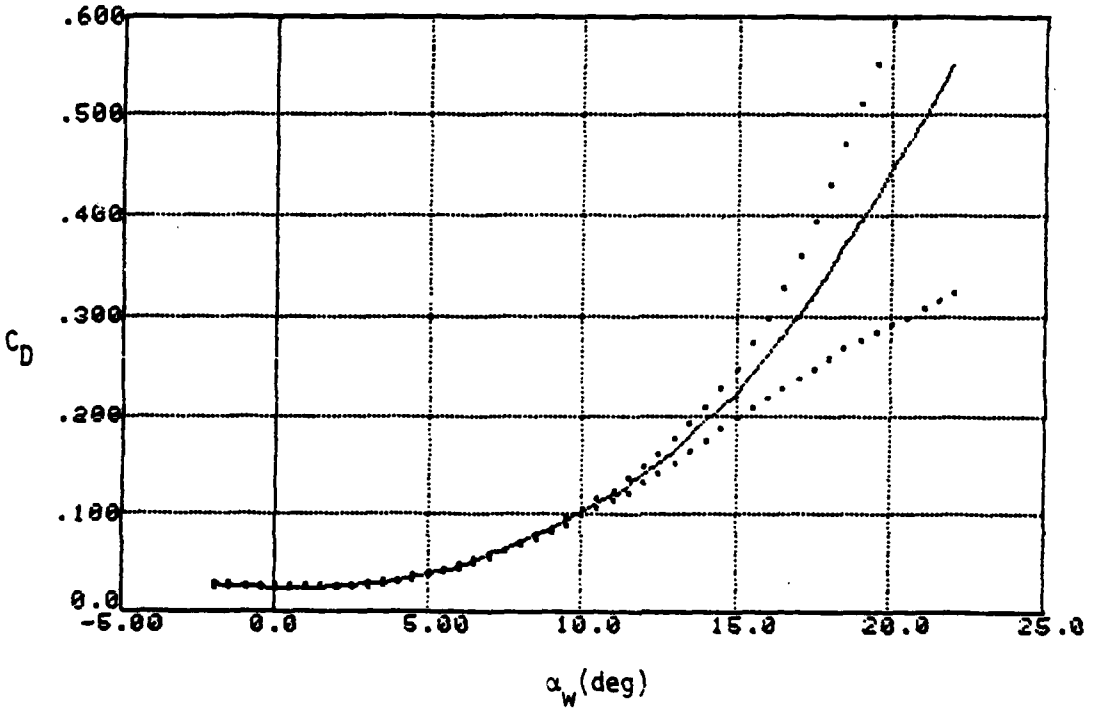

Figure 5.24 Drag Coefficient - Cruise (M = .8)

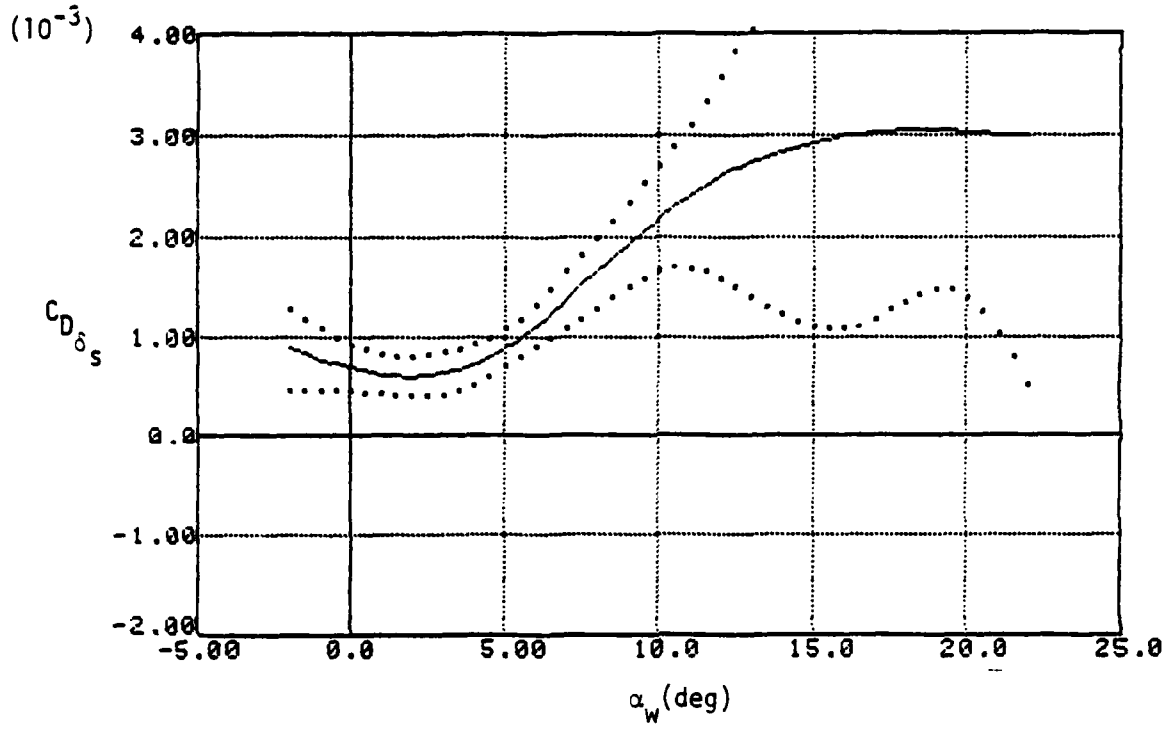

Figure 5.25 Drag Coefficient due to Stabilator - Cruise (M = .8)

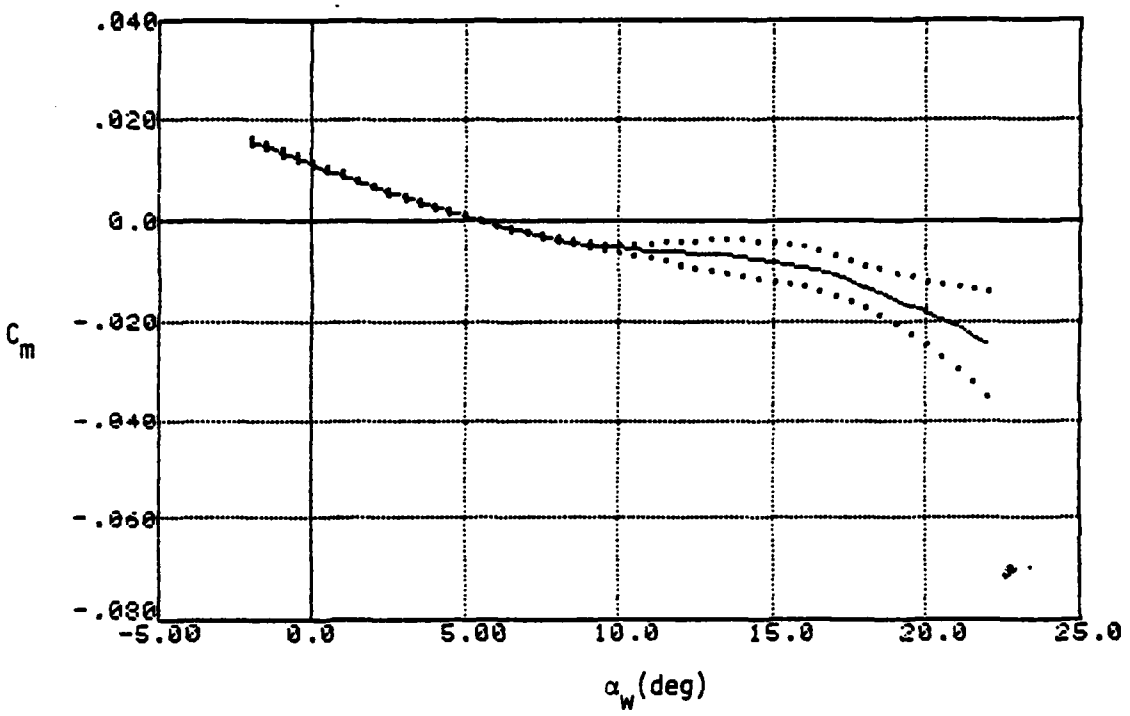

Figure 5.26 Pitching Moment Coefficient - Cruise (M = .8)

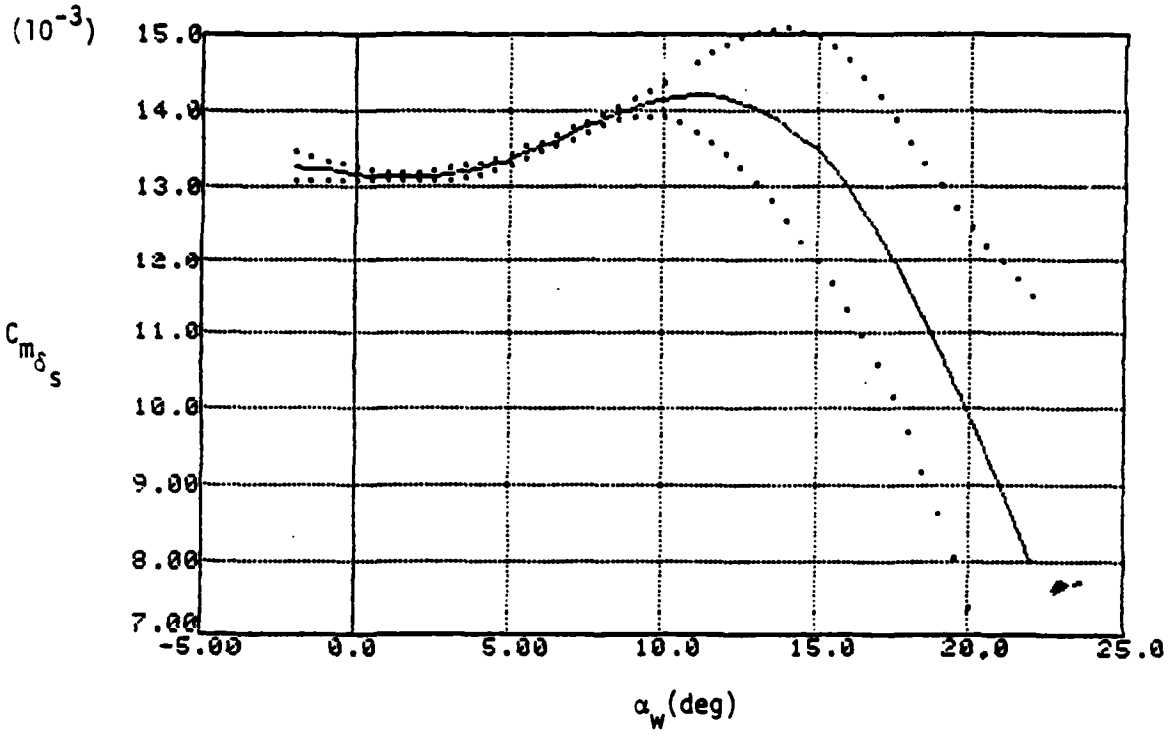

Figure 5.27 Pitching Moment Coefficient due to Stabilator - Cruise (M = .8)

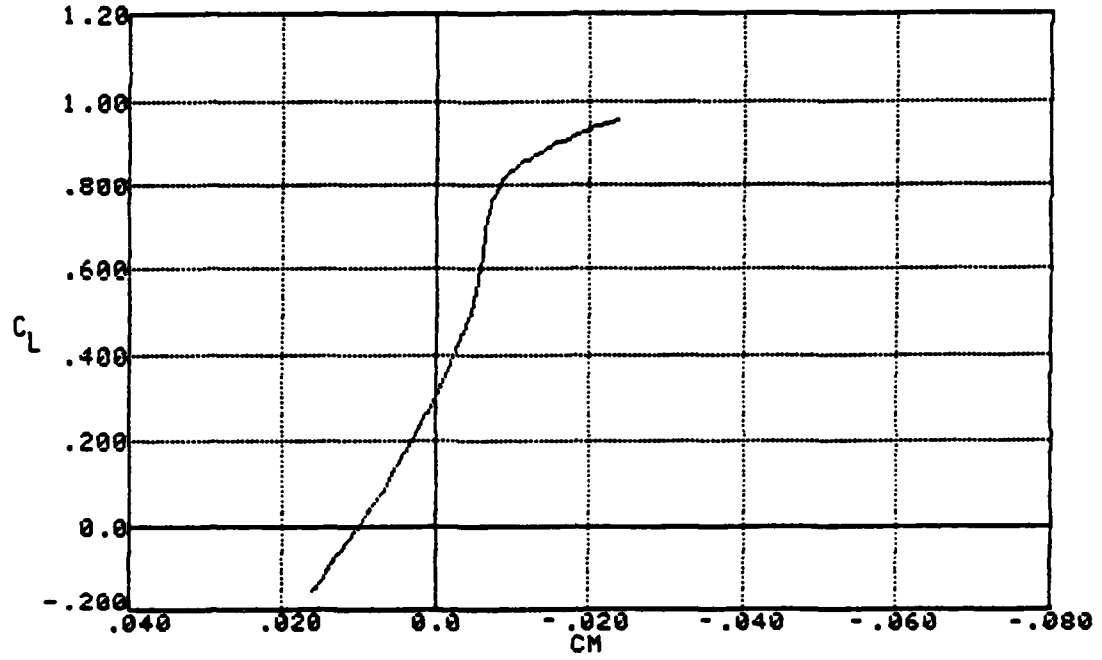

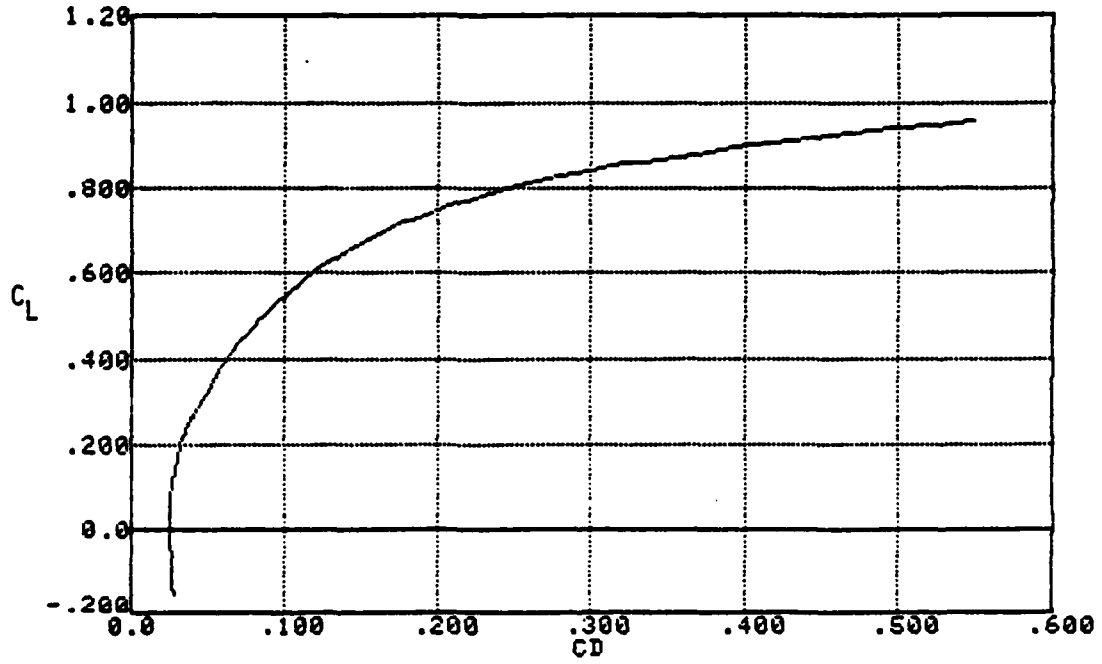

Figure 5.28 C_D and C_m versus C_L - Cruise (M = .8)

Table 5.2

Pitching Moment Coefficient Due to Pitch Rate

FLAP CONFIGURATION	CLEAN CONFIGURATION	STORE EFFECT
	$C_{m_{\hat{q}}} \pm 2\sigma$	$\Delta C_{m_{\hat{q}}} \pm 2\sigma$
TO	-6.40 ± 0.18	-0.22 ± 0.30
PA	-7.45 ± 0.50	-0.24 ± 0.30
CR (M = 0.7)	-5.74 ± 0.12	-0.55 ± 0.28
CR (M = 0.8)	-6.28 ± 0.08	—

Table 5.3

Lift Coefficient Due to Pitch Rate

FLAP CONFIGURATION	CLEAN CONFIGURATION	STORE EFFECT
	$C_{L_{\hat{q}}} \pm 2\sigma$	$\Delta C_{L_{\hat{q}}} \pm 2\sigma$
TO	5.16 ± 0.74	0.84 ± 1.11
PA	8.23 ± 0.96	-1.64 ± 0.88
CR (M = 0.7)	4.00 ± 4.16	-1.54 ± 2.28
CR (M = 0.8)	3.76 ± 0.75	—

5.2 LONGITUDINAL CHARACTERISTICS AT HIGH ANGLE OF ATTACK

This sections presents the F-4S longitudinal characteristics at low speed (M = 0.4) and high angle of attack (5 to 35 deg). The test maneuvers used, taken from the Phase II flight test are:

- Tape 3, File 3 - stall with pitch doublet at 30,000 ft and Mach 0.4.
- Tape 3, File 6 - pitch doublets at 37,000 ft and Mach 0.4.

The results are presented in the same format as those of Section 5.3:

(1) Figure 5.29 shows a time history plot of one test maneuver with both the actual recorded test data and the estimated measurement derived from the identified aerodynamic model.

(2) Figures 5.30 through 5.35 present the identified aerodynamic coefficients in stability axis, referenced to c.g. = 33 percent and $\delta_S = 0$. The estimation uncertainty is shown by the $\pm 2\sigma$ bounds.

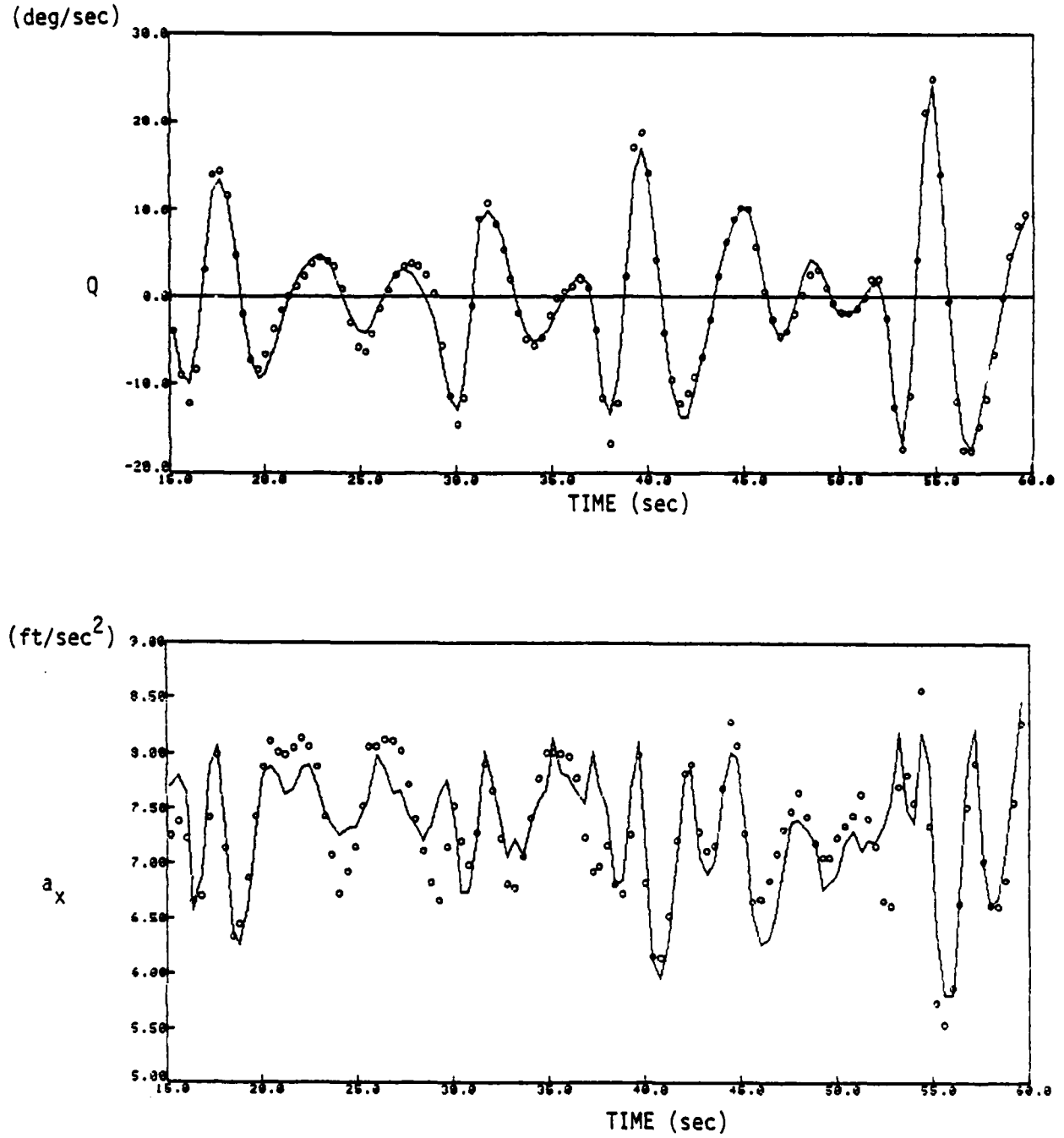

Figure 5.29 Time History Plot - Longitudinal High Angle of Attack

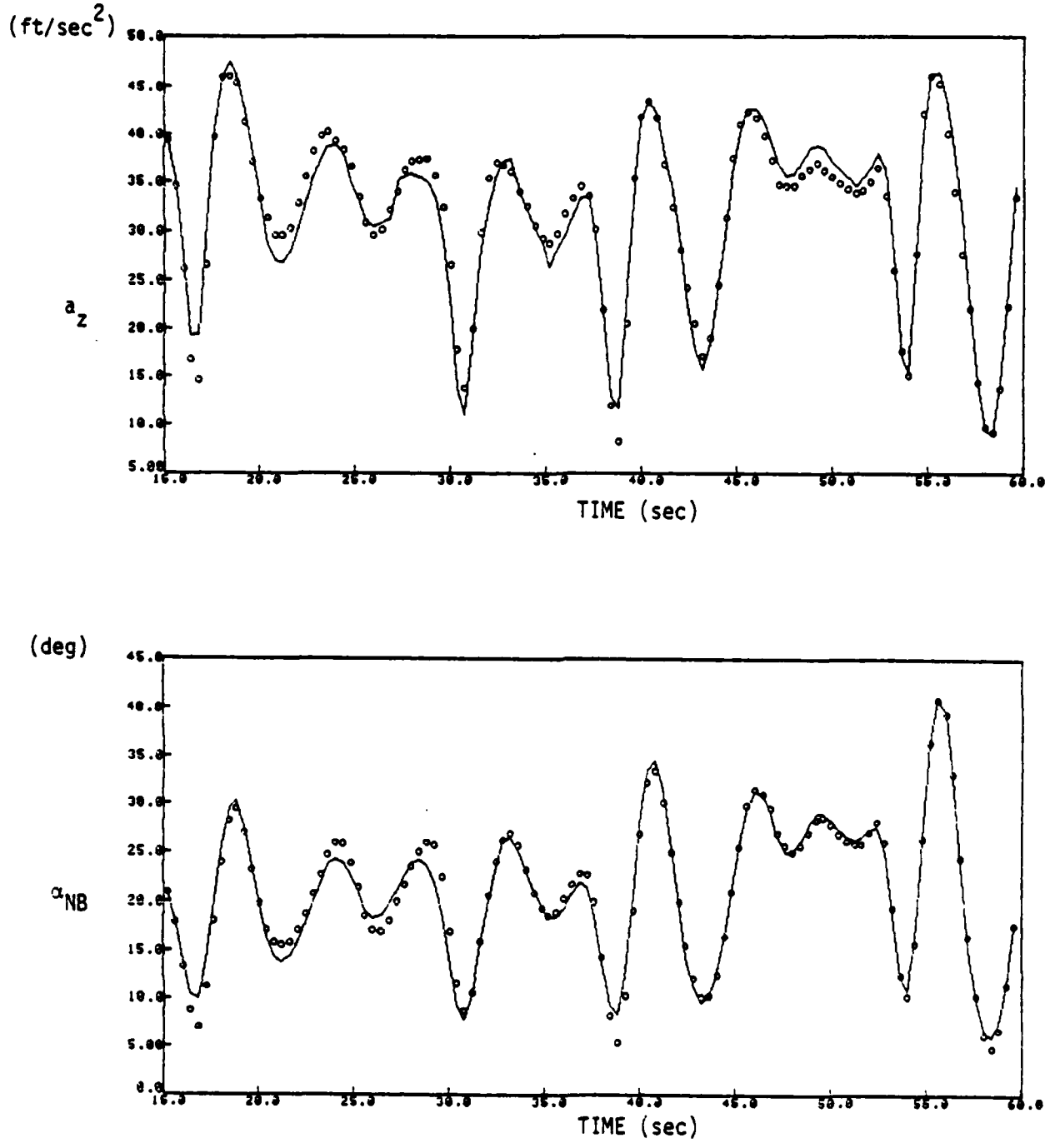

Figure 5.29 (Continued)

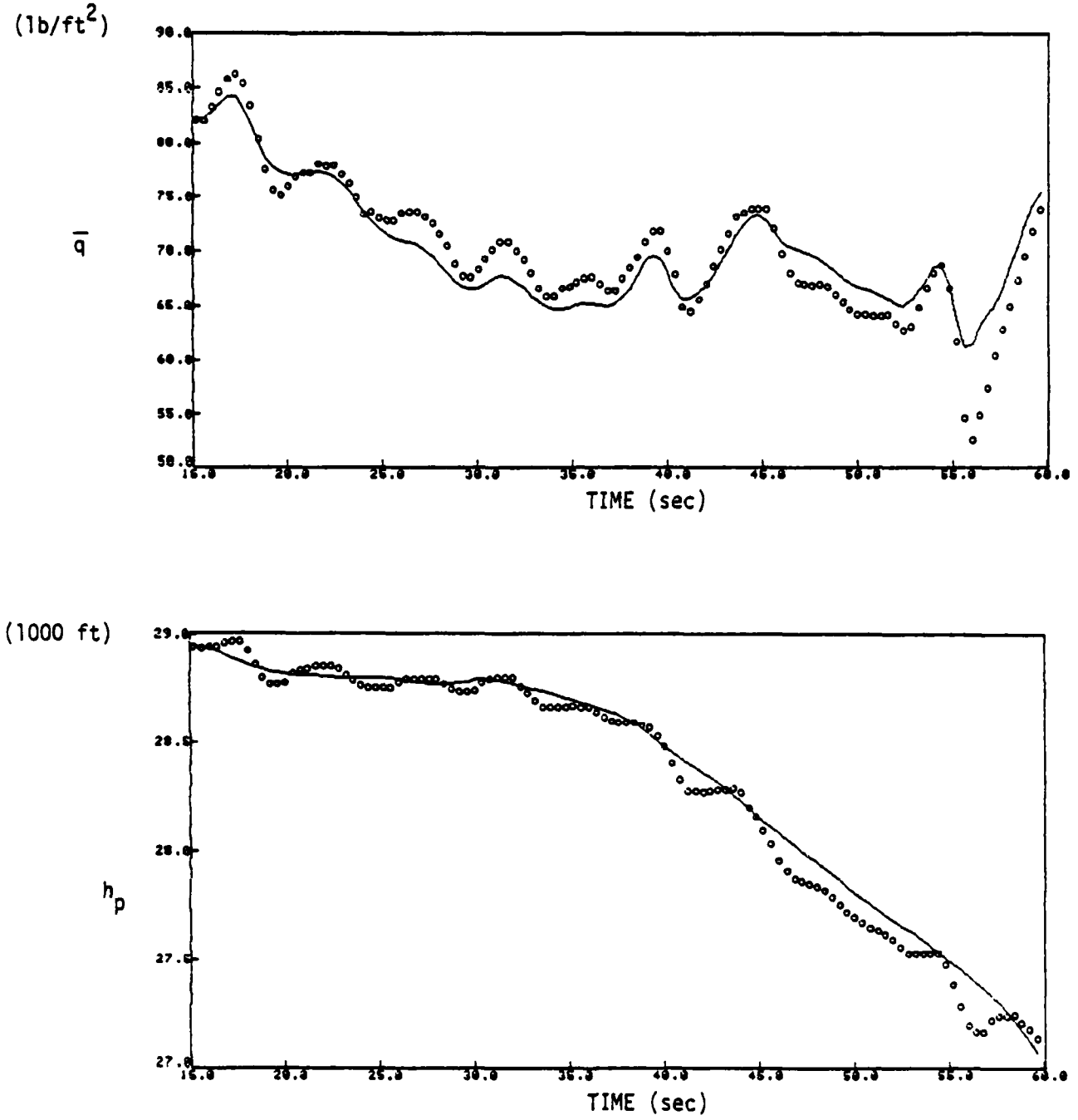

Figure 5.29 (Continued)

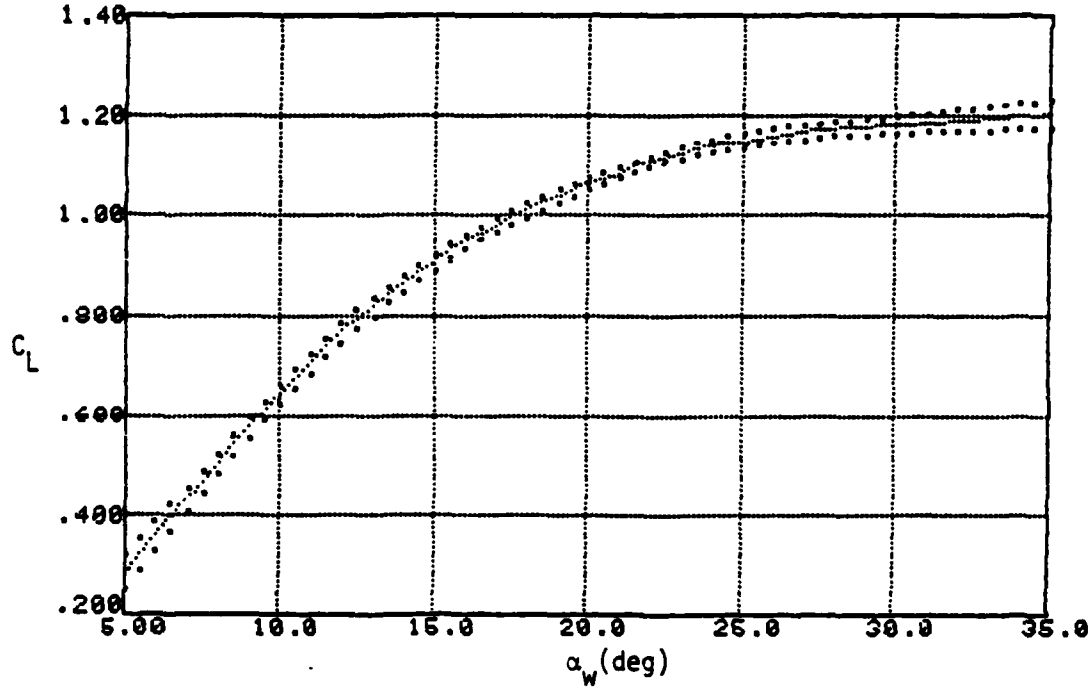

Figure 5.30 Lift Coefficient - High Angle of Attack

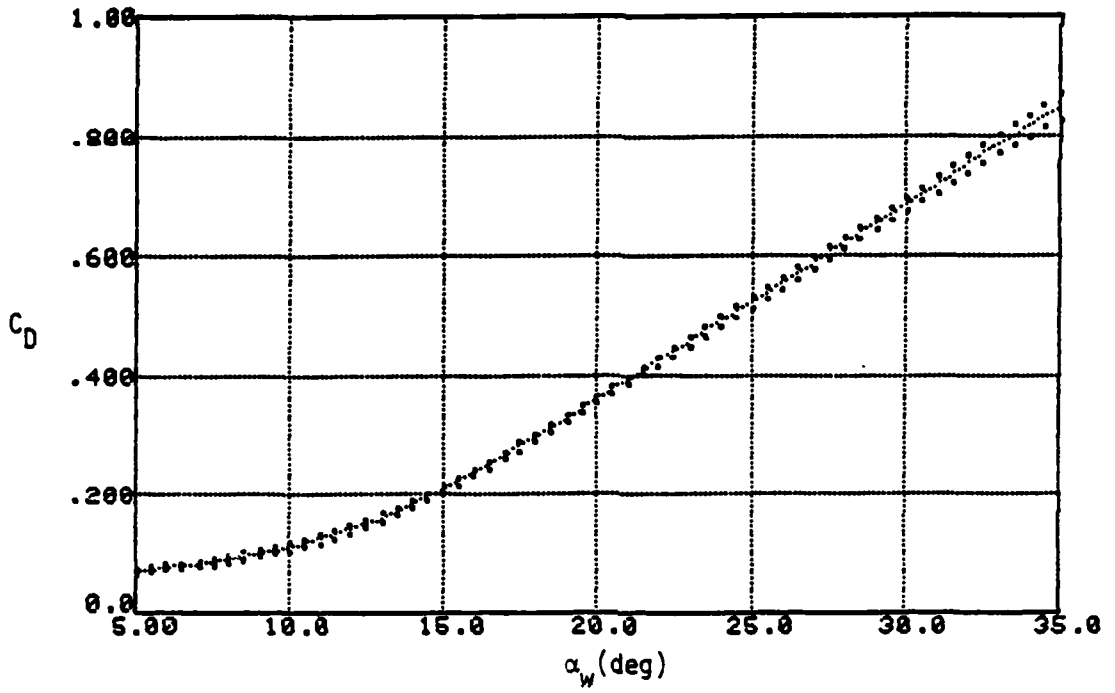

Figure 5.31 Drag Coefficient - High Angle of Attack

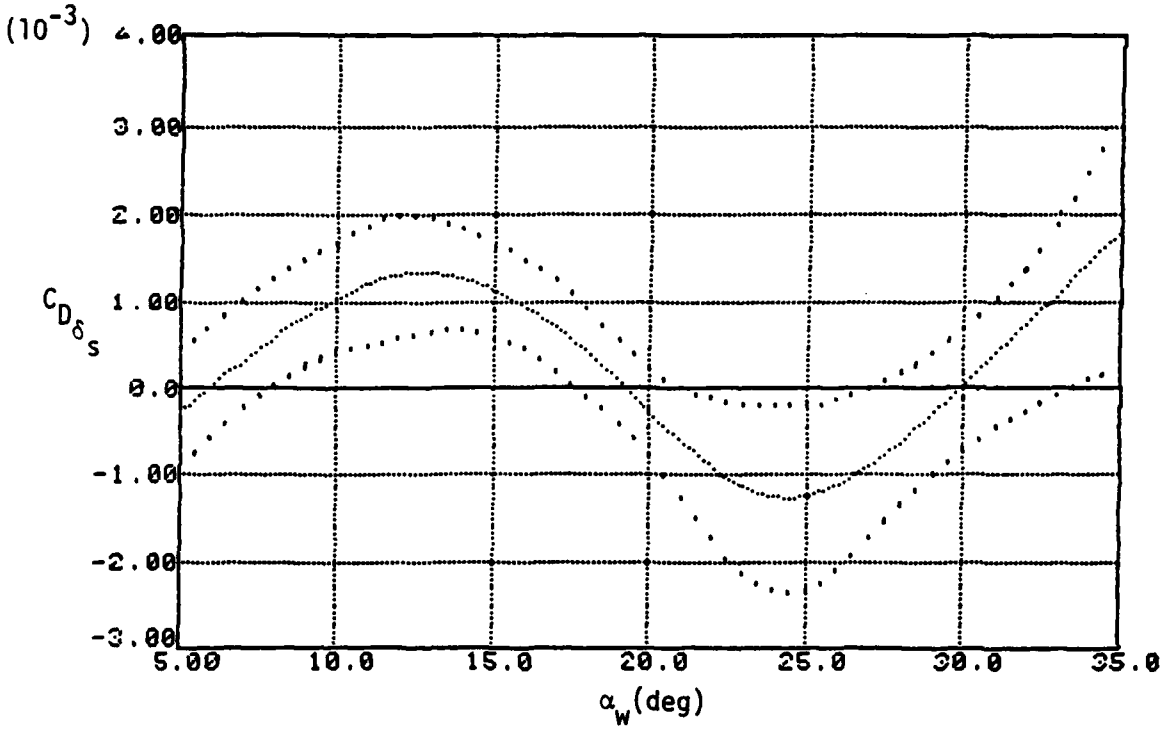

Figure 5.32 Drag Coefficient due to Stabilator Deflection - High Angle of Attack

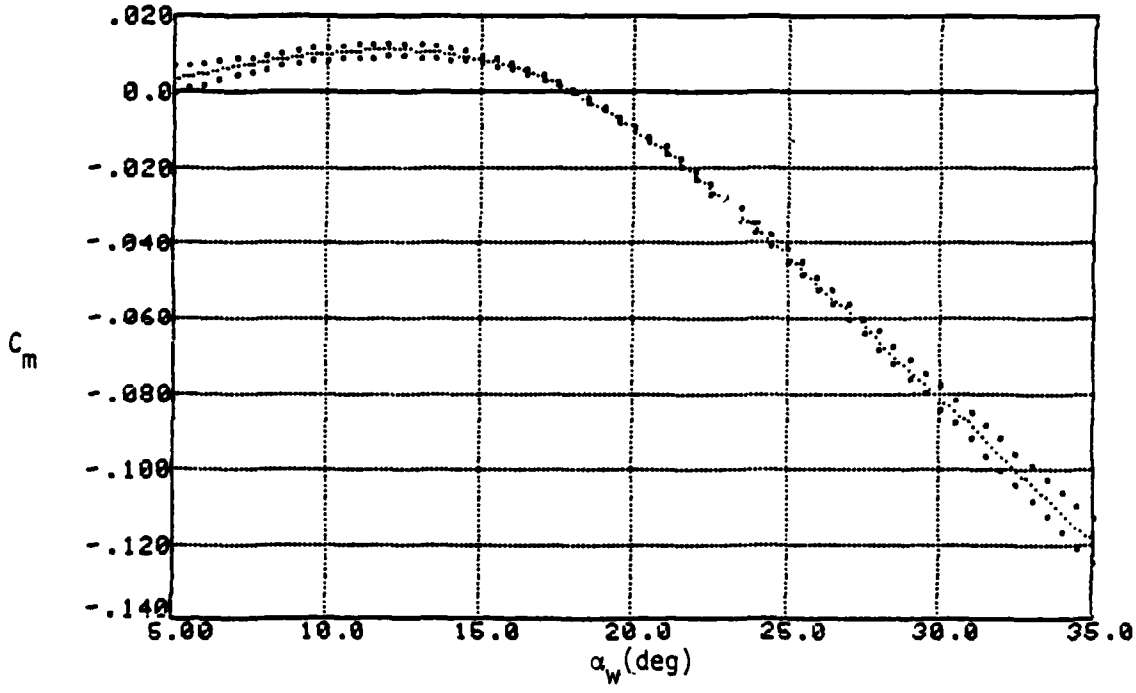

Figure 5.33 Pitching Moment Coefficient - High Angle of Attack

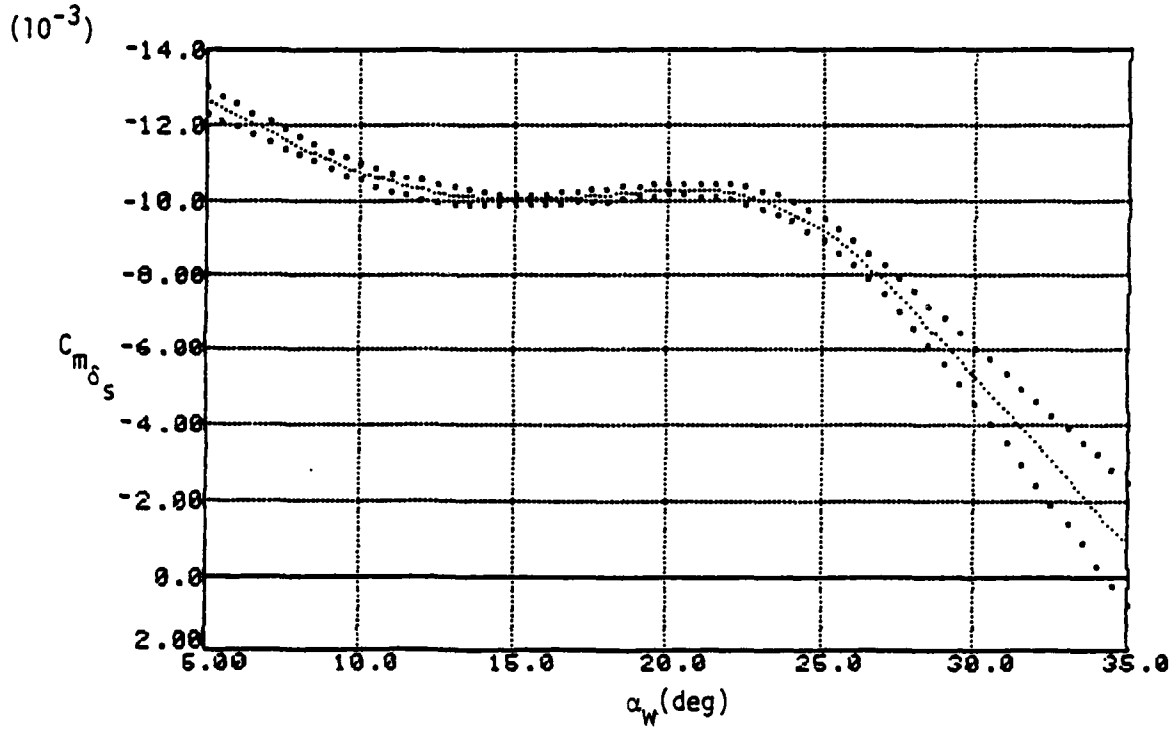

Figure 5.34 Pitching Moment Coefficient due to Stabilator Deflection - High Angle of Attack

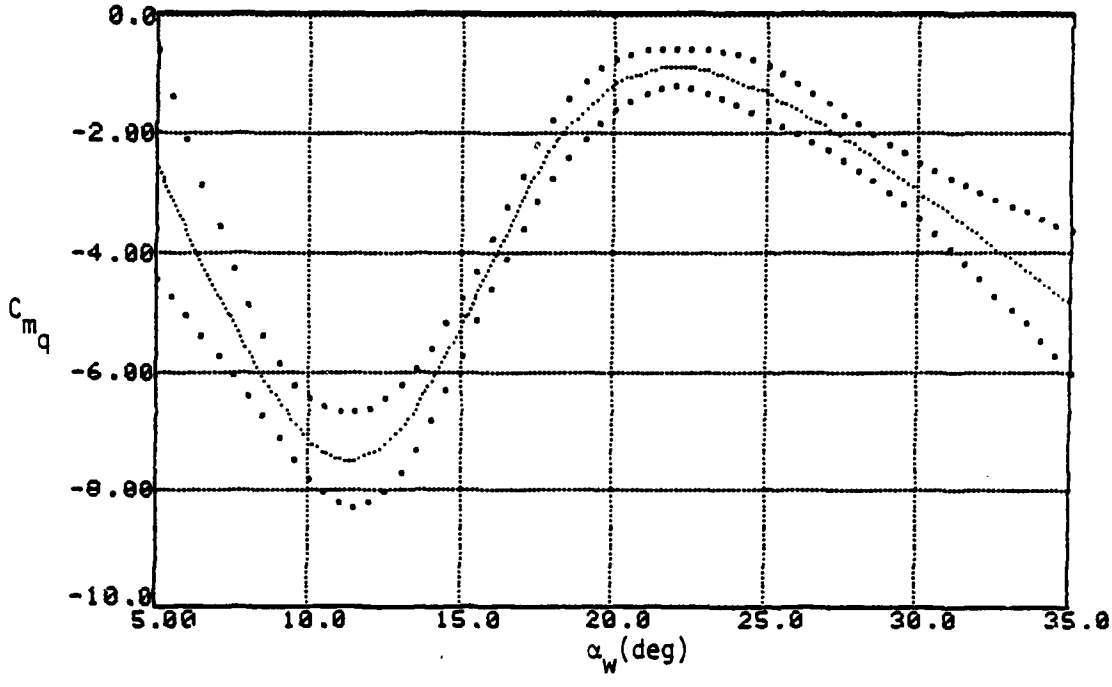

Figure 5.35 Pitching Moment Coefficient due to Pitch Rate - High Angle of Attack

5.3 LATERAL-DIRECTIONAL CHARACTERISTICS

5.3.1 General

The F-4S lateral/directional characteristics, presented in this section, were identified in two distinct phases. The initial processing covered the full low to high angle-of-attack range and was based on the Phase II flight tests. The final processing provided more accurate estimates for the low angle-of-attack range and was based on the Phase III flight tests conducted. The final processing was based on improved thrust and c.g. location models.

5.3.2 Instrumentation Considerations

Initial Processing

In the initial data processing, the following maneuvers from Flight WD7 were used:

- Tape 2, File 3 - aileron doublet
- Tape 2, File 5 - sequential doublets
- Tape 3, File 3 - stall and pitch doublet
- Tape 3, File 4 - stall and aileron doublet
- Tape 3, File 5 - stall and rudder doublet
- Tape 3, File 6 - pitch doublet

where the longitudinal maneuvers were included to aid i instrumentation calibration. All the maneuvers were flown at Mach 0.4 with the altitude varying between 30,000 and 37,000 feet.

A net thrust propulsion model was used (see Table A.6 in Appendix A for details). The only instrumentation problem was with the roll-rate gyro. As a result, the derivative of roll attitude was used to reconstruct roll rate.

Final Processing

The maneuvers used for the second phase were the pitch, aileron, and rudder pumping at Mach 0.7 from Flight 3, Record 46. A more accurate propulsion model representing both gross thrust and inlet ram force effect was used (see Table A.7 in Appendix A). An updated model of c.g. location as a function of fuel consumption was also used. The maneuvers covered only the low angle-of-attack range and a linear aerodynamic model (angle of attack perturbation relative to α = 5 deg) was sufficient. Here, too, the derivative of roll attitude was used to reconstruct roll rate. A time history plot of the second phase maneuvers is shown in Figure 5.36.

5.3.3 Combined Initial and Final Estimates

Before the initial estimates could be revised using the final processing results, the latter had to be corrected for Mach number effects. The aerodynamic coefficients variations with Mach number between Mach 0.7 and Mach 0.4 (at α = 5 deg) were obtained from Ref. 43 (MDC A2013). The initial estimate at α = 5 deg and the corrected estimate from the second phase (both at Mach 0.4) were combined according to:

$$C = K_1 C_1 + K_2 C_2$$

$$\sigma = \sqrt{\sigma_1^2 + \sigma_2^2}$$

where

C = revised coefficient

C_1 = initial coefficient estimate (Phase II)

C_2 = final coefficient estimate (Phase III) corrected for Mach effects

σ, σ_1, σ_2 = the corresponding standard deviation

and

$$K_1 = \sigma^2/(\sigma_1^2 + \sigma_2^2)$$

$$K_2 = 1 - K_1$$

The revised coefficient (C) was then used instead of the initial coefficient as the $\alpha = 5$ deg knot in the cubic spline representation of each aerodynamic derivative.

These results are shown in Figures 5.37 through 5.44 in the following manner:

(1) The top plot of each figure shows the initial estimate as a function of angle of attack and the $\pm 2\sigma$ uncertainty bounds.

(2) The estmate from the second phase, at $\alpha_w = 5$ deg, are also shown on the top plot. The square (□) is the value for Mach 0.7 and the star (*) is the corrected value at Mach 0.4.

(3) The revised estimate is shown on the bottom plot of each figure. The circle (○) at $\alpha_w = 5$ deg, emphasizes the only spline knot that was changed. The other knots (at 15, 25, and 35 deg) are the same as those of the initial estimate.

NOTE: The lateral/directional results are in body axis, whereas the longitudinal results are in stability axis.

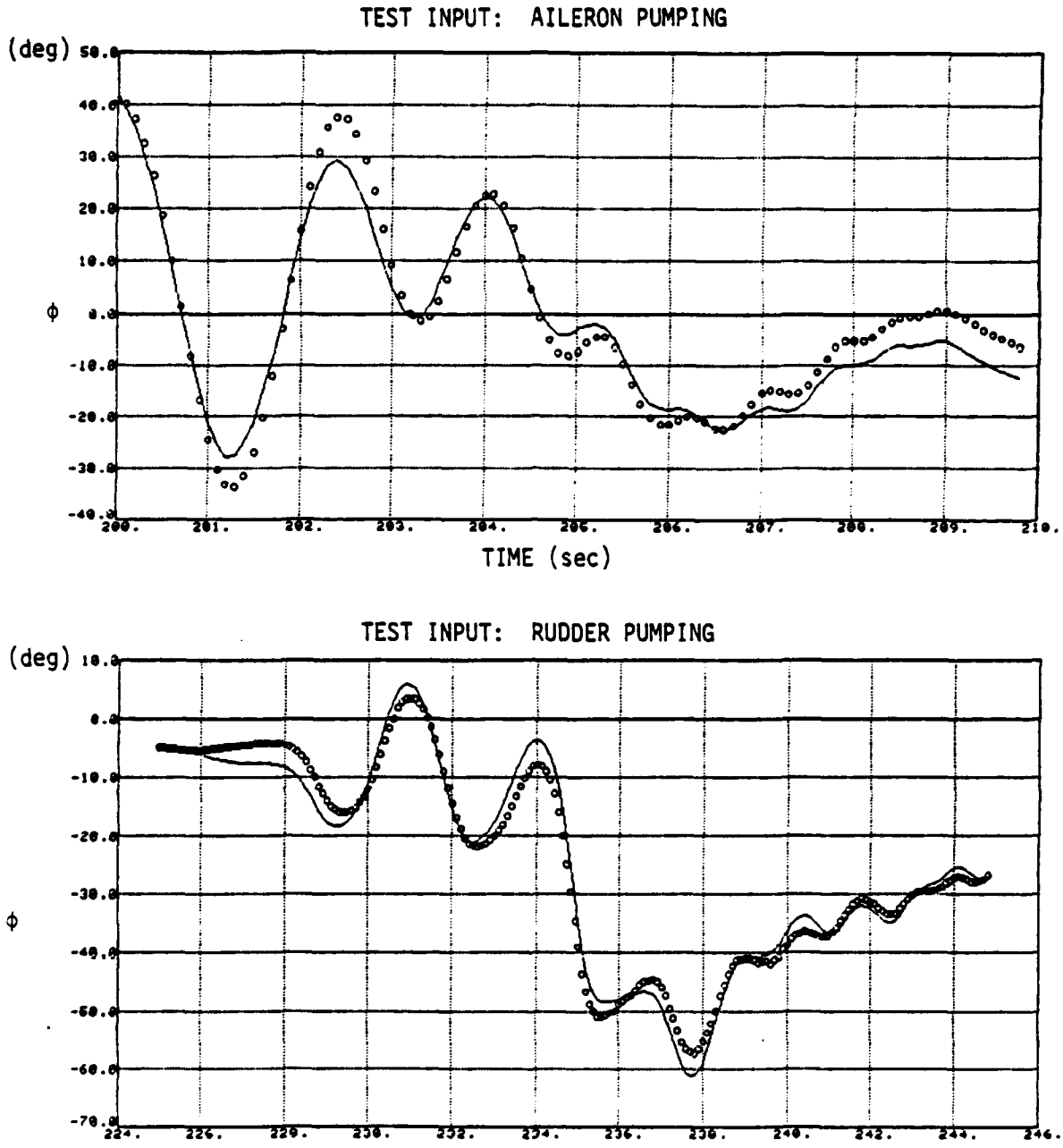

Figure 5.36 Time History Plots - Lateral/Directional

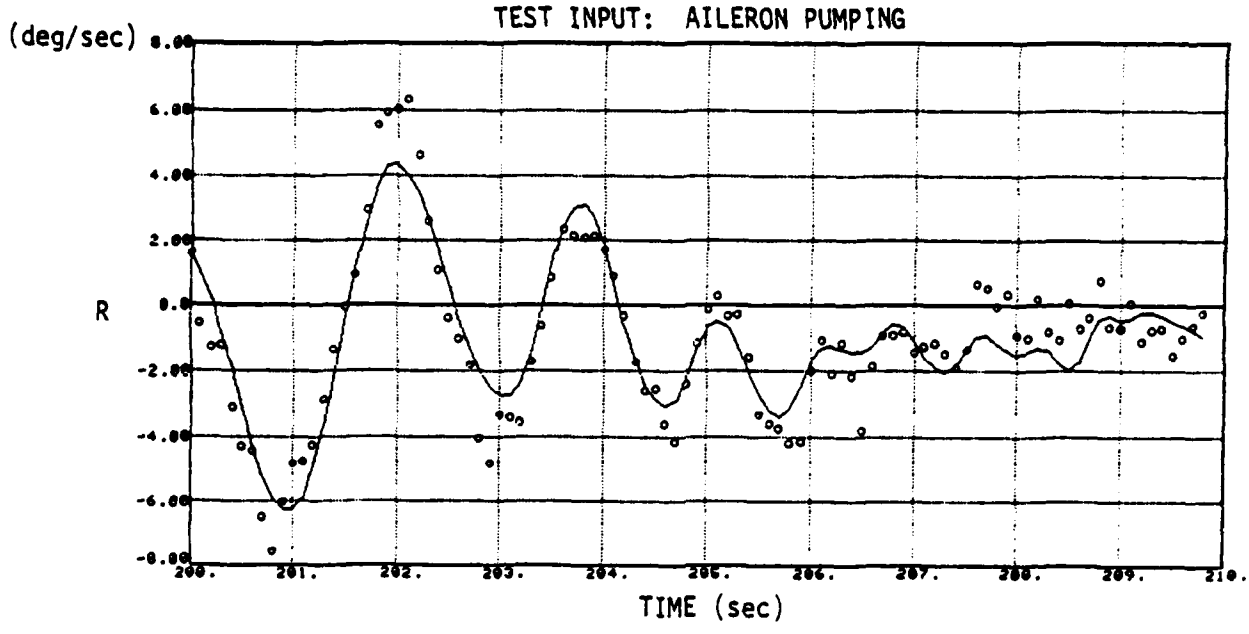

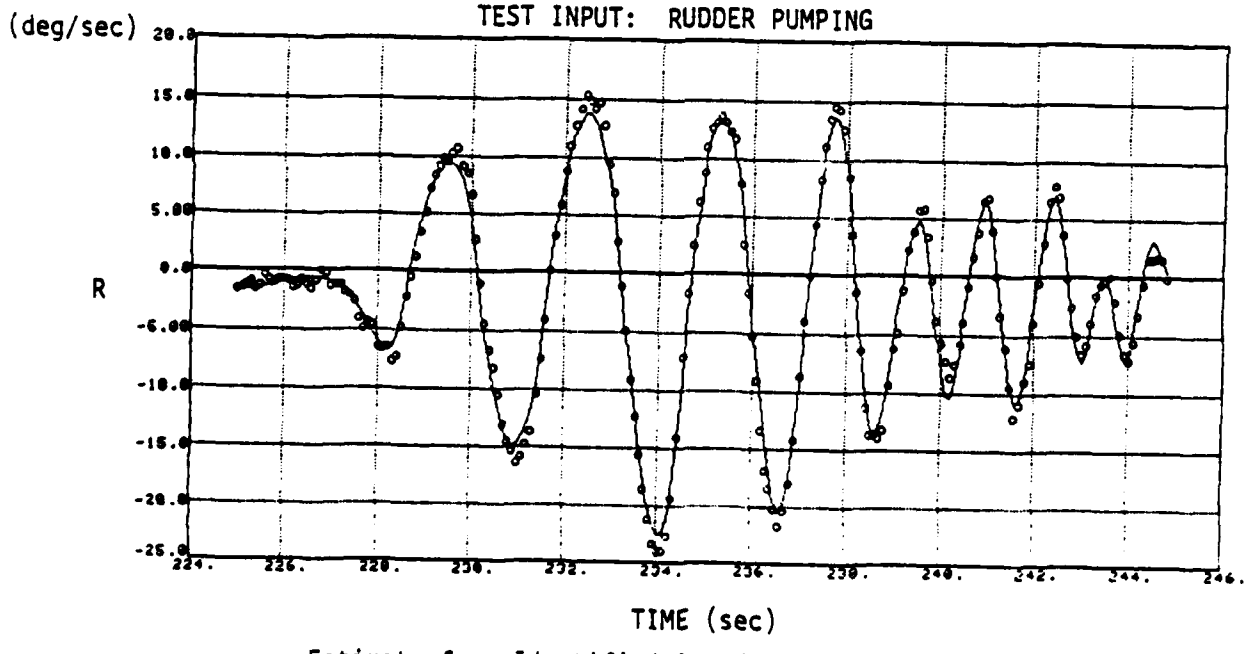

——— Estimate from Identified Aerodynamic Model

o o o o Flight Test Data

Figure 5.36 (Continued)

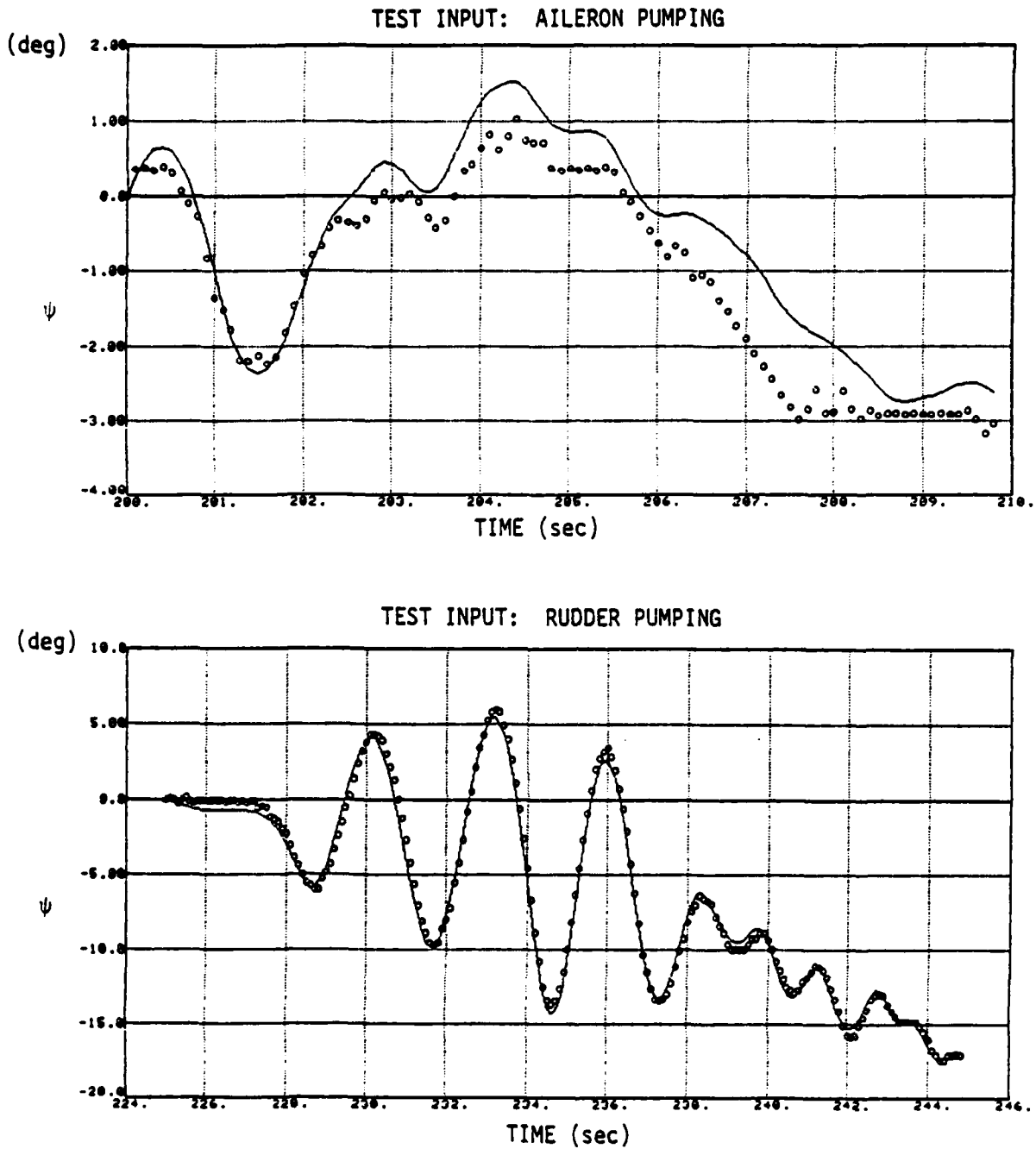

Figure 5.36 (Continued)

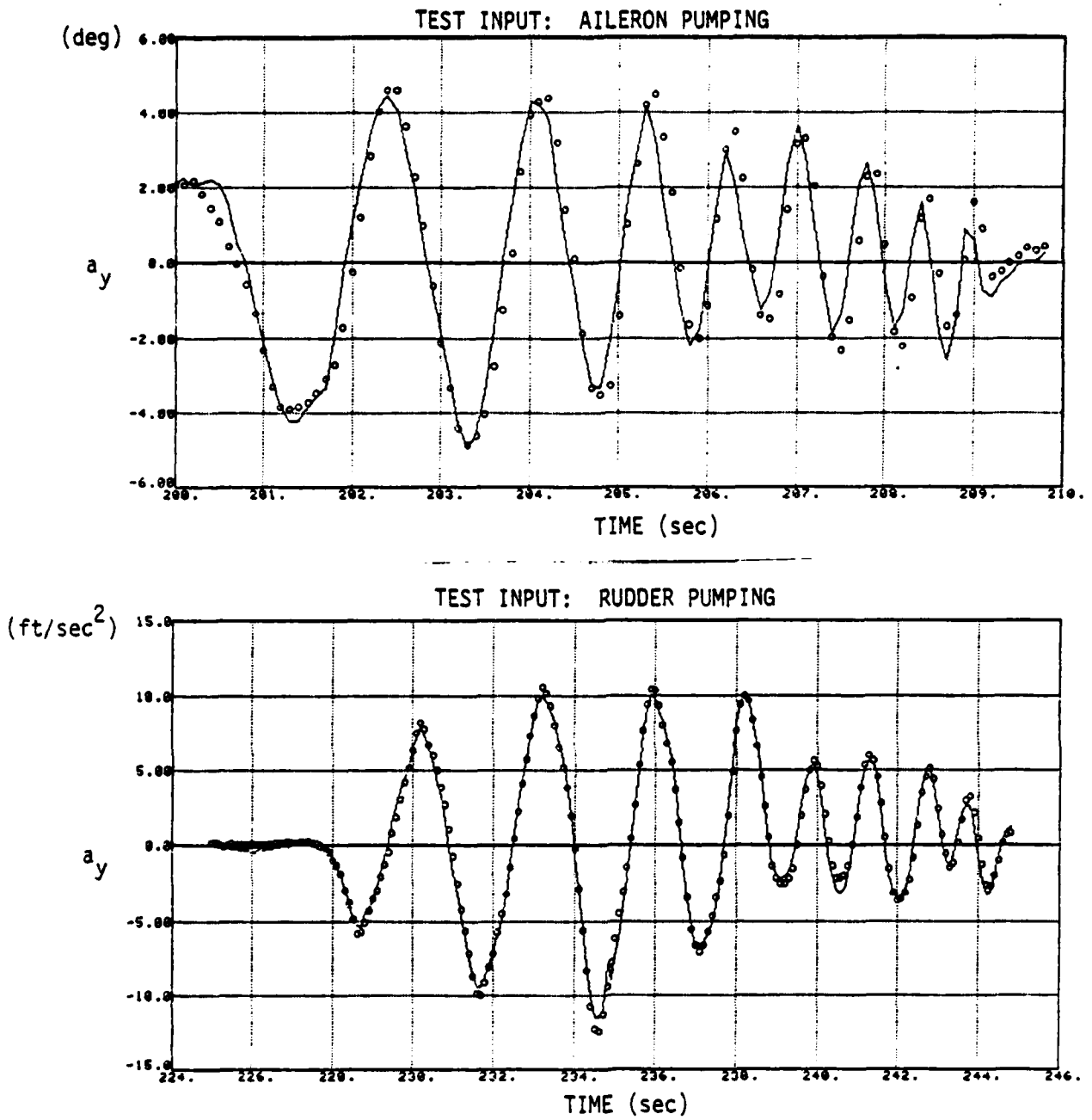

Figure 5.36 (Continued)

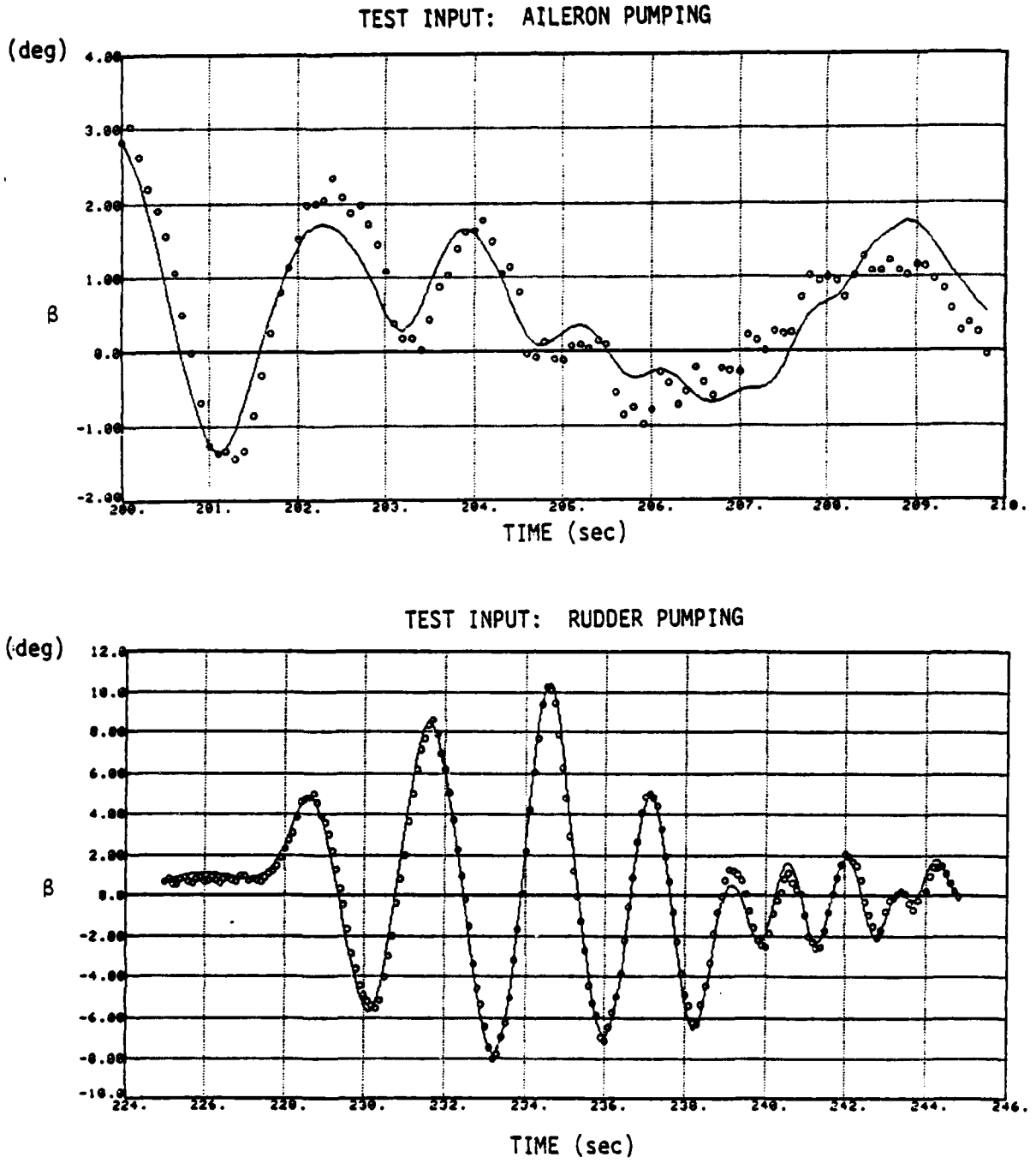

Figure 5.36 (Continued)

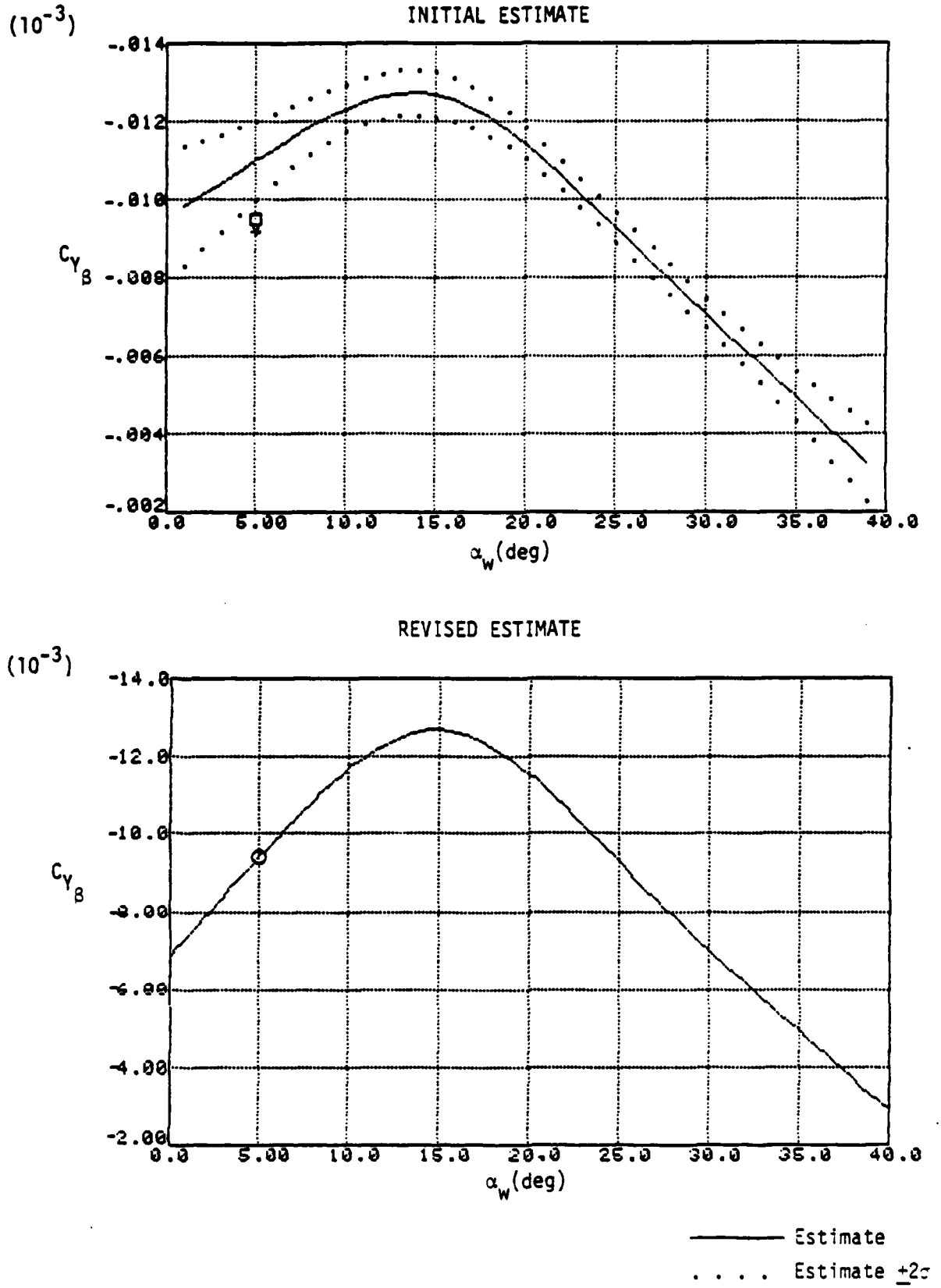

Figure 5.37 Side Force Coefficient due to Sideslip

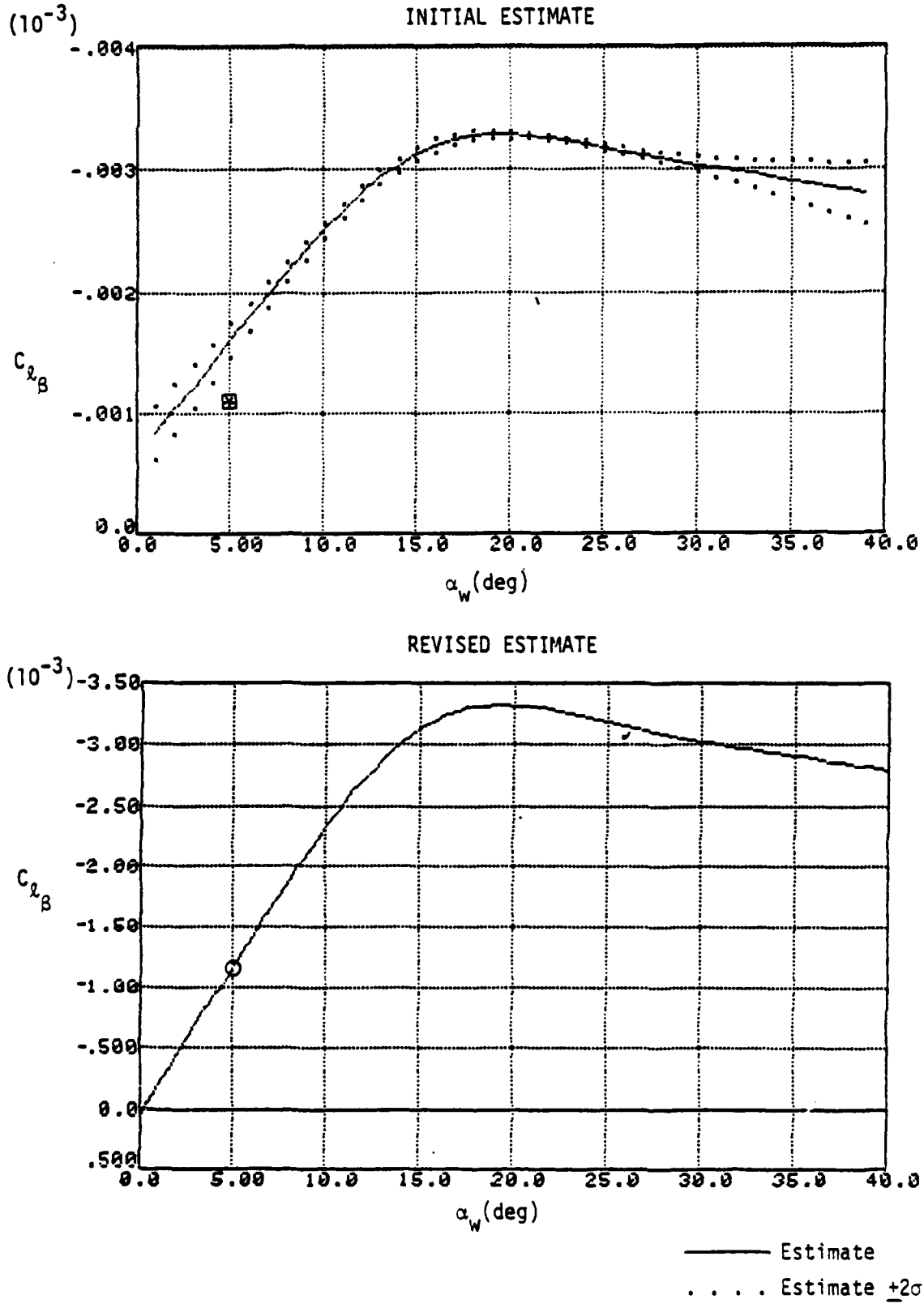

Figure 5.38 Rolling Moment Coefficient due to Sideslip (body axis)

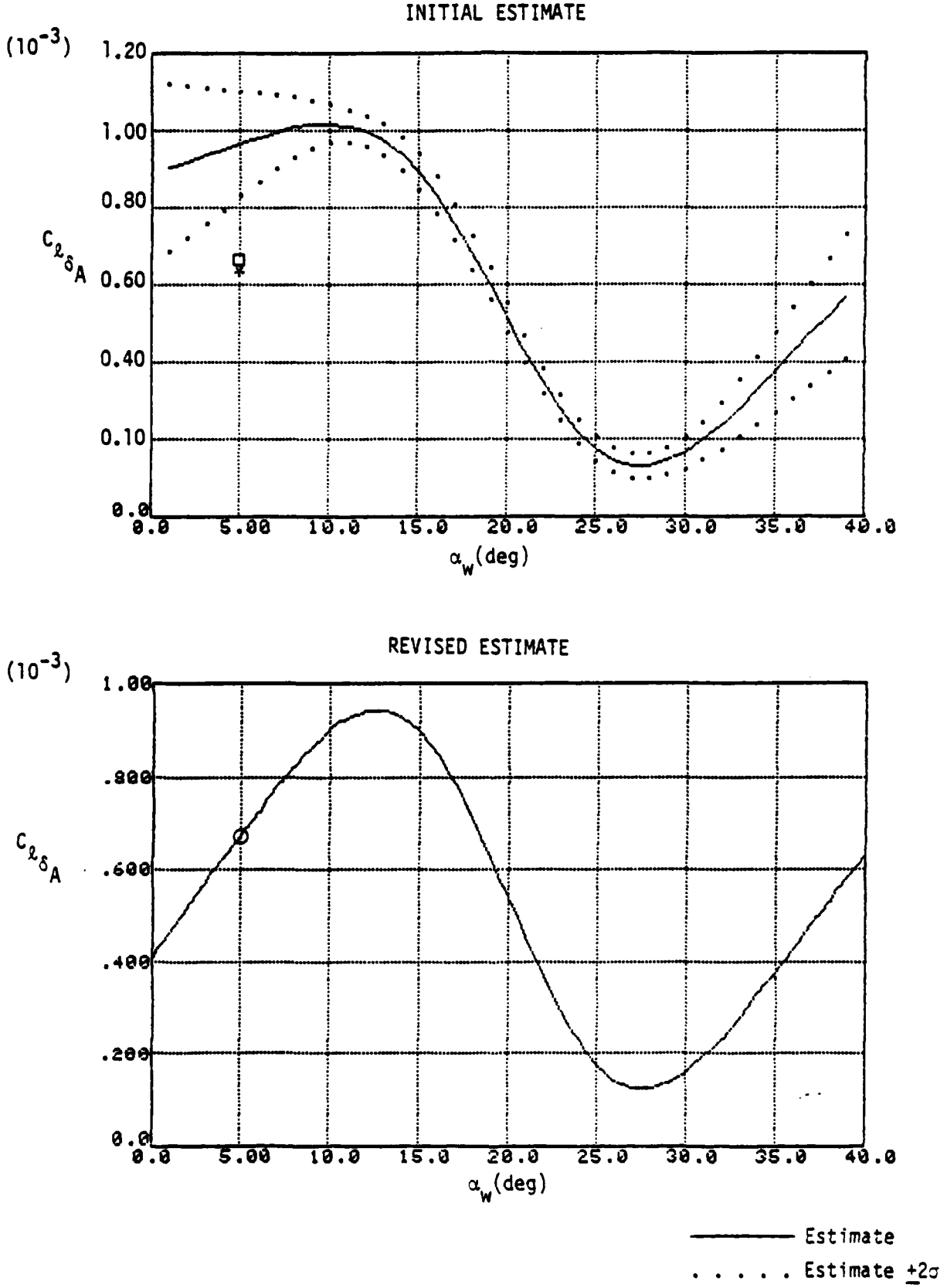

Figure 5.39 Rolling Moment Coefficient due to Aileron (body axis)

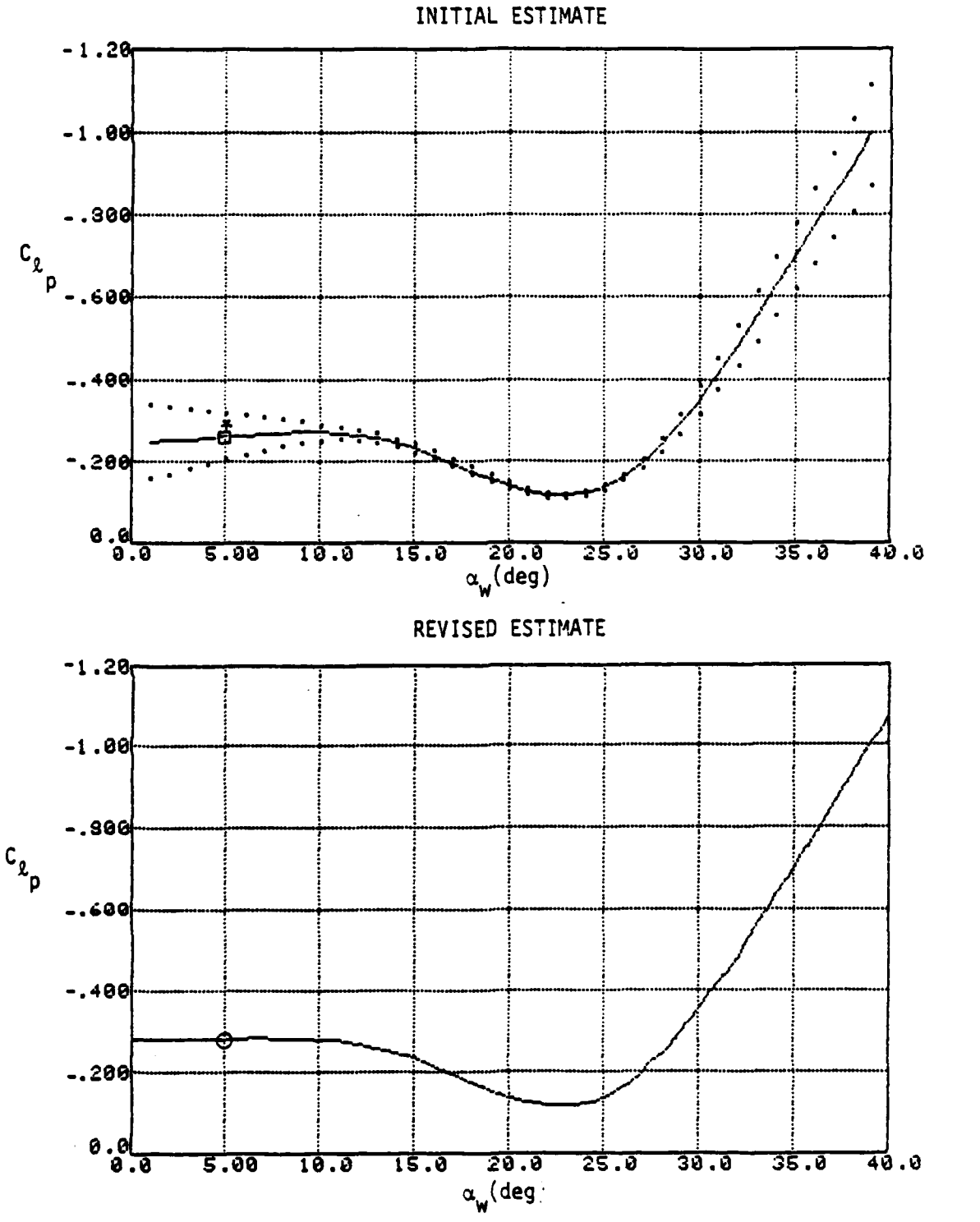

Figure 5.40 Rolling Moment Coefficient due to Roll Rate (body axis)

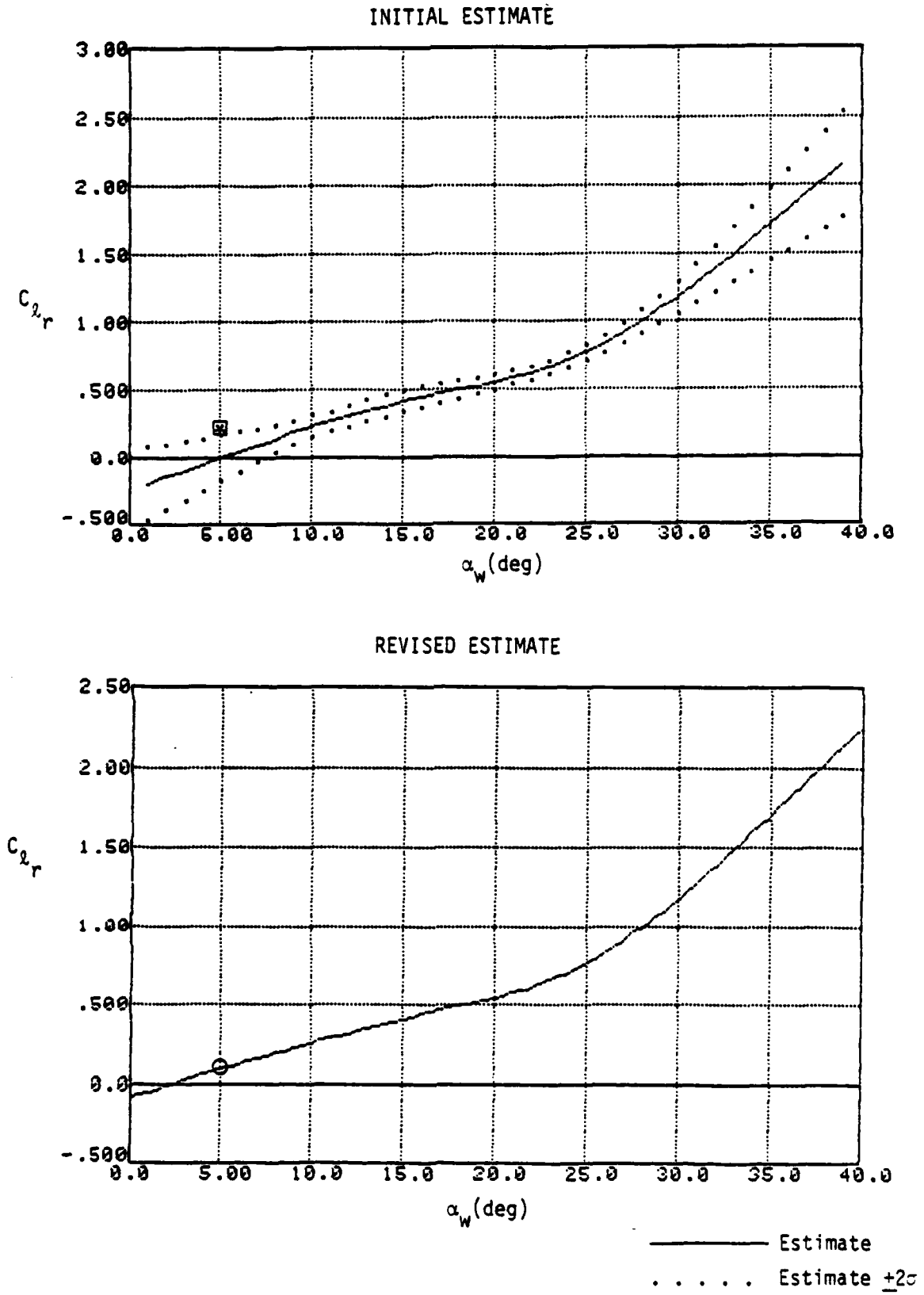

Figure 5.41 Rolling Moment Coefficient due to Yaw Rate (body axis)

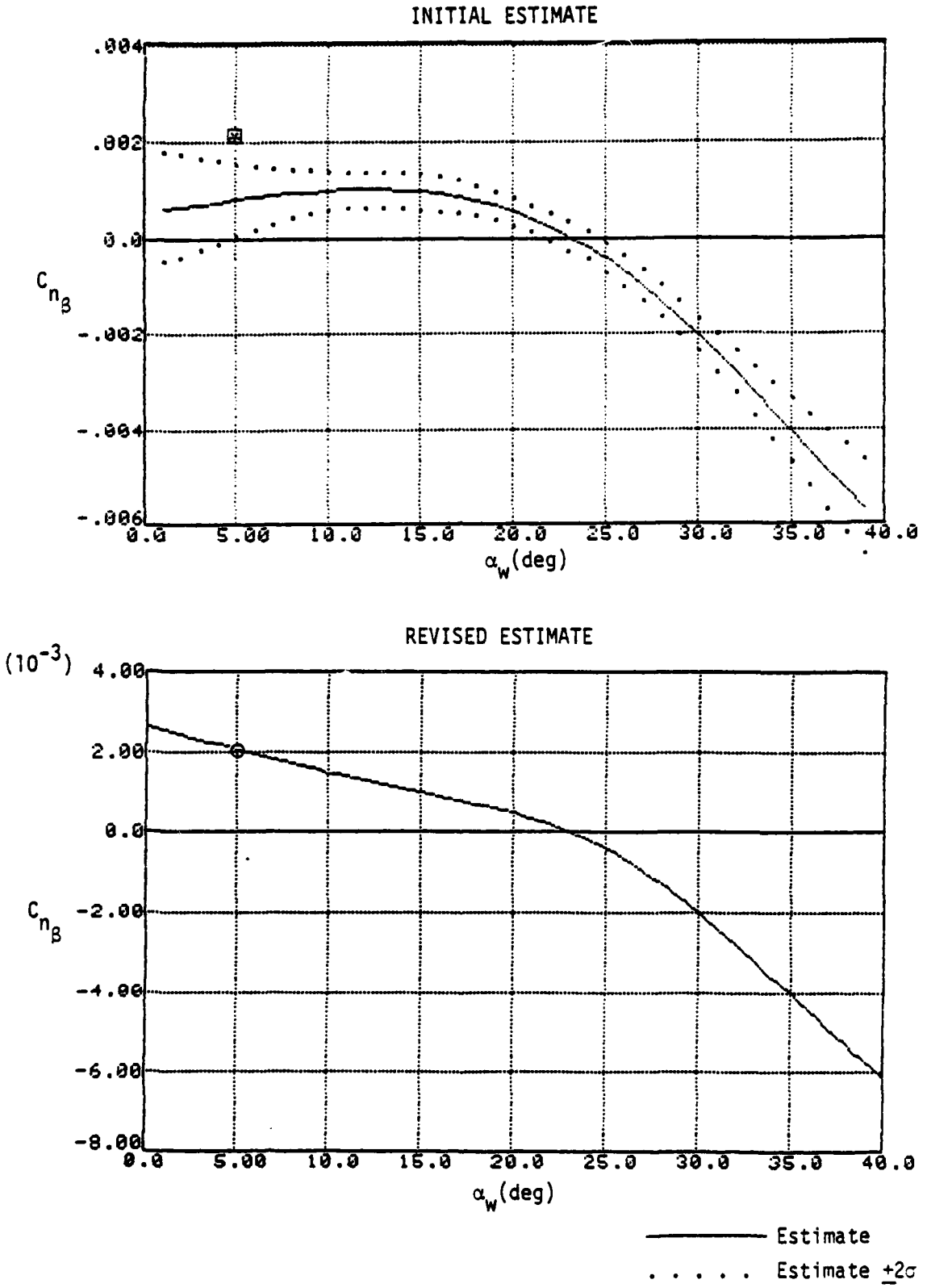

Figure 5.42 Yawing Moment Coefficient due to Sideslip (body axis)

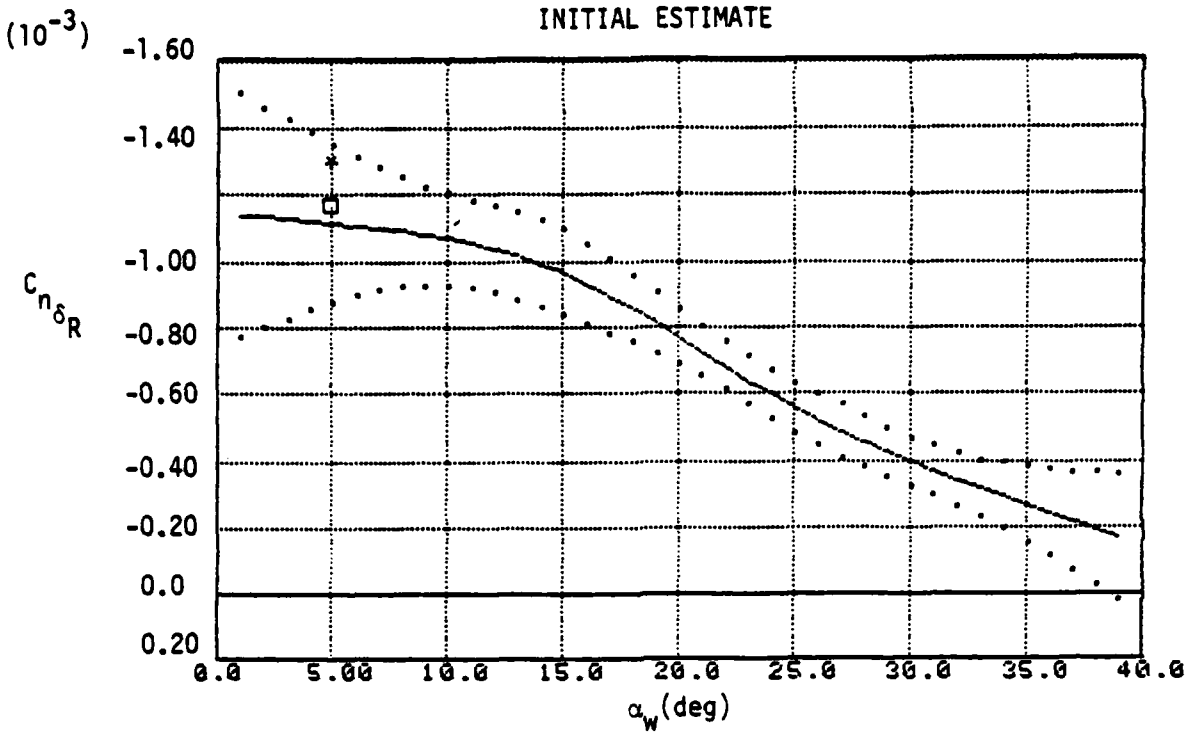

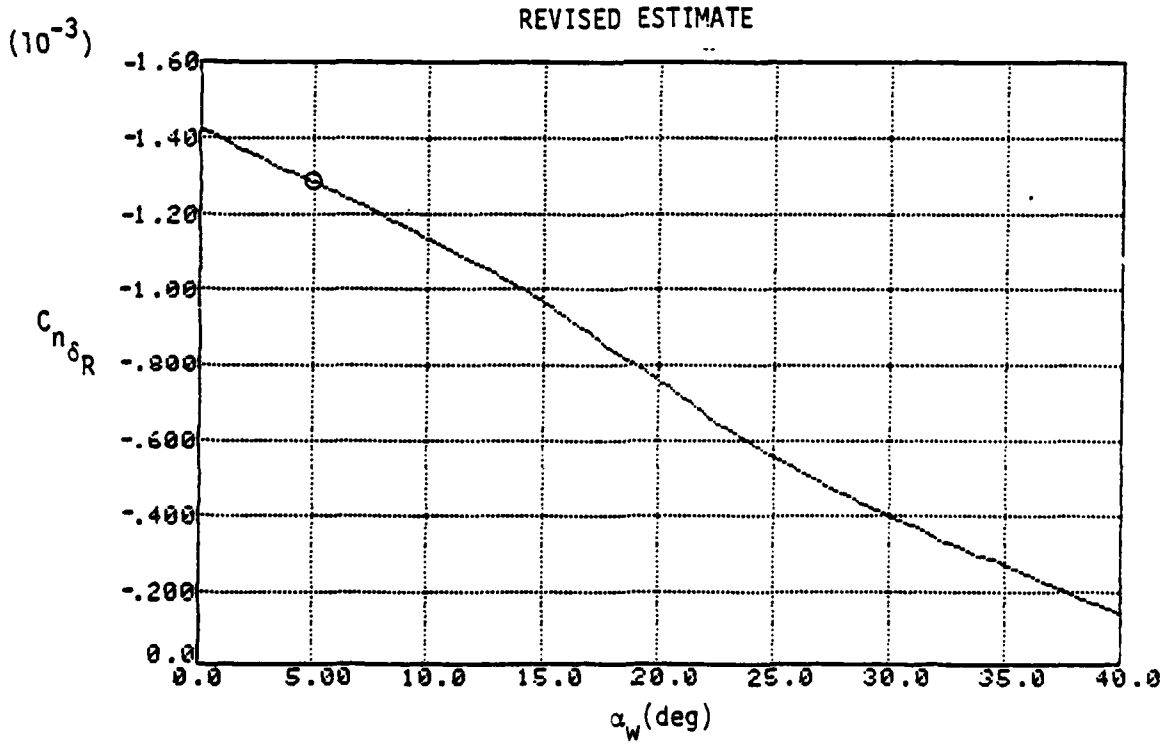

Figure 5.43 Yawing Moment Coefficient due to Rudder (body axis)

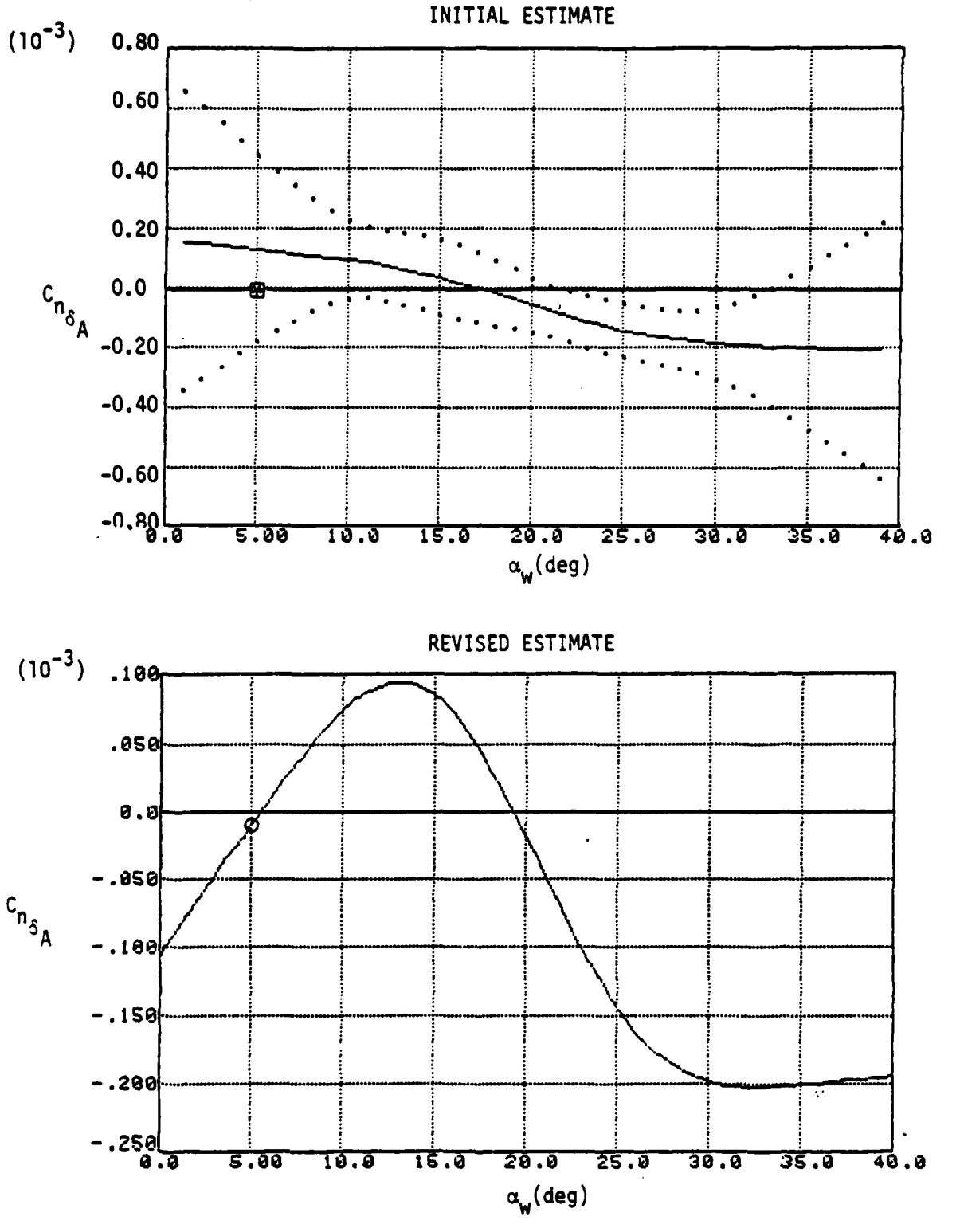

Figure 5.44 Yawing Moment Coefficient due to Aileron (body axis)

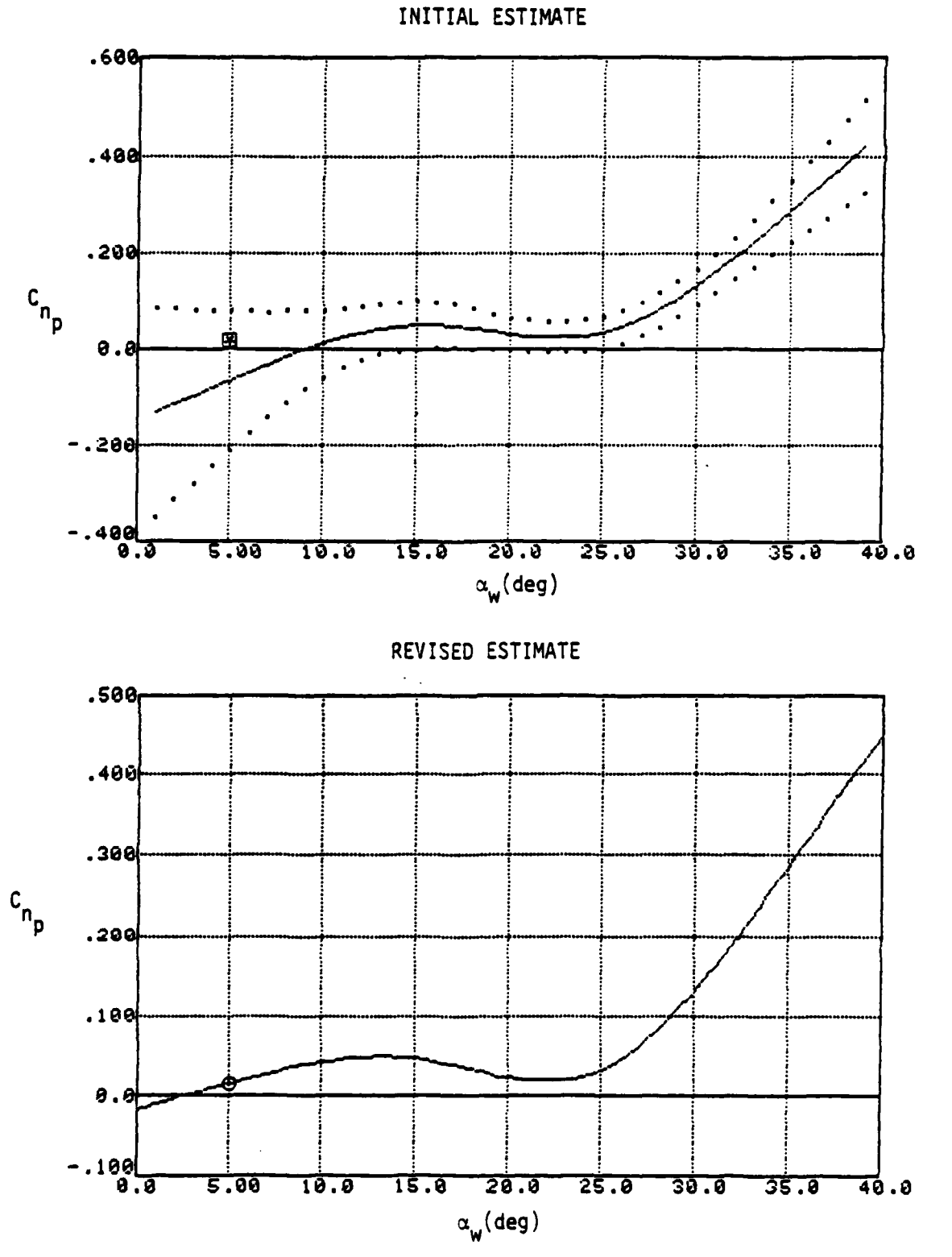

Figure 5.45 Yawing Moment Coefficient due to Roll Rate (body axis)

5.4 PROPULSION SYSTEM MODELING AND IDENTIFICATION

For the Phase II flight test processing, a simplified model of the propulsion system was used to separate thrust effects from the applied forces and moments. The model was based on representing the engines by corrected net thrust as a function of corrected fuel flow. This model was identified from flight test data. The result of this identification is presented in Figure 5.46. The difference between the identified and preflight models for corrected net thrust is a bias in fuel flow of 58 lbs/hr based on a pressure altitude of h_p = 30,000 ft. The accuracy of the flight test fuel flow sensor is 150 lbs/hr.

The propulsion model was revised to separately represent gross thrust and inlet airflow terms for the data processed from the Phase III flight test program. These models were not identified. Status check performance data for the F-4S engines were used directly. Details of this model are presented in Appendix A.

5.5 MODEL VALIDATION

The validity of the parameter estimates can be established from three different considerations.

(1) Engineering judgement: are the estimates reasonable from the point of view of general agreement with preflight predictions

(2) Estimation uncertainty: what is the magnitude of the + 2σ bands about the estimate

(3) Prediction accuracy: How well does the identified model predict flight test measurements for many test maneuvers Does the identified model predict these measurements better than a model based on preflight parameters

Figures 5.47 and 5.48 compare identified aerodynamic characteristics with preflight predictions. The purpose of this presentation is to show the reasonableness of the identified parameters. The identified data are from the Phase II analysis and repeat data presented in Section 5.3.

Figure 5.47 presents rudder and lateral control power estimates as functions of angle of attack. The flight derived control power estimates show

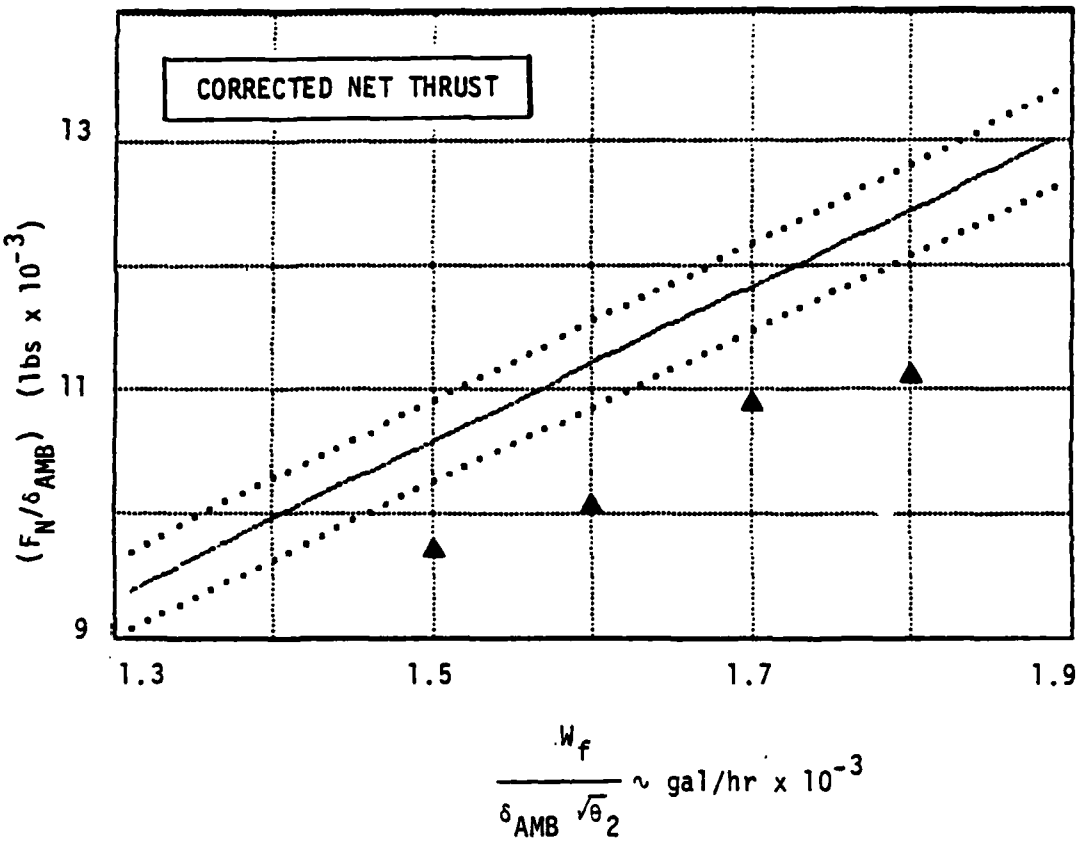

Figure 5.46 Identified Net Thrust Model

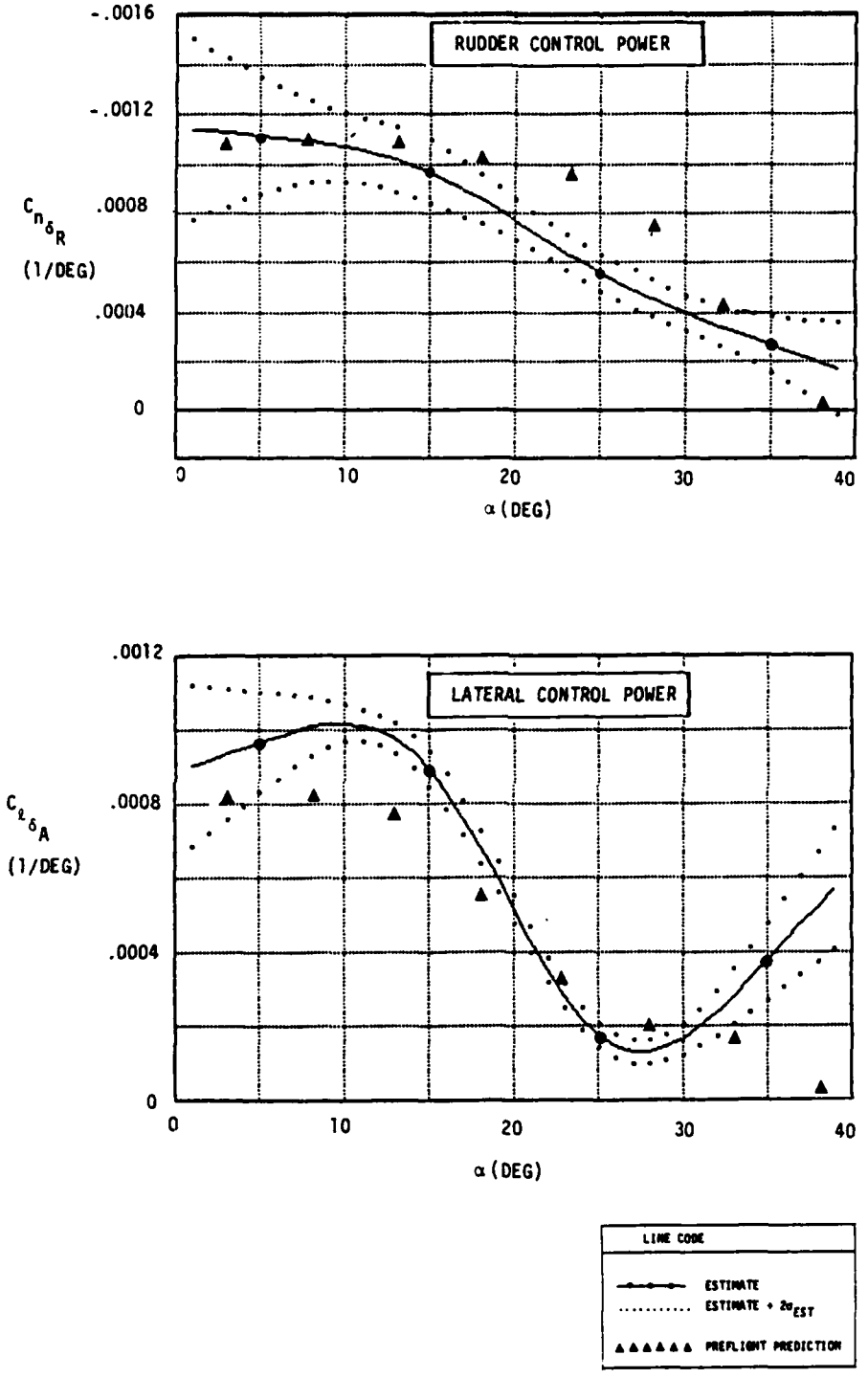

Figure 5.47 Comparison Between Flight-Identified and Preflight-Predicted Lateral/Directional Control Terms (continued on next page)

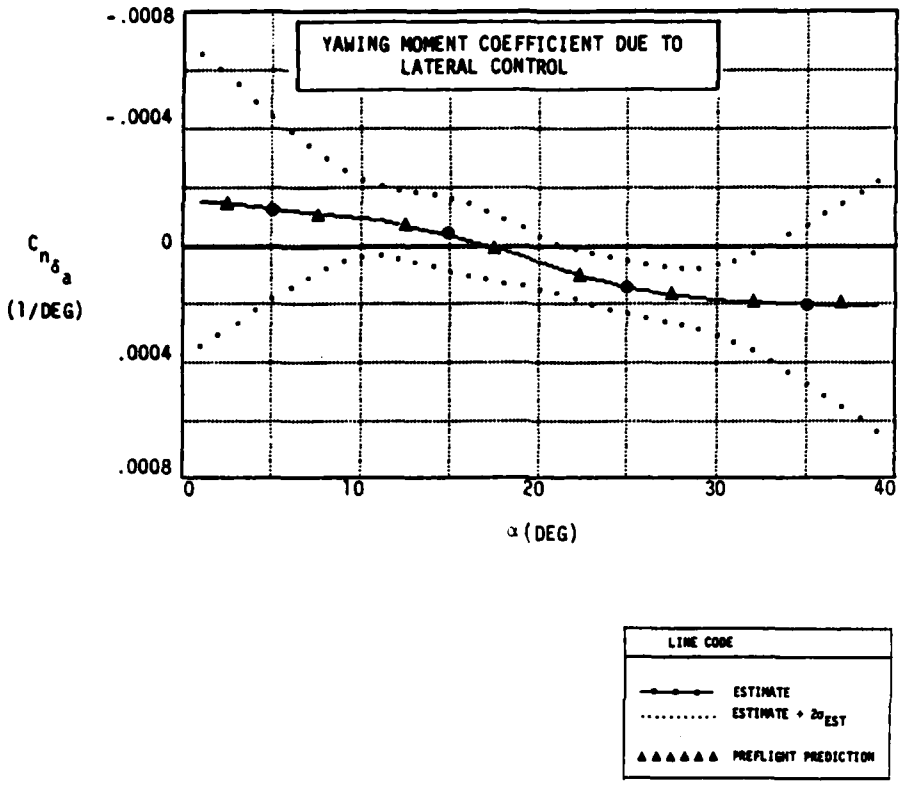

Figure 5.47 (Continued)

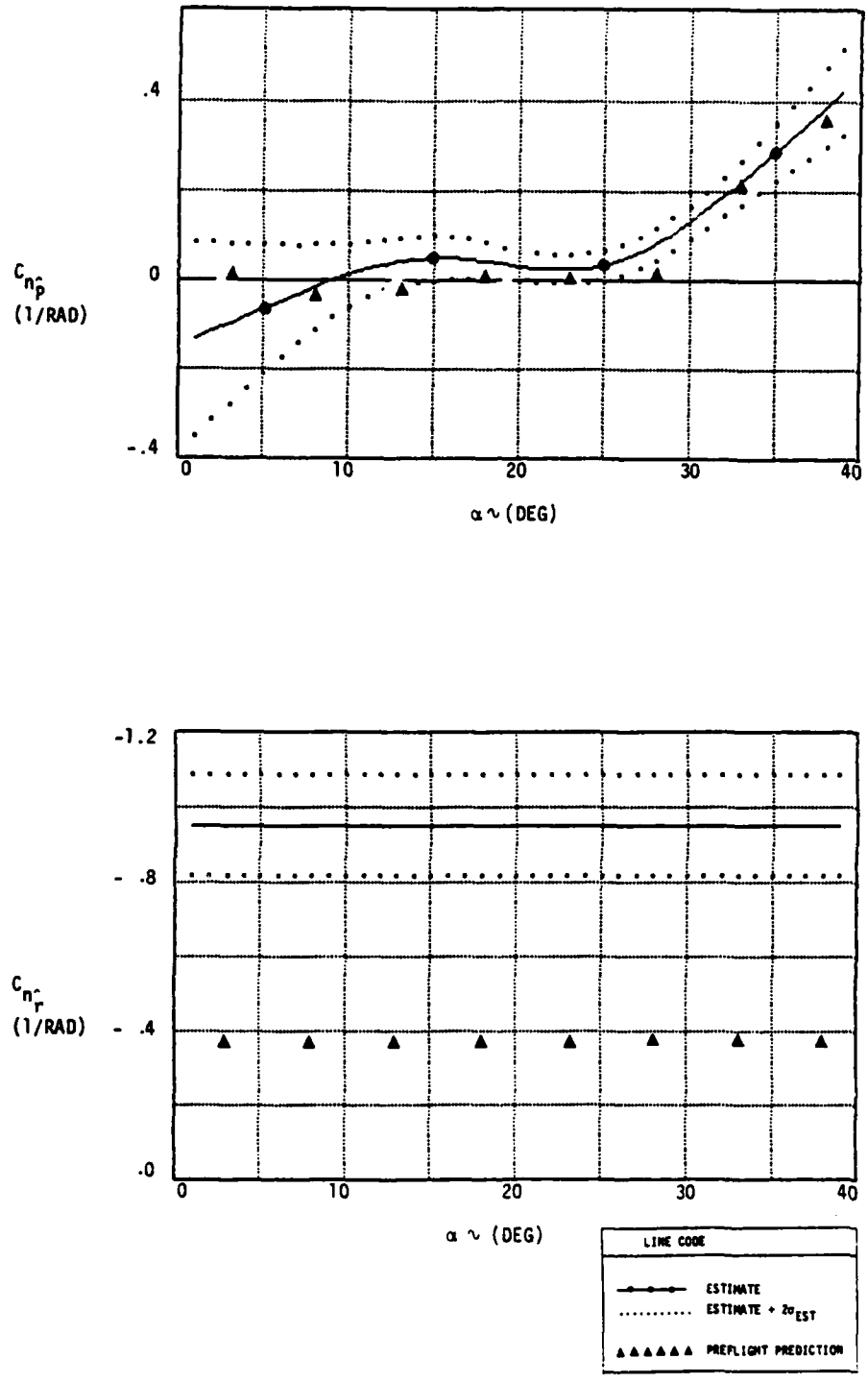

Figure 5.48 Comparison Between Flight-Identified and Preflight-Predicted Lateral/Directional Dynamic Derivatives (continued on next page)

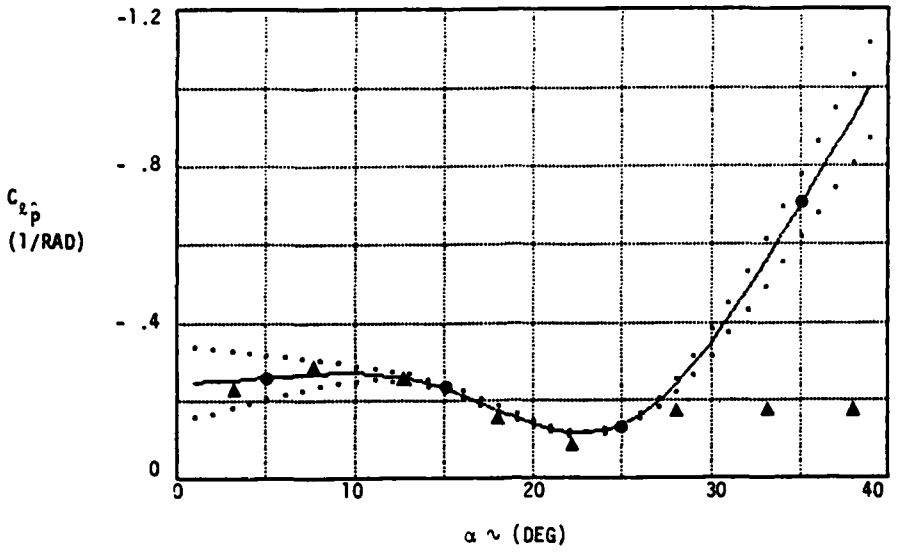

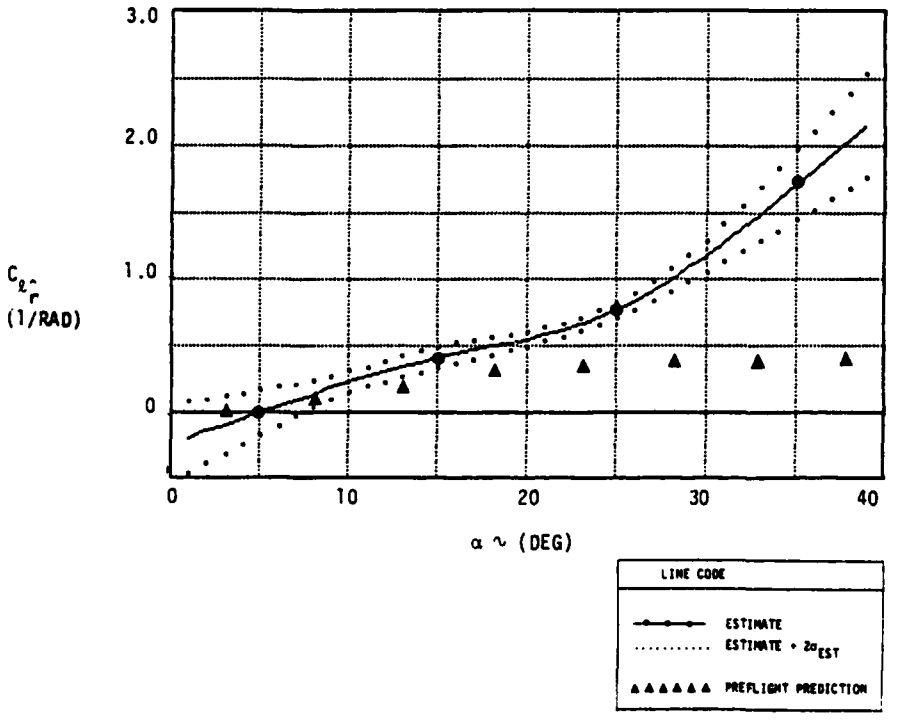

Figure 5.48 (Continued)

good agreement with preflight data in terms of trends with angle of attack with slight differences in the actual value of the derivative. The uncertainty of the lateral control derivatives ($C_{\ell_{\delta_a}}$ and $C_{n_{\delta_a}}$) as shown by the fanning of the $\pm 2\sigma$ curves is due to the lack of lateral control excitation at low and high α. In general, when the uncertainty boundaries are large for some parts of the flight regime, this information can be used for planning additional flight test conditions.

Identified values for roll rate and yaw rate stability derivatives for the F-4S are presented in Figure 5.48. Good agreement is evident between preflight prediction and identified values for $C_{n_{\hat{p}}}$ and $C_{\ell_{\hat{p}}}$ (for $\alpha <$ 30). The identified value for $C_{n_{\hat{r}}}$ is much greater than the preflight prediction, although both are independent of angle of attack. Significant differences exist between identified and predicted values of C_{ℓ_r} for $\alpha >$ 20°. The mid-span wing pylon, which protrudes beyond the wing leading edge for the flight test aircraft, could contribute to some of the differences between the flight identified and preflight predicted values for $\alpha > 20°$. The wing pylon would shed a vortex that would alter wing aerodynamics at high α.

5.6 FLIGHT MEASUREMENT PREDICTIONS

The ability of the identified aerodynamic and net thrust models to reproduce flight test measurements for the six test maneuvers analyzed from Phase II flight test data is tabulated in Figure 5.49. Figure 5.50 summarizes the root mean square residuals between the flight test measurements and estimates of the measurements. The predicted measurements are generated from a simulation of the F-4S based on the identified aerodynamic, thrust, and instrumentation models. The simulation is run with actual flight test time histories of the control commands.

MEASUREMENT	UNITS	RMS RESIDUAL FOR COMBINED SIX MANEUVERS IDENT. AERO/PROP CALIBRATED INS.	PREFLIGHT AERO/PROP CALIBRATED INS.
P	deg/sec	6.15	13.81
Q	deg/sec	2.85	11.61
R	deg/sec	1.78	11.04
$\alpha N/B$	deg	1.07	2.82
$\beta N/B$	deg	.98	2.35
q	psf	2.22	6.56
h_p	ft	94.00	215.00
n_x	g's	.009	.028
n_y	g's	.012	.016
n_z	g's	.036	.073

Note: Measure Residual = Actual Measurement - Estimate of Measurement

Figure 5.49 Effect of Model Parameters on Measurement Residuals

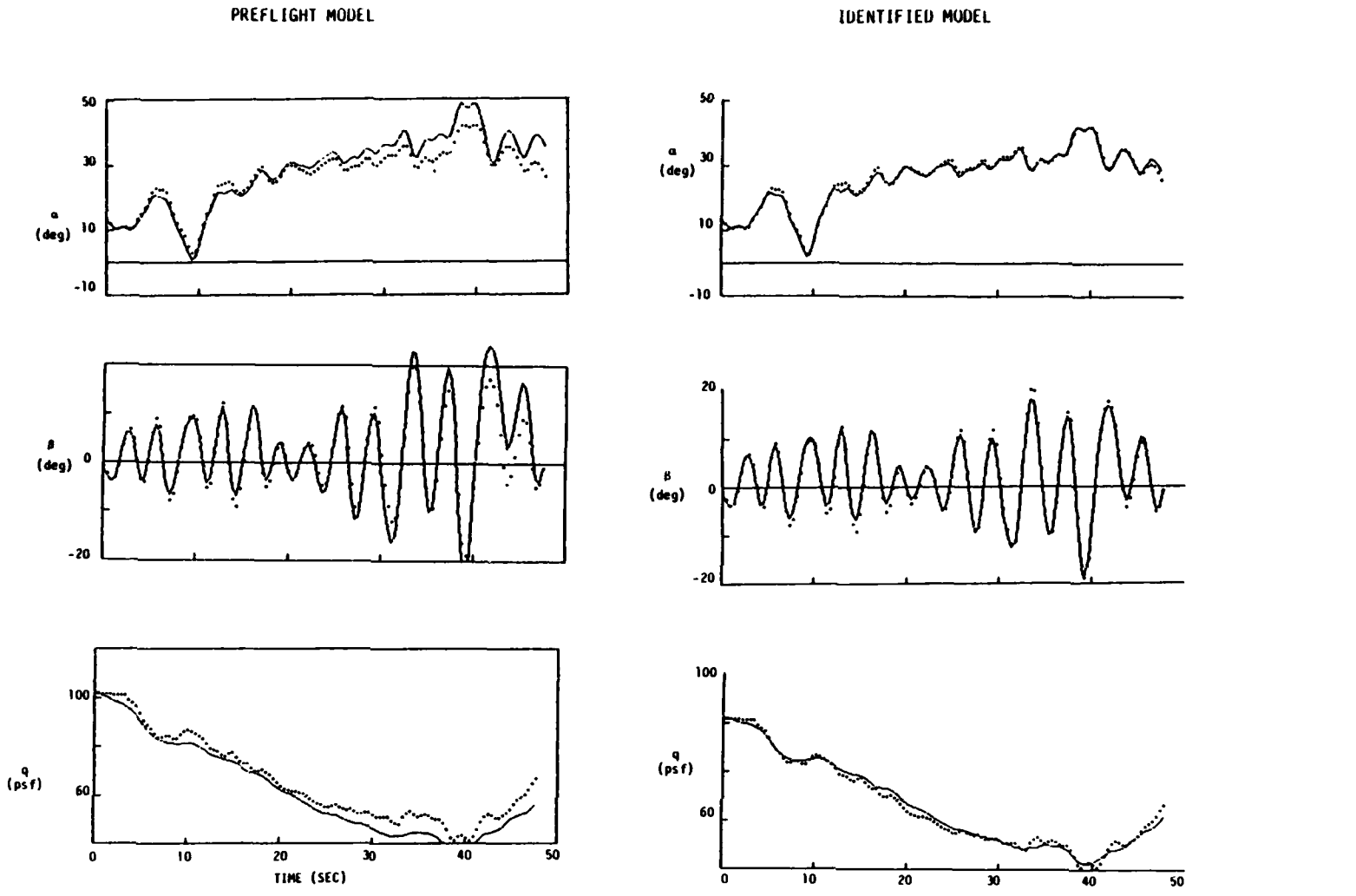

Figure 5.50 Measurement Prediction Improvement Due to Identified Parameters
(continued on next page)

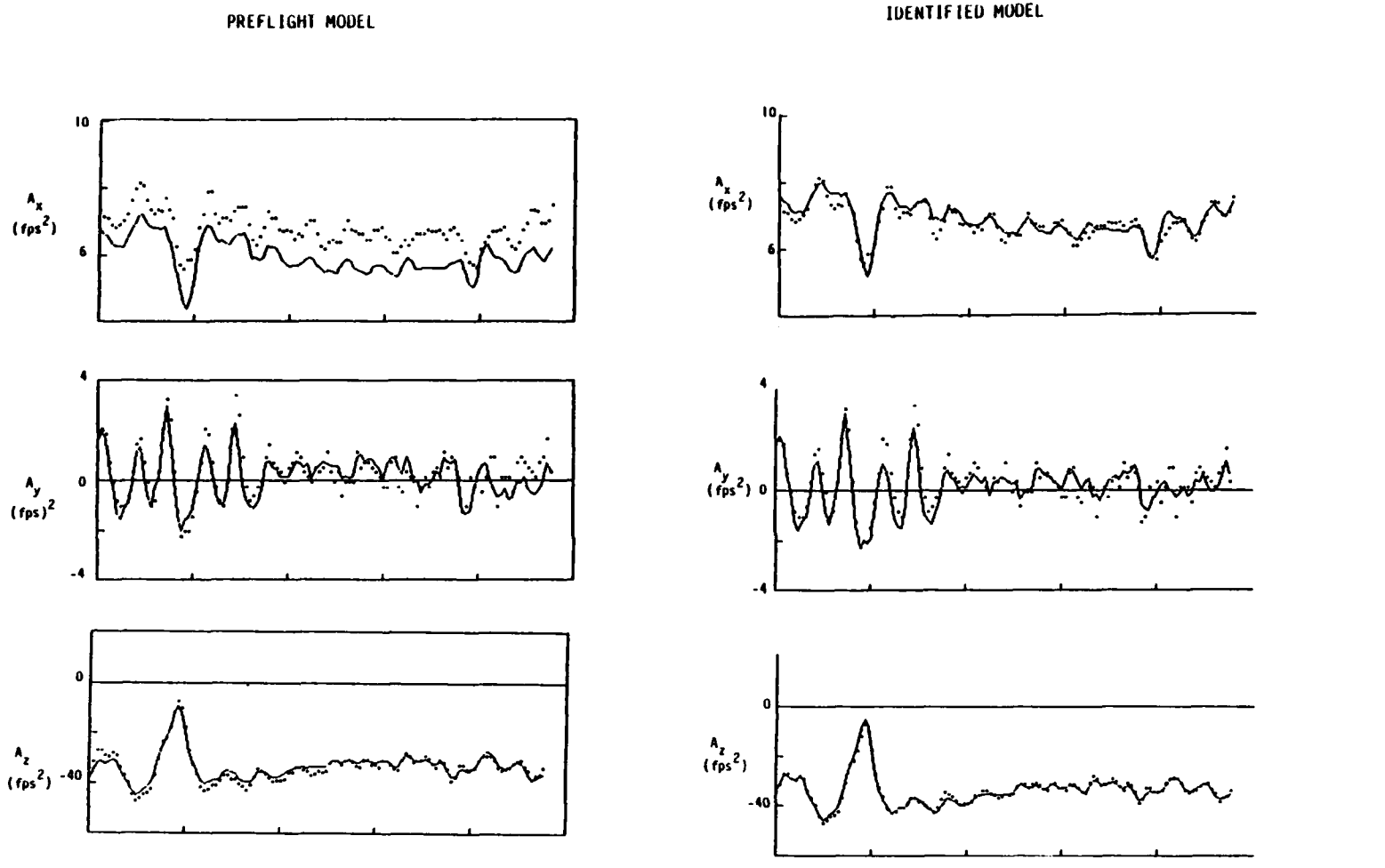

Figure 5.50 Measurement Prediction Improvement Due to Identified Parameters
(continued on next page)

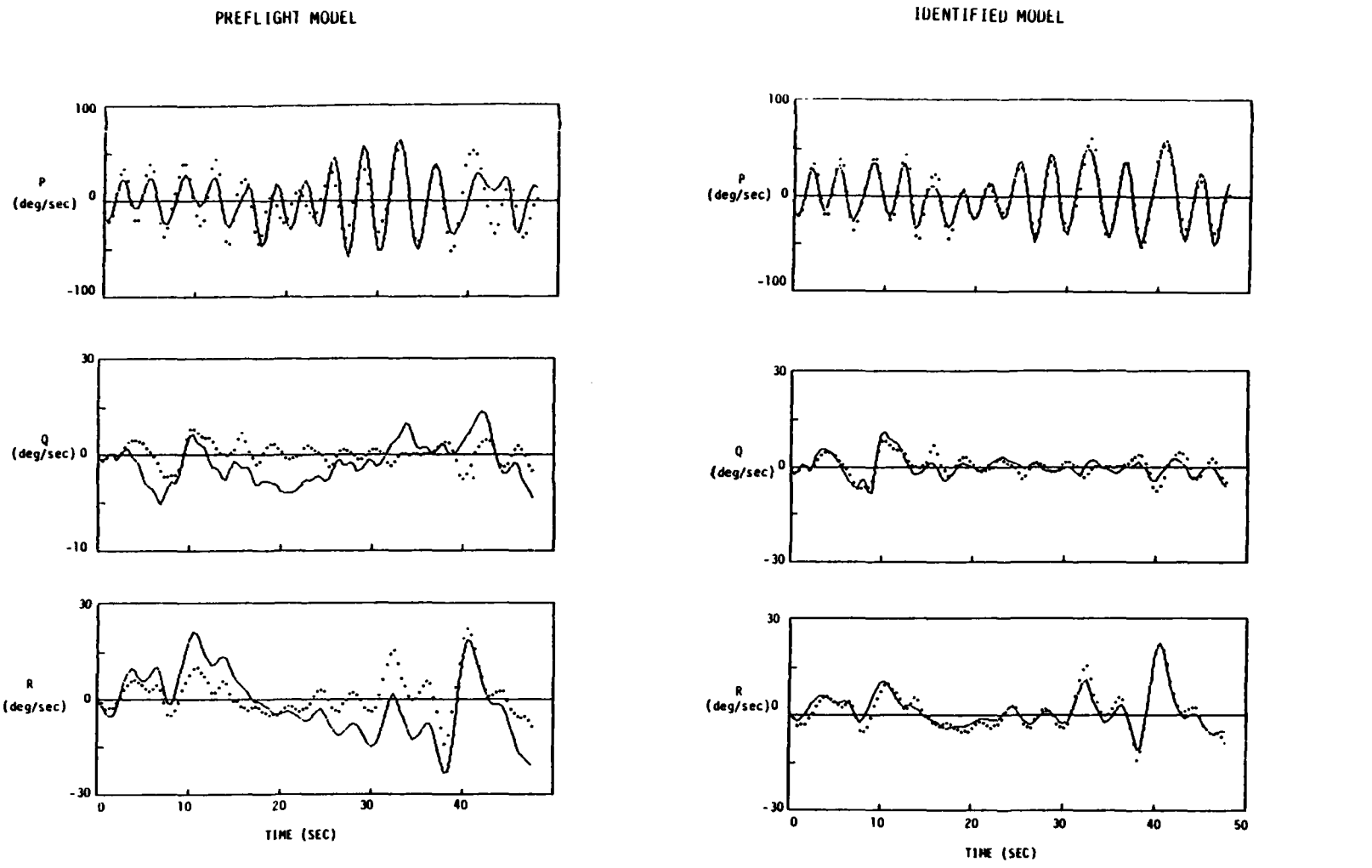

Figure 5.50 Measurement Prediction Improvement Due to Identified Parameters (concluded)

To gain some feeling for the relative worth of the identified model, the F-4S simulation was configured with the preflight aerodynamic data and run with the flight test control inputs. The resulting measurement residuals are also presented in Figure 5.49. In all cases, the identified model provides a better explanation of the flight test measurements. Figure 5.50 compares the time histories of the flight test measurements, predictions based on the identified model and predictions based on the preflight model for one of the flight conditions analyzed.

VI. SUMMARY AND CONCLUSIONS

The results presented in this report demonstrate the operational status of a nonlinear system identification data processing technique which is currently being used at the Naval Air Test Center. The following specific conclusions are noted.

(1) Nonlinear system identification data processing techniques can be used to identify aerodynamic, propulsion system and instrumentation calibration models from a common set of flight test conditions.

(2) Aircraft response predictions are improved with the identified model relative to prediction based on a preflight model.

(3) Extraction of performance, stability and control, and high angle of attack characteristics from a single model has been illustrated.

(4) The capability for identifying nonlinear aerodynamic models in a format compatible with preflight predictions has been demonstrated.

(5) A methodology for determining the accuracy of the parameter estimates was presented.

(6) Dynamic test techniques, which require nonlinear system identification data processing techniques, can improve test productivity.

(7) It is feasible to identify both aerodynamic and propulsion model data from a common set of flight test data. Only a very simplified propulsion model was identified in the analysis covered by this report. To aid the identification of propulsion models, it is recommended that the test conditions include throttle transients and that measurements of fan inlet pressure (P_{T2}), turbine exit on tail pipe pressure (P_{T56}), and nozzle area (A_8) also be included. A_8 could possibly be reconstructed from nozzle actuator displacements.

APPENDIX A
F-4S MATHEMATICAL MODEL

This appendix describes the F-4S mathematical simulation model implemented by the SCIDNT system identification computer program. The simulation models the following aspects of aircraft dynamics:

- rigid body nonlinear three degree of freedom rotation and three degree of freedom translation;
- aerodynamic and propulsion system forces and moments;
- winds (north, east, and down components); and

The simulation also models sensors which are commonly employed during aircraft flight testing. These sensors are

- angle of attack and sideslip vanes mounted on a nose boom;
- impact pressure;
- true airspeed;
- pressure altitude;
- three orthogonal axis accelerometers;
- three orthogonal axis angular rate gyros;
- vertical and directional gyros.

Provision is also made for modeling scale factor, misalignment, and bias errors in all sensors.

The following is a list of the subsections describing the simulation model:

A.2 Measurement Equations

A.2.1 Inertial Sensor

A.2.2 Air Data Sensors

A.2.3 Sensor Moment Arms

A.1 STATE EQUATIONS

A.1.1 Definition of States

Table A.1 lists the 10 states used in the simulation model. This list is made up of three basic classes of states

- fuselage translational and rotational motion,
- attitude dynamics, and
- altitude dynamics.

The units listed are in generic length (L), mass (M), time (T), and angle (rad). The program works effectively for any consistent set of units such as International or English. The geometric quantities cg_X, cg_Z, X_{REF}, and Z_{REF} will be scaled by 1/12 before being used to compute X_{cg} and Z_{cg} (see A.1.3.1). This will simplify the use of inches for the first four terms and feet for the second two. Dimensional constants such as air density must also use consistent units. Table A.2 illustrates these definitions.

A.1.2 Fuselage Rigid Kinematics and Dynamics

The detailed differential equations which describe the rigid body states and the kinematic relationships are

- Body Fixed Inertial Velocities

$$\frac{dU}{dt} = VR - WQ + g\ T_{L2B}(1,3) + \left(\frac{1}{m}\right) F_X$$

$$\frac{dV}{dt} = WP - UR + g\ T_{L2B}(2,3) + \left(\frac{1}{m}\right) F_Y$$

Table A.1
State Definitions

SYMBOL	DESCRIPTION	UNITS
U	x body axis component of inertial space velocity of body-fixed origin	ft/sec
V	y body axis component of inertial space velocity of body-fixed origin	ft/sec
W	z body axis component of inertial space velocity of body-fixed origin	ft/sec
P	x body axis component of angular rotation (roll rate)	rad/sec
Q	y body axis component of angular rotation (pitch rate)	rad/sec
R	x body axis component of angular rotation (yaw rate)	rad/sec
ϕ	Euler roll angle	rad
θ	Euler pitch angle	rad
ψ	Euler yaw angle	rad
h	Altitude (positive u_p)	ft

Table A.2
Dimensional Parameters

CONSTANTS

SYMBOL	DESCRIPTION	UNITS
g	Acceleration due to gravity	fps^2
ρ	Density of air	$slug-ft^3$
m	Mass of aircraft	slugs
I_x	Roll moment of inertia = $(y^2+z^2)dm$	$slug-ft^2$
I_y	Pitch moment of inertia = $(x^2+z^2)dm$	$slug-ft^2$
I_z	Yaw moment of inertia = $(x^2+y^2)dm$	$slug-ft^2$
I_{xy}	x-y product of inertia = $xy\ dm$	$slug-ft^2$
I_{xz}	x-z product of inertia = $xz\ dm$	$slug-ft^2$
I_{yz}	y-z product of inertia = $yz\ dm$	$slug-ft^2$

$$\frac{dW}{dt} = UQ-VP + g\ T_{L2B}(3,3) + \left(\frac{1}{m}\right) F_Z$$

- Body Axis Rotation Rates ($I_{xy}=I_{yz}=0$)

$$\frac{dP}{dt} = C_1RQ + C_2PQ + C_3M_{TX} + C_4M_{TZ}$$

$$\frac{dQ}{dt} = C_5RP + C_6(R^2-P^2) + C_7M_{TY}$$

$$\frac{dR}{dt} = C_8PQ + C_9RQ + C_4M_{TX} + C_{10}M_{TZ}$$

- Euler Angles

$$\frac{d\phi}{dt} = P + Q \sin\phi \tan\theta + R \cos\phi \tan\theta$$

$$\frac{d\theta}{dt} = Q \cos\phi - R \sin\phi$$

$$\frac{d}{dt} = (Q \sin\phi + R \cos\phi)/\cos\theta$$

- Altitude

$$\frac{dh}{dt} = -T_{L2B}(1,3)\ U - T_{L2B}(2,3)\ V - T_{L2B}(3,3)\ W$$

In these equations, the matrix T_{L2B} is a direction cosine matrix which relates the local earth-fixed coordinate system to the fuselage body-fixed coordinate system. The gravity vector is aligned with the z axis in the earth-fixed frame. The x y z axes of the body-fixed frame are aligned with the reference geometric axes of the fuselage. The nine elements of T_{L2B} are:

$$T_{L2B}(1,1) = \cos\theta \cos\psi$$

$$T_{L2B}(2,1) = \sin\phi \sin\theta \cos\psi - \cos\phi \sin\psi$$

$$T_{L2B}(3,1) = \sin\phi \sin\psi + \cos\phi \sin\theta \cos\psi$$

$$T_{L2B}(1,2) = \cos\theta \sin\psi$$

$$T_{L2B}(2,2) = \cos\phi \cos\psi + \sin\phi \sin\theta \sin\psi$$

$$T_{L2B}(3,2) = \cos\phi \sin\theta \sin\psi - \sin\phi \cos\psi$$

$$T_{L2B}(1,3) = -\sin\phi$$

$$T_{L2B}(2,3) = \cos\theta \sin\phi$$

$$T_{L2B}(3,3) = \cos\theta \cos\phi$$

For any vector x, the components in the local frame and the components in the body frame are related by

$$[\underset{\sim}{X}]_{\substack{BODY \\ AXIS}} = [T_{L2B}] \quad [\underset{\sim}{X}]_{\substack{LOCAL \\ AXIS}}$$

The inertia terms C_i, i=1 to 10 are

$$C_1 = \frac{(I_y - I_z)\, I_z - I_{xz}^2}{I_x I_z - I_{xz}^2}$$

$$C_2 = \frac{(I_x - I_y + I_z)\, I_{xz}}{I_x I_z - I_{xz}^2}$$

$$C_3 = \frac{I_z}{I_x I_z - I_{xz}^2}$$

$$C_4 = \frac{I_{xz}}{I_x I_z - I_{xz}^2}$$

$$C_5 = \frac{I_z - I_x}{I_y}$$

$$C_6 = \frac{I_{xz}}{I_y}$$

$$C_7 = \frac{1.0}{I_y}$$

$$C_8 = \frac{(I_x - I_y)\ I_x + I_{xz}^2}{I_x I_z - I_{xz}^2}$$

$$C_9 = \frac{(I_y - I_z - I_x)\ I_{xz}}{I_x I_z - I_{xz}^2}$$

$$C_{10} = \frac{I_x}{I_x I_z - I_{xz}^2}$$

The use of inertia terms in this form assumes symmetry through a vertical plane of the aircraft (i.e. $I_{xy}=I_{yz}=0$). The aircraft inertial tensor terms are

I_x roll moment of inertia = $\int(y^2 + z^2)dm$

I_y pitch moment of inertia = $\int (x^2 + z^2)dm$

I_z yaw moment of inertia = $\int(x^2 + y^2)dm$

I_{xz} x-z product of inertia = $\int xz\ dm$,

and are defined for the body axis system.

A.1.3 Applied Forces and Moments

A.1.3.1 Modeling Approach

The applied force and moment terms are formulated from aerodynamic and propulsion system contributions (see Table A.3). To permit multimaneuver identification processing, the moment models are referenced to a

Table A.3

Applied Forces and Moments (Body Axis)

Axial Force

$$F_x = F_{Ax} + F_{Tx}$$

Side Force

$$F_y = F_{Ay} + F_{Ty}$$

Vertical Force

$$F_z = F_{Az} + F_{Tz}$$

Rolling Moment

$$M_x = M_{Ax} + M_{Tx} - F_y \cdot Z_{cg}$$

Pitching Moment

$$M_y = M_{Ay} + M_{Ty} - F_y \cdot Z_{cg} - F_z \cdot X_{cg}$$

Yawing Moment

$$M_z = M_{Az} + M_{Tz} - F_y \cdot X_{cg}$$

where

$F_{(\cdot)}$, $M_{(\cdot)}$ = total applied forces and moments

$F_{A(\cdot)}$, $M_{A(\cdot)}$ = aerodynamic forces and moments

$F_{T(\cdot)}$, $M_{T(\cdot)}$ = propulsion forces and moments

X_{cg}, Y_{cg}, Z_{cg} = moment arm transfers between the MRC and the cg

user-specified "moment reference center" and then are corrected by conventional moment arm transfers for the c.g. location of each maneuver.

The moment arm transfers are defined by

$$X_{cg} = .0833\ (cg_X - X_{REF}) \quad \text{(ft)}$$

$$Z_{cg} = .0833\ (cg_Z - Z_{REF}) \quad \text{(ft)}$$

where cg_X: cg Body Station location (inches)

cg_Z: Water Line location (inches)

X_{REF}: Moment Reference Center Body Station (inches) - longitudinal

$Y_{REF} = 0$

Z_{REF}: Moment Reference Center Water Level (inches) - vertical.

The aerodynamic force and moment models are defined in terms of nondimensional coefficients which are dimensionalized by the appropriate reference geometry and by the dynamic pressure. The aerodynamic nondimensional coefficients are further expanded by nondimensional derivatives represented by single cubic spline in α and β. The aerodynamic derivatives are defined in Table A.4 for the body axis system and in Table A.5 for the stability axis system.

The propulsion forces and moments are defined in terms of corrected fuel flow and corrected engine RPM. Two models were used in the F-4S analysis. The first was a simplified model using net thrust as a function of corrected fuel flow. The second was a more accurate model using gross thrust and inlet ram force as a function of corrected fuel flow and corrected engine RPM. These two models are defined in Tables A.6 and A.7, respectively.

Table A.4

Aerodynamic Model in Body Axis

$$F_{Ax} = \bar{q}S\ C_x$$

$$F_{Ay} = \bar{q}S\ C_y$$

$$F_{Az} = \bar{q}S\ C_z$$

$$M_{Ax} = \bar{q}S\ b\ C_{\ell_{REF}}$$

$$M_{Ay} = \bar{q}S\ \bar{c}\ C_{m_{REF}}$$

$$M_{Az} = \bar{q}S\ b\ C_{n_{REF}}$$

where

$$C_x = C_x(\alpha) + C_{x_{|\delta_S|}}(\alpha) \cdot |\delta_S|$$

$$C_y = C_{y_\beta}(\alpha) \cdot \beta + K_{C_{n_{\delta_R}}} \cdot C_{n_{\delta_R}}(\alpha) \cdot \delta_R + C_{y_{\delta_A}}(\alpha) \cdot \delta_A + C_{y_{P_\alpha}} \cdot \hat{P} \cdot \alpha + C_{y_R} \cdot \hat{R}$$

$$C_z = C_z(\alpha) + K_{C_{m_{\delta_S}}} \cdot C_{m_{\delta_S}}(\alpha) \cdot \delta_S + C_{z_Q} \cdot \hat{q}$$

Table A.4 (Continued)

$$C_{\ell_{REF}} = C_{\ell_\beta}(\alpha) \cdot \beta + C_{\ell_{\delta_R}} \cdot \delta_R + C_{\ell_{\delta_A}}(\alpha) \cdot \delta_A + C_{\ell_P}(\alpha) \cdot P^* + C_{\ell_R}(\alpha) \cdot R^*$$

$$C_{m_{REF}} = C_m(\alpha) + C_{m_{\delta_S}}(\alpha) \cdot \delta_S + C_{m_{|\beta|}}(\alpha) \cdot |\beta| + C_{m_Q} \cdot Q^* + C_{m_{|\delta_A|}}(\alpha) \cdot |\delta_A|$$

$$+ C_{m_{|\delta_R|}}(\alpha) \cdot |\delta_R|$$

$$C_{n_{REF}} = C_n^b(\alpha, \beta) + C_{n_{\delta_R}}(\alpha) \cdot \delta_R + C_{n_{\delta_A}}(\alpha) \cdot \delta_A + C_{n_P}(\alpha) \cdot P^* + C_{n_R} \cdot R^*$$

Notation:

$C(\alpha)$ = a single cubic spline in α

$$= \sum_{i=1}^{k} C(\alpha = \alpha_i)\, f_i(\alpha)$$

$C(\alpha, \beta)$ = a bicubic spline in α and β, which is antisymmetric in β

$$= \sum_{i=1}^{k} \sum_{j=2}^{k} C(\alpha = \alpha_i, \beta = \beta_j)\, f_i(\alpha)\, g_j(\beta) \qquad (\text{for } \beta > 0)$$

$$= -C(\alpha, -\beta); \quad C(\alpha, 0) = 0 \qquad (\text{for } \beta \leq 0)$$

Table A.5
Aerodynamic Model in Stability Axis

$$F_{Sx} = \bar{q} S_w C_D$$

$$F_{Sy} = \bar{q} S_w C_y$$

$$F_{Sz} = - \bar{q} S_w C_L$$

$$M_{Sx} = \bar{q} S_w b_w C_{\ell_{REF}}$$

$$M_{Sy} = \bar{q} S_w \bar{c}_w C_{m_{REF}}$$

$$M_{Sz} = \bar{q} S_w b_w C_{n_{REF}}$$

where

$F_{S(\cdot)}$, $M_{S(\cdot)}$ = aerodynamic forces and moments in stability axis.

As the equations of motion are solved in body axis, the following stability axis to body axis transformation is used:

$$F_{Ax} = F_{Sx} \cos \alpha_B - F_{Sz} \sin \alpha_B$$

$$F_{Ay} = F_{Sy}$$

$$F_{Az} = F_{Sx} \sin \alpha_B + F_{Sz} \cos \alpha_B$$

$$M_{Ax} = M_{Sx} \cos \alpha_B - M_{Sz} \sin \alpha_B$$

$$M_{Ay} = M_{Sy}$$

$$M_{Az} = M_{Sx} \sin \alpha_B + M_{Sz} \cos \alpha_B$$

Table A.5 (Continued)

The aerodynamic coefficients are expanded as follows:

$$C_D = C_D(\alpha) + C_{D_{|\delta_S|}}(\alpha) \cdot |\delta_S|$$

$$C_y = C_{y_\beta}(\alpha) \cdot \beta + C_{y_{\delta_R}} \cdot \delta_R + C_{y_{|\delta_A|}}(\alpha) \cdot |\delta_A| + C_{y_P}(\alpha) \cdot \hat{P} + C_{y_R} \cdot \hat{R}$$

$$C_L = C_L(\alpha) + K_{C_{m_{\delta_S}}} \cdot C_{m_{\delta_S}}(\alpha) \cdot \delta_S + C_{L_Q} \cdot \hat{Q}$$

$$C_{\ell_{REF}} = C_{\ell_\beta}(\alpha) \cdot \beta + C_{\ell_{\delta_R}}(\alpha) \cdot \delta_R + C_{\ell_{\delta_A}}(\alpha) \cdot \delta_A + C_{\ell_P}(\alpha) \cdot \hat{P} + C_{\ell_r}(\alpha) \cdot \hat{R}$$

$$C_{m_{REF}} = C_m(\alpha) + C_{m_{\delta_S}}(\alpha) \cdot \delta_S + C_{m_Q}(\alpha) \cdot \hat{q}$$

$$C_{n_{REF}} = C_{n_\beta}(\alpha) \cdot \beta + C_{n_{\delta_R}}(\alpha) \cdot \delta_R + C_{n_{\delta_A}}(\alpha) \cdot \delta_A + C_{n_P}(\alpha) \cdot \hat{P} + C_{n_R}(\alpha) \cdot \hat{R}$$

NOTE: Though physically and numerically different, the same symbols are used for body axis and stability axis lateral rolling and yawing moment coefficients ($C_{\ell_{REF}}$ and $C_{n_{REF}}$). The side force coefficient (C_y) is physically and numerically the same in both axis systems.

Table A.6

Propulsion Model Using Net Thrust

$$F_{Tx} = (F_{N_L} + F_{N_R}) \cos \theta_T$$

$$F_{Ty} = 0$$

$$F_{Tz} = -(F_{N_L} + F_{N_R}) \sin \theta_T$$

$$M_{Tx} = |\ell_{N_y}| \, (F_{N_L} + F_{N_R}) \sin \theta_T$$

$$M_{Ty} = \ell_{N_z} (F_{N_L} + F_{N_R}) \cos \theta_T$$

$$M_{Tz} = |\ell_{N_y}| \, (F_{N_L} + F_{N_R}) \cos \theta_T$$

where

F_{N_L}, F_{N_A} = left and right engine net thrust

ℓ_{N_y}, ℓ_{N_z} = lateral and vertical net thrust moment arm relative to MRC

θ_T = thrust line inclination relative to x-axis

and

$$FN_{(\cdot)} = \left(\frac{F_N}{\delta_{AMB}} \right)_{(\cdot)} \cdot \delta_{AMB}$$

$$\left(\frac{F_N}{\delta_{AMB}} \right)_{(\cdot)} = f_n \left(\frac{\dot{w}_f}{\delta_{AMB} \cdot \sqrt{\theta_2}} \right)$$

where

f_n = corrected net thrust versus corrected fuel flow curve identified from flight test data (see Section 5.4).

Table A.7

Propulsion Model Using Gross Thrust

$$F_{Tx} = \sum_{i=L,R} (F_{G_i} \cos \theta_T - F_{I_i} \cos \alpha_B \cos \beta)$$

$$F_{Ty} = - \sum_{i=L,R} (F_{I_i} \sin \beta)$$

$$F_{Tz} = - \sum (F_{G_i} \sin \theta_T + F_{I_i} \sin \alpha_B \cos \beta)$$

$$M_{Tx} = \sum_{i=L,R} [F_{G_i} \ell_{G_{y_i}} \sin \theta_T + F_{I_i}(\ell_{I_{z_i}} \sin \beta - \ell_{I_{y_i}} \cos \beta \sin \alpha_B)]$$

$$M_{Ty} = \sum_{i=L,R} [F_{G_i}(\ell_{G_{y_i}} \sin \theta_T + \ell_{G_{z_i}} \cos \theta_T) + F_{I_i}(\ell_{I_{x_i}} \sin \alpha_B \cos \beta - \ell_{I_{z_i}} \cos \alpha_B \cos \beta)]$$

$$M_{Tz} = \sum_{i=L,R} [- F_{G_i} \ell_{G_{y_i}} \cos \theta_T + F_{I_i}(- \ell_{I_{x_i}} \sin \beta + \ell_{I_{y_i}} \cos \alpha_B \cos \beta)]$$

where

F_{G_L}, F_{G_R} = left and right engine gross thrust

F_{I_L}, F_{I_R} = left and right inlet ram force

$\ell_{G_{y_{(\ )}}}$, $\ell_{G_{z_{(\ )}}}$ = gross thrust moment arms relative to MRC

$\ell_{I_{x_{(\ )}}}$, $\ell_{I_{y_{(\ )}}}$, $\ell_{I_{z_{(\ )}}}$ = inlet ram force moment arms relative to MRC

and

Table A.7 (Continued)

Gross Thrust

$$F_{G_{(\cdot)}} = \left(\frac{F_G}{\delta_{AMB}}\right)_{(\cdot)} \cdot \delta_{AMB}$$

$$\left(\frac{F_G}{\delta_{AMB}}\right)_{(\cdot)} = f_g\left(\frac{w_{f(\cdot)}}{\delta_{AMB} \cdot \theta_{AMB}}\right)$$

Inlet Ram Force

$$F_{I_{(\cdot)}} = \dot{m}_{a_{(\cdot)}} \cdot V_T$$

$$\dot{m}_{a_{(\cdot)}} = \left(\frac{\dot{m}_a \sqrt{\theta_{T_2}}}{\delta_{T_o}}\right)_{(\cdot)} \frac{\delta_{T_o}}{\sqrt{\theta_{T_2}}}$$

$$\left(\frac{\dot{m}_a \sqrt{\theta_{T_2}}}{\delta_{T_o}}\right)_{(\cdot)} = f_m\left(\frac{N_{2_{(\cdot)}}}{\sqrt{\theta_{T_2}}}\right)$$

where

$\left(\frac{F_G}{\delta_{AMB}}\right)$ = corrected gross thrust versus corrected fuel flow curve (see Figure A.1)

Table A.7 (Concluded)

$\left(\frac{\dot{m}_a \sqrt{\theta_{T_2}}}{\delta_{T_o}}\right)$ = corrected air mass flow versus corrected RPM curve supplied by the manufacturer (see Figure A.2)

NOTE: For some of the flights, the fuel flow measurement was not available. Calculated fuel flow as a function of corrected RPM was used instead (see Figures A.3 and A.4).

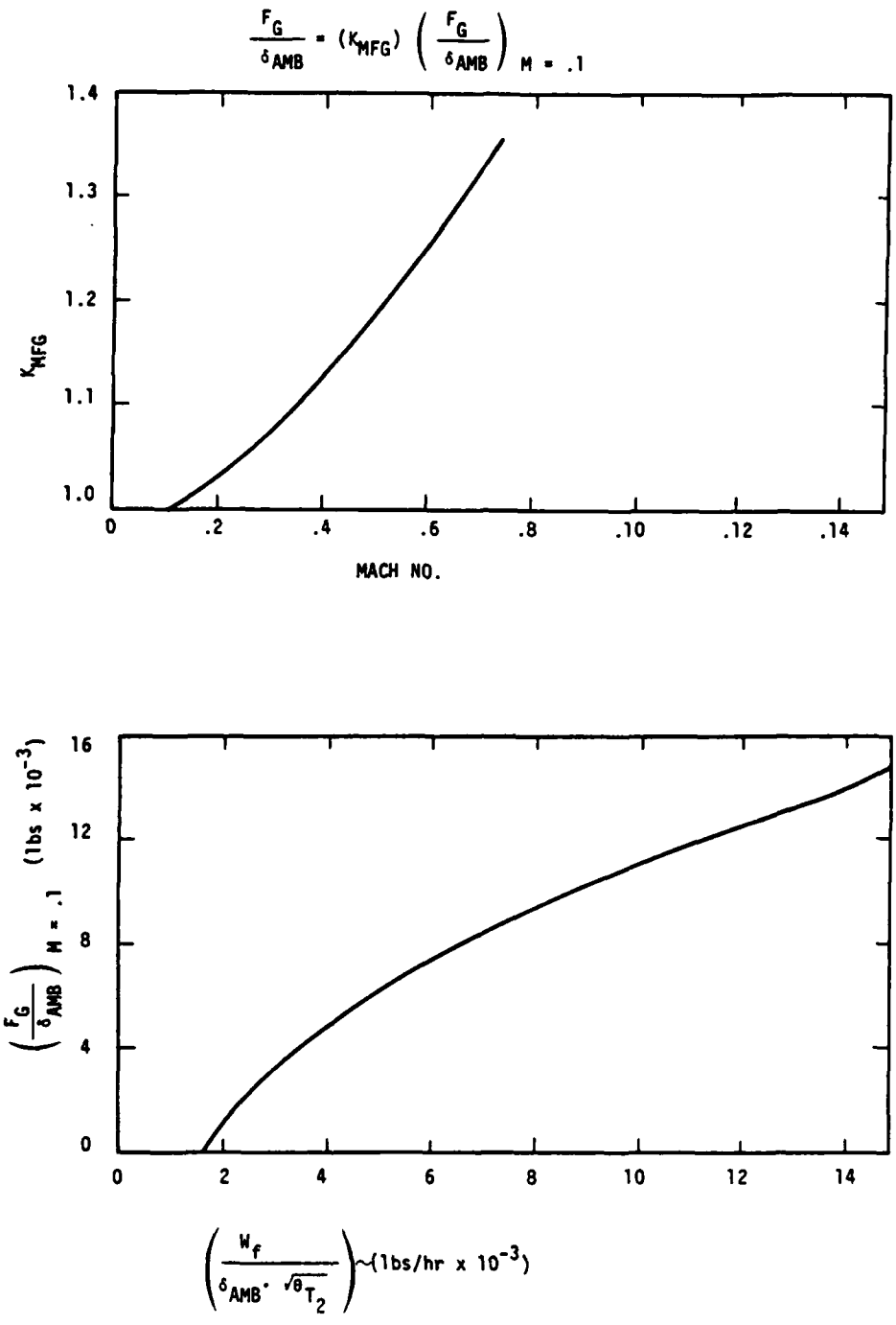

Figure A.1 Corrected Gross Thrust Versus Corrected Fuel Flow

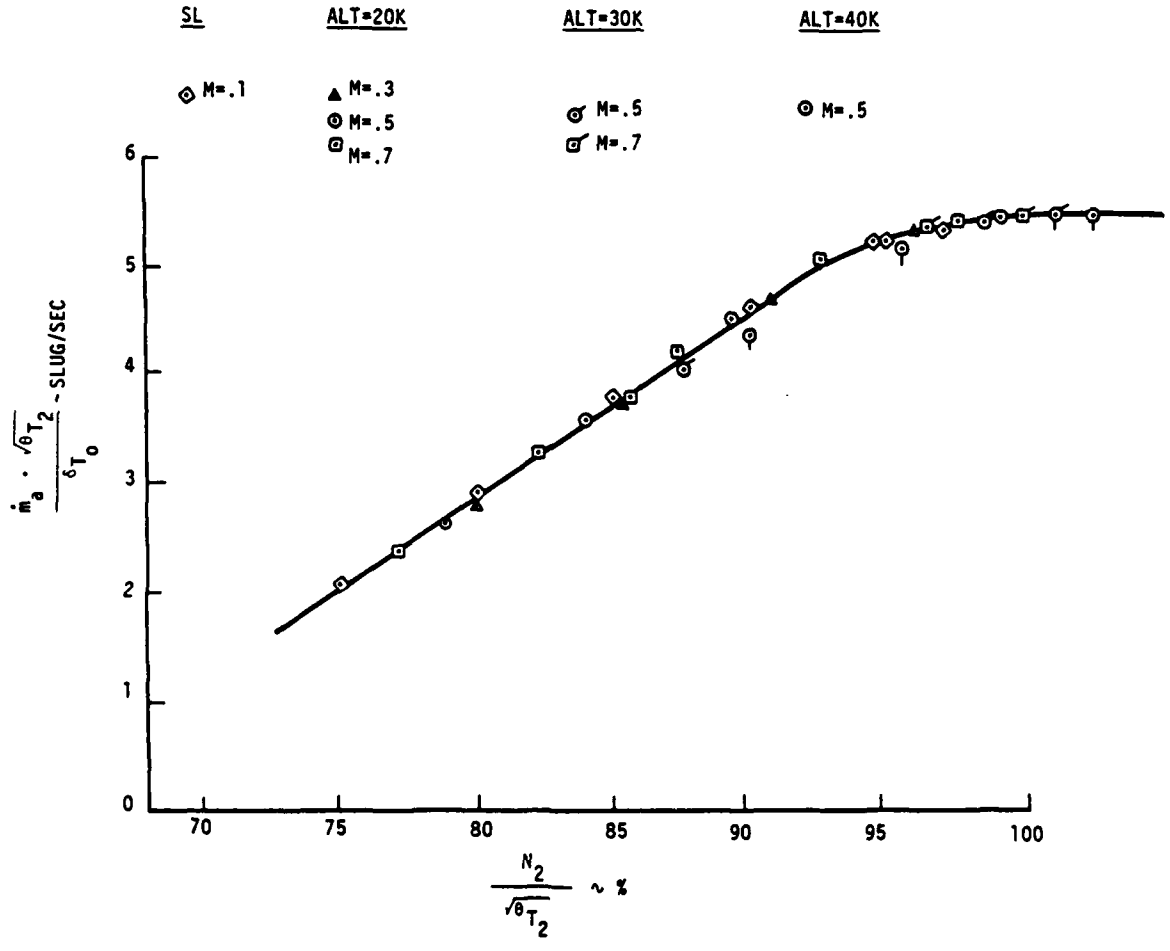

Figure A.2 Corrected Air Mass Flow Versus Corrected RPM

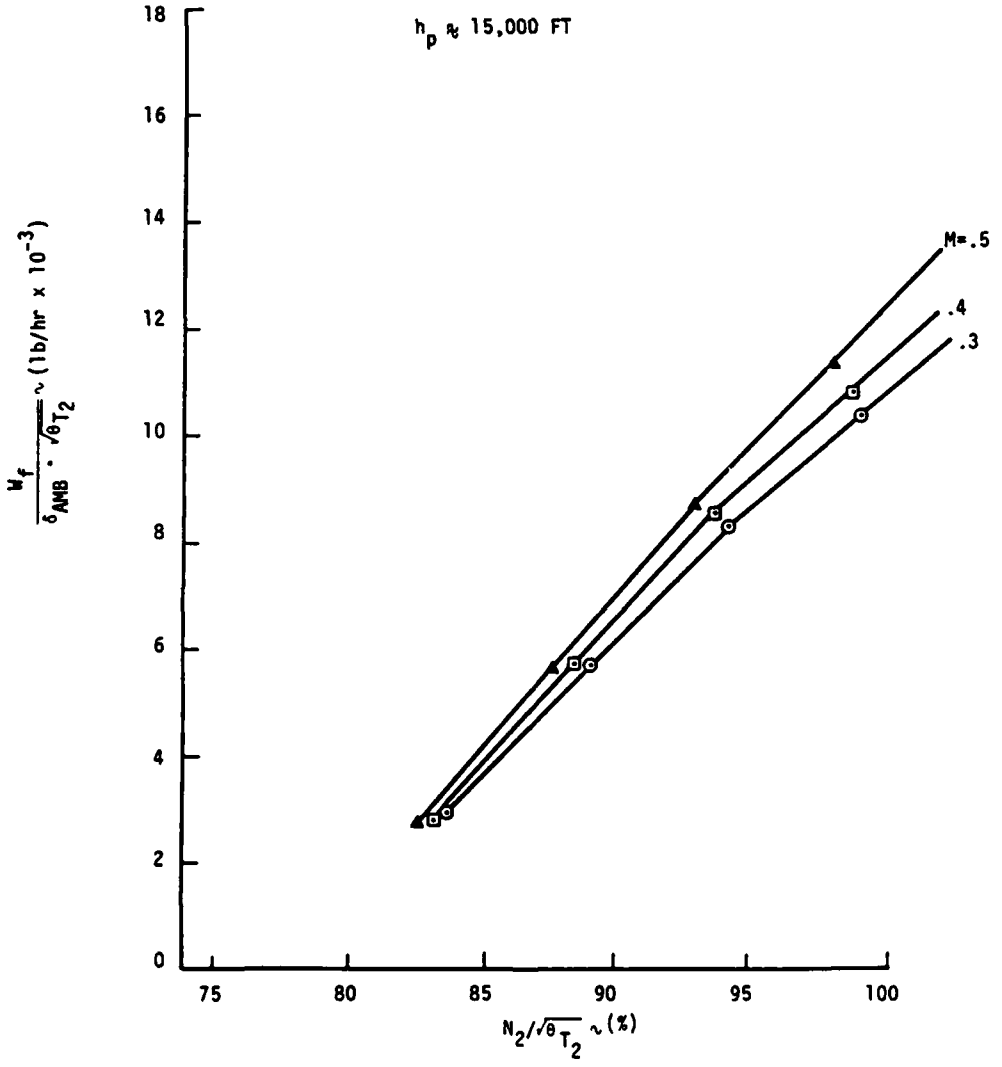

Figure A.3 Corrected Fuel Flow Versus Corrected RPM

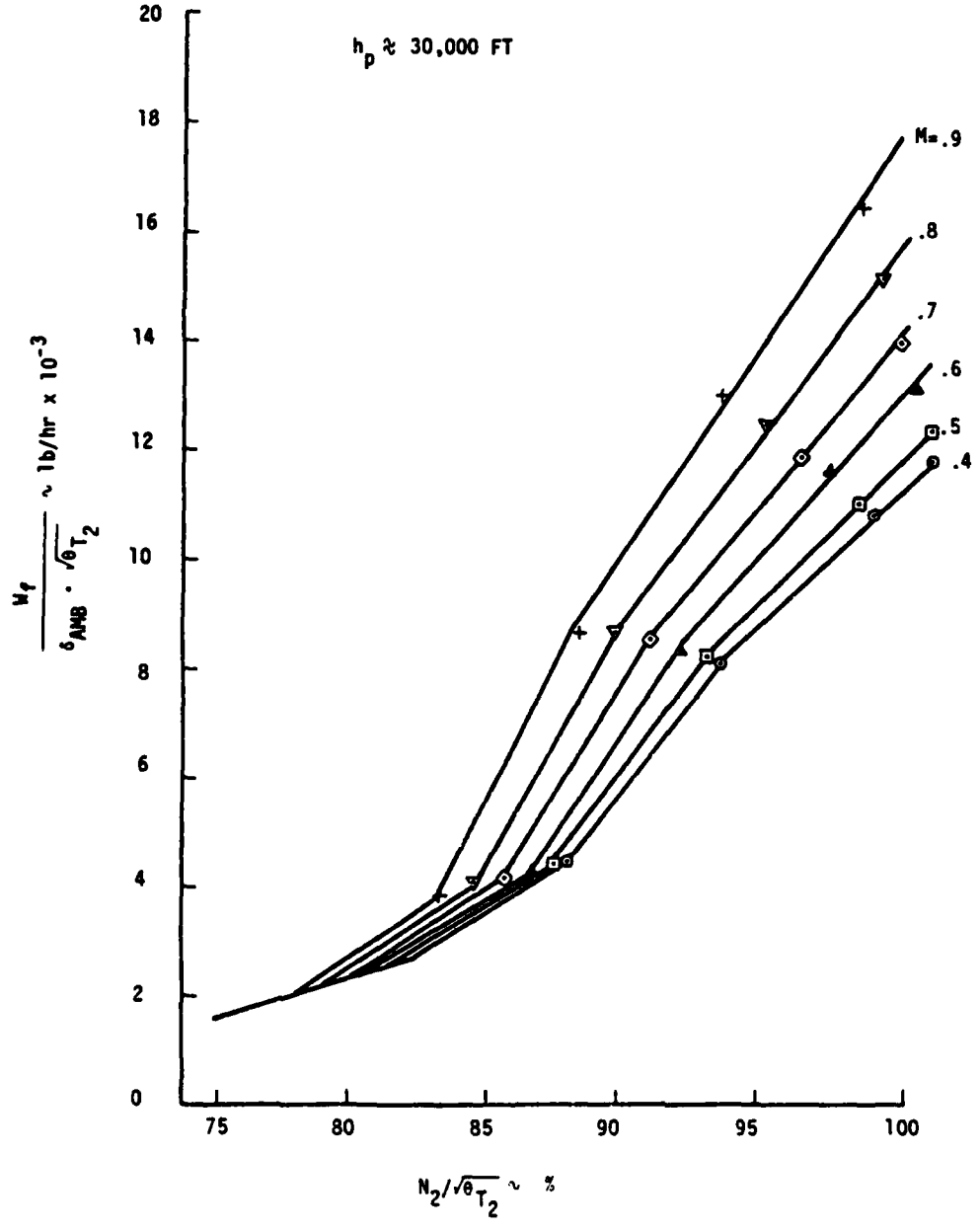

Figure A.4 Corrected Fuel Flow Versus Corrected RPM

A.1.4.2 Expansion Variables

The expansion variables are the independent arguments for the applied force and moment terms. These variables fall into four classes and they can be calculated as a part of the simulation or read-in as "control variables."

- Airspeed, Angle of Attack, Sideslip
- Body Rotational Rates
- Control Positions
- Atmospheric Variables

- Airspeed, Angle of Attack and Sideslip

The airspeed components are reconstructed from the inertial velocity components (U,V,W) and the body axis wind velocity components (U_W, V_W, W_W):

$$U_A = U - U_W$$

$$V_A = V - V_W$$

$$W_A = W - W_W$$

The body axis wind velocity components are derived from wind components which are defined in an earth fixed axis system (i.e., V_N (north), V_E (east), V_D (down)). The transformation from earth to body axis wind components is

$$\begin{Bmatrix} U_W \\ V_W \\ W_W \end{Bmatrix} = [T_{L2B}] \begin{Bmatrix} V_N \\ V_E \\ V_D \end{Bmatrix}$$

Airspeed: $$V_T = \sqrt{U_A^2 + V_A^2 + W_A^2}$$

angle of attack: $$\alpha = \tan^{-1}\left(\frac{W_A}{U_A}\right)$$

angle of sideslip: $$\beta = \tan^{-1}\left(\frac{V_A}{U_A}\right)$$

END

FILMED

10-84

DTIC